AN INVESTIGATION OF THE Ta^{181} NUCLEUS

Thesis by

Arthur H. Muir, Jr.

In Partial Fulfillment of the Requirements

For the Degree of

Doctor of Philosophy

California Institute of Technology
Pasadena, California

1960

ACKNOWLEDGEMENTS

It is a pleasure for the author to acknowledge the kind assistance offered him by all of the personnel of the Physics 34 group. In particular, he is very much indebted to Dr. Felix Boehm for suggesting this study and for his interest, advice, and encouragement which contributed greatly to it. It is also a pleasure to acknowledge the continued support and encouragement of Dr. Jesse W. M. DuMond. The author has benefited greatly from discussion with Dr. U. Hauser, Dr. G. Manning, Dr. G. Nijgh, Mr. John Rogers, and other members of the group. In addition, he wishes to express his gratitude to his wife for her help in the preparation of the manuscript.

Finally, the author would like to express his appreciation to the U.S. Atomic Energy Commission for the financial support of this research.

ABSTRACT

The nuclear levels of Ta^{181} were investigated by the study of the β-decay of Hf^{181} and the electron capture decay of W^{181}. The previously reported 476 kev transition from the Hf^{181} decay was found not to be in coincidence with the 482 kev transition, thus ruling out the level proposed at 958 kev. Evidence for weak M-shell conversion lines of a ~6 kev transition in the Hf^{181} decay was found with a 180° β-spectrometer. A β-spectrometer investigation of the W^{181} decay revealed strong M-shell conversion lines which correspond to a transition of 6.25 ± 0.3 kev in energy. On the basis of the above mentioned results and other considerations, it is concluded that the 476 kev transition in the Hf^{181} decay occurs between the 482 kev level and the new 6 kev level. A 6 kev γ-ray was also found in the W^{181} decay with an argon proportional counter. From these studies, the conversion coefficient of the 6 kev transition was determined to be $\alpha_T = 44 \pm 7$. The conversion coefficient and the M-subshell conversion ratios require that the 6 kev transition is of E1 multipolarity. From this assignment and other experimental and theoretical considerations, it is concluded that the 6 kev level is the 9/2− [514] Nilsson intrinsic state. Arguments can also be made that the previously reported 152 kev transition in the W^{181} decay occurs between a new 11/2− rotational level at 158 kev and the 6 kev level. From a measurement of the tantalum L/K x-ray intensity ratio, the W^{181} electron capture L/K branching ratio (to the ground state and the 6 kev level) is found to be $P_L/P_K = 0.359$, and the W^{181} decay energy is found to be 176^{+44}_{-22} kev. The branchings of this decay to the various Ta^{181} levels are as follows: 158 kev (0.12%), 136 kev (0.075%), 6.25 kev (~35%), and 0 kev (~65%). All findings and proposals are consistent with the unified model of the nucleus.

TABLE OF CONTENTS

PART I

INTRODUCTION

Atomic nuclei with large spheroidal deformations can, in many respects, be understood on the grounds of the Nilsson model (1) of intrinsic single particle nucleonic states. This model has proved to be particularly successful in explaining the spins, parities, and magnetic moments of nuclear ground states and it describes the properties of many excited states as well. On the other hand, it is well known that aspects of the collective motion of deformed nuclei can be understood in terms of the Bohr-Mottelson collective model (2). For each intrinsic configuration, collective vibrational and rotational modes of nuclear excitation may also exist. It has been found that many observed low-lying excited states of deformed nuclei can be interpreted as rotational levels based on intrinsic states. Energy level spacings in rotational bands, in particular, are given extremely accurately by the theory. The combined description of nucleonic single particle and collective motion giving rise to intrinsic and rotational states is referred to as the "unified model".

The nuclei to which this unified model applies best are those in the regions $150 < A < 190$ and $A > 220$. From measurements of quadrupole moments, nuclei in these regions are known to possess strong spheroidal deformations (3). Recently Mottelson and Nilsson (4) have reviewed the spectra of odd mass number nuclei in the regions $150 < A < 190$ and $230 < A < 250$, and have interpreted the observed spectra in terms of the unified model.

One of the most frequently studied* deformed nuclei is Ta^{181}. The nearly 100% natural abundance of tantalum isotope 181 makes it an ideal case for Coulomb excitation studies. Hf^{181}, which β-decays to Ta^{181} (with a half-life of 45 days), is readily produced by neutron capture in Hf^{180}. Finally, W^{181} is known to decay by electron capture (6), (7), (8) to Ta^{181} (with a half-life of 145 days), although this decay is not as well studied as the Hf^{181} decay.

Mottelson and Nilsson's (4) interpretation of the reported Ta^{181} levels in terms of Nilsson intrinsic states (1), (4) and collective rotational levels (2) is shown in the level scheme of Fig. 1.1. The K = 7/2+ (I = 7/2, 9/2, 11/2) ground state rotational band is well known from Coulomb excitation experiments (5). A second rotational band (I = 1/2, 3/2) is found (9) which is based on the K = 1/2+ intrinsic state at 615 kev. A 5/2+ intrinsic level occurs at 482 kev, and there are suggestions for a 9/2− intrinsic state at 152 kev (10), and for a 1/2− intrinsic state at 958 kev (9). The assignments for the ground state, as well as for the levels at 136, 301, 482, and 615 kev, seem quite certain.

Despite the many studies of this level scheme, several problems still exist. Boehm and Marmier (9) found a weak 476 kev transition in the Hf^{181} decay. The probable multipolarity assignment was given as M2, and they suggested that this transition might occur between a 1/2− intrinsic level at 958 kev and the well known 482 kev level. Debrunner et al. (8), however, reported that a coincidence experiment excluded

---

* See references (5) through (10) and the list of references for Table A II, Appendix III.

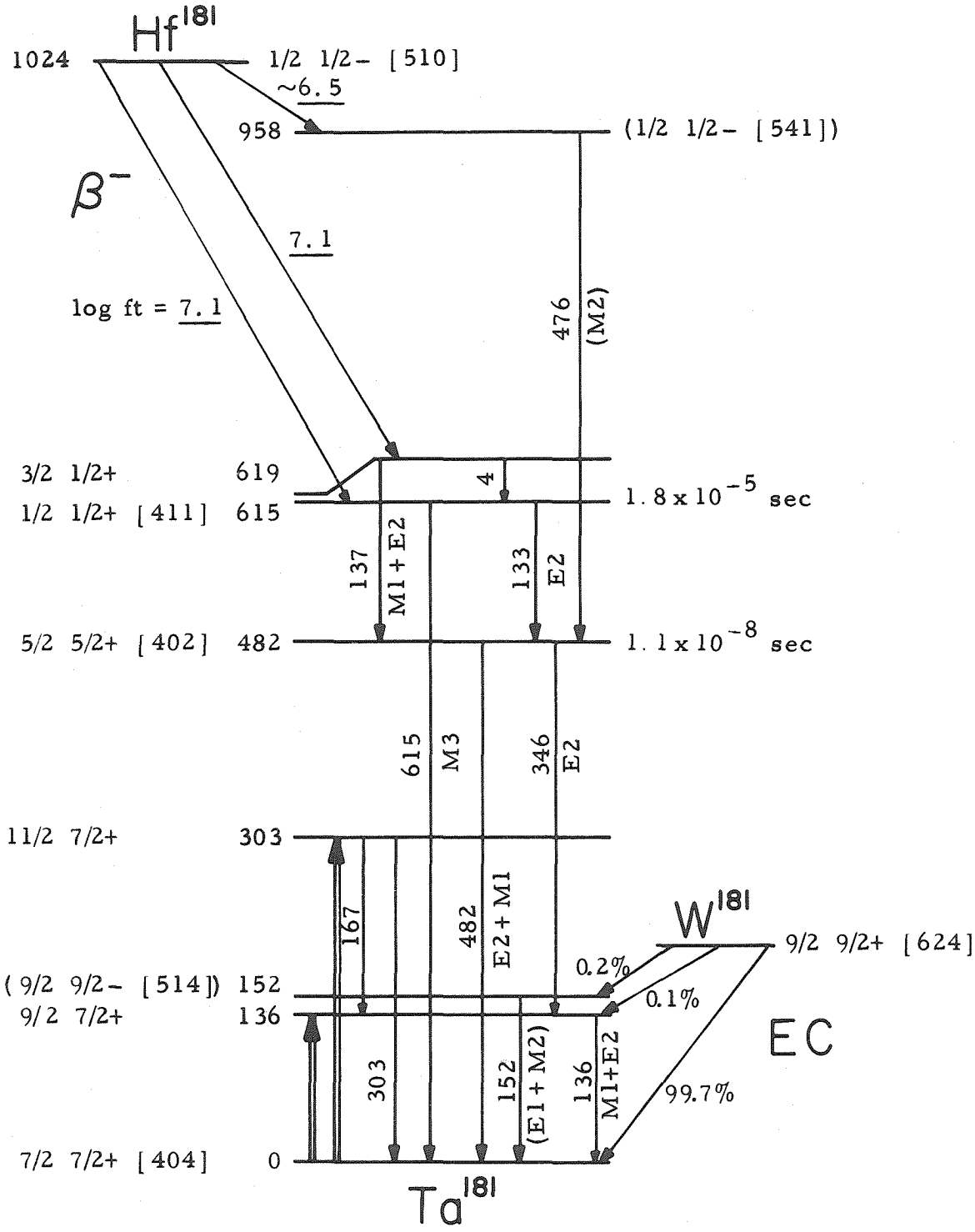

Fig. 1.1. Levels in Ta^{181} appearing in Hf^{181} β-decay, W^{181} electron capture decay, and Coulomb excitation. Level assignments are according to Mottelson and Nilsson, reference 4. Energies are given in kev.

the 476 kev transition from being in cascade with the 482 kev transition.

In addition, there were contradictions and ambiguities in the W^{181} decay. Cork et al. (6) found 136 and 152 kev transitions in this decay. Bisi et al. (7) subsequently reported seeing no evidence for these transitions, and from L/K x-ray intensity ratio measurements estimated the W^{181} electron capture decay energy to be 92 ± 10 kev. On the other hand, Debrunner et al. (10) found both the 136 and 152 kev transitions and established that they were not in cascade. From x-ray – γ-ray coincidence measurements these authors concluded that the W^{181} decay energy must lie between 160 and 200 kev. Debrunner and co-workers' choice of E1 + M2 for the 152 kev transition multipolarity was based on K-shell internal conversion coefficient measurements and on nuclear model considerations. This assignment should not be considered as unique, for the conversion data would also allow this transition to be classified as M1. Consequently the choice of spin 9/2 and negative parity for the level Debrunner et al. propose at 152 kev is subject to question. This assignment is given in parentheses in Fig. 1.1.

The present work was undertaken to clarify some of these problems and to attempt an improvement in the understanding of the nuclear excitation of Ta^{181}. Part II describes the various instruments used in these studies. The critical 476, 482 kev coincidence experiment has been repeated and is described in Part III A. A negative result was found, in agreement with Debrunner et al. (8).

With a 476, 482 kev cascade ruled out, a search was made for low energy transitions in the Hf^{181} decay. A new low energy transition might help locate the 476 kev transition. Some evidence for the conversion electrons from a ~6 kev transition was found in the β-ray

spectrometer results reported in Part III B. The W^{181} decay was also investigated and strong conversion lines of a 6.25 kev transition were found. These results, the coincidence experiment, and decay energy and branching considerations lead to the conclusion that Ta^{181} has a level at 6 kev.

The proportional counter measurements of Part III C allow the 6 kev transition conversion coefficient and multipolarity to be determined. A careful measurement of the W^{181} decay L/K x-ray intensity ratio discussed in Part III D enables the electron capture decay energy to be calculated. The result is in agreement with the predictions of Debrunner et al. (10). Finally, with the aid of the β-ray spectrometer and scintillation spectrometer measurements of Part III G, the W^{181} decay branchings to the various Ta^{181} levels are determined. Log ft values of these transitions are given as well.

In Part IV the experimental results are summarized and interpreted in terms of the nuclear models (1), (2). A new Ta^{181} level scheme is presented, in which the 152 kev transition occurs between a level at 158 kev and the 6 kev level. The 476 kev transition takes place between the 482 and 6 kev levels. The spin and parity assignments for all levels appear to be in excellent agreement with nuclear model considerations (1), (2). The significant results of this work are presented in brief in the decay scheme of Fig. 4.3, p.82 (compare with Fig. 1.1).

PART II

EXPERIMENTAL APPARATUS AND TECHNIQUES

The various experimental apparatuses used in the measurements, and also the methods of source production and preparation, will now be described briefly.

A. Coincidence Apparatus

In order to check for possible coincidences between the 476 and 482 kev γ-rays in the Hf^{181} decay, a standard fast-slow triple coincidence circuit was employed. Fig. 2.1 is a schematic representation of the detectors and associated coincidence instrumentation. The fast coincidences were analyzed by a Garwin (11), (12) fast coincidence circuit. A Detectolab model DZ4 fast-slow coincidence circuit was used to analyze the triple coincidences. By means of this arrangement, an improved fast resolving time was obtained over that which could have been obtained by use of the commercial triple coincidence analyzer alone.

The detectors were standard sodium iodide scintillation crystals mounted directly on the faces of photomultiplier tubes. The photomultiplier assemblies, which had 0.002" aluminum foil windows in front of the crystals, were mounted horizontally at an angle of 180^{o} with respect to each other. For most of the measurements the crystals were about one-half inch apart and the source was located midway in between.

The signal for each slow preamplifier came from the tenth dynode of the photomultiplier tube, while that for each fast preamplifier was

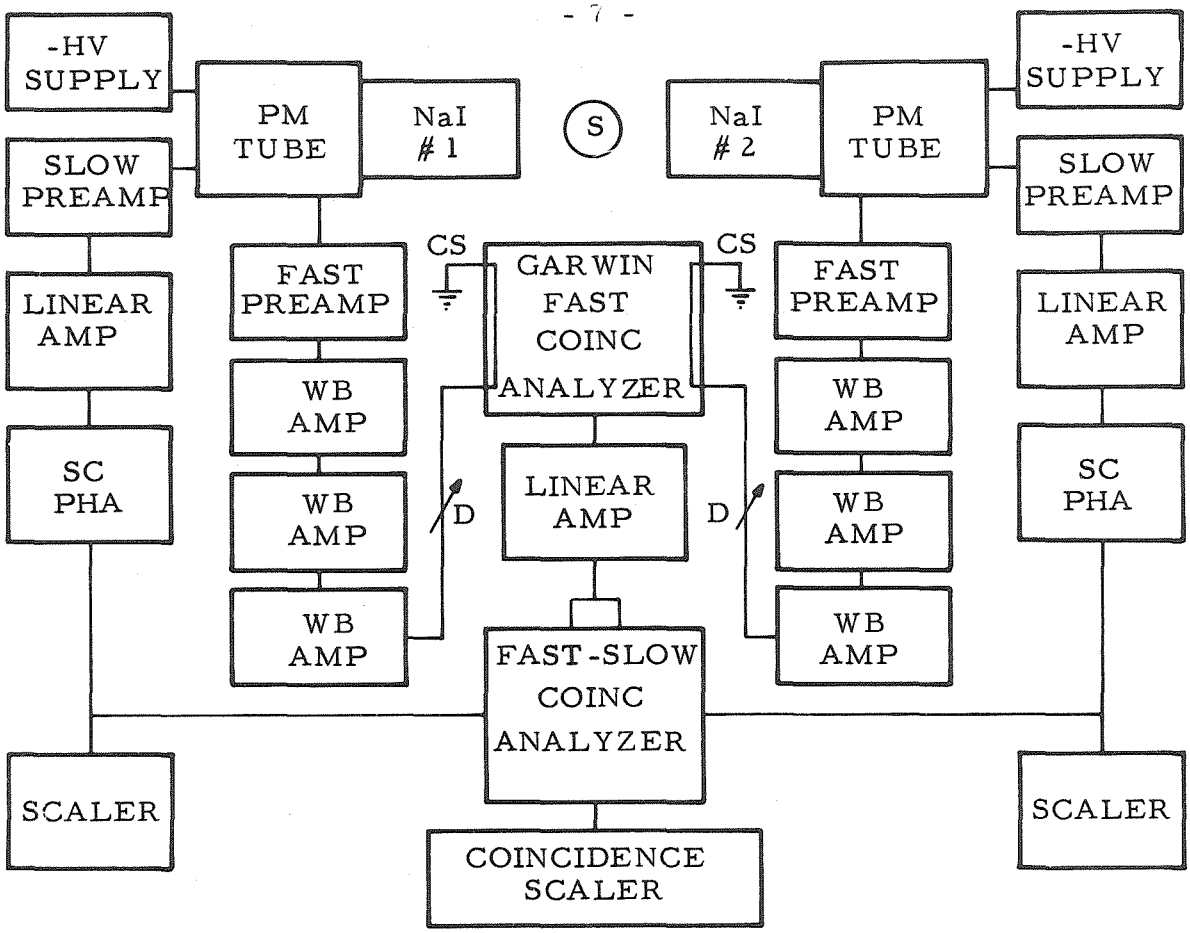

Fig. 2.1. Fast-slow coincidence circuit block diagram.

NOTES:

-HV SUPPLY is Baird Atomic model 312 super stable regulated high voltage supply.
PM TUBE is DuMont type 6292 photomultiplier tube.
NaI is Harshaw Chemical Co. Tl-activated scintillation crystal: #1 – 1 1/2" x 1"; #2 – 1 1/2" x 1 1/2".
S is radioactive source.
SLOW PREAMP is Baird Atomic model 219 preamplifier.
LINEAR AMP is Baird Atomic model 218 linear amplifier.
SC PHA is Detectolab model DZ15 single channel pulse height analyzer.
SCALER is Baird Atomic model 1030 scaler.
COINCIDENCE SCALER is Baird Atomic model 131A cold cathode glow tube scaler.
FAST-SLOW COINC ANALYZER is Detectolab model DZ4 fast-slow coincidence circuit.
WB AMP is Hewlett-Packard model 460A wide band amplifier.
FAST PREAMP is a modified Garwin fast coincidence preamplifier (11).
GARWIN FAST COINC ANALYZER is a modified Garwin fast coincidence analyzer (12).
D is variable length delay line, 185 ohm nominal impedance.
CS is fast clipping stub, 93 ohm nominal impedance.

taken from the anode. Pulse shaping for the fast signals was accomplished by appropriate adjustment of the gains of the wide band amplifiers and of the bias on the G7A diode clipper installed on the output of each middle wide band amplifier. Further fast pulse shaping was provided by shorted delay line clipping stubs in parallel with each Garwin circuit input channel. The clipping stubs were coaxial cable of 93 ohms nominal impedance.* In determining the coincidence circuit fast resolving time, variable length delay cable was used between the fast amplifier outputs and the Garwin circuit inputs. This line was ultra-low capacitance coaxial cable of 185 ohms nominal impedance.†

Annihilation radiation from the Na^{22} decay was used to adjust the pulse shaping parameters and to measure the fast resolving time of the Garwin analyzer. The annihilation radiation is particularly suitable because of its closeness in energy to 480 kev. With about 1100 volts on the photomultiplier tubes, and with 4 ft long clipping stubs in the fast coincidence analyzer, the pulses on the input grids of the analyzer were a little over 1 volt negative and had a rise time of about 0.01 μ sec. Upon proper adjustment of the operating conditions, a fast resolving time of $2\tau_f = 4.4 \times 10^{-8}$ sec was achieved. The resolving time was determined from the prompt coincidence resolution curve obtained by counting coincidences with different lengths of delay cable feeding the fast inputs.

The slow resolving time of the fast-slow coincidence analyzer was

---

* The 93 Ω cable was RG 62/U, which has a delay of 1.2 mμ sec/ft.

† The 185 Ω cable was either Hewlett Packard cable no. 812-52 or RG 114/U, or combinations of the two, both of which have delays of 1.1 mμ sec/ft.

determined in two ways. First, with the fast input switched out of the circuit, the two slow inputs were fed with pulses from a variable delay double pulse generator. The known delay was varied until coincidences were no longer recorded and this gave the resolving time. The slow resolving time was also measured by comparing the observed fast triple coincidence rate, N_f, with the observed slow coincidence rate, N_s, for the annihilation radiation. It can be readily shown that the slow resolving time is given by

$$2\tau_s = \frac{N_s - N_f}{N_1 N_2} + 2\tau_f \quad ,$$

where N_1 and N_2 are the two singles counting rates. Both methods gave essentially the same result, namely $\tau_s = 2\ \mu$ sec, which is in agreement with the manufacturer's specifications.

In looking for coincidences between the 476 and 482 kev γ-rays, each of the single channel pulse height analyzers was carefully energy calibrated and then set to correspond to a photopeak at about 480 kev. The channel widths were 4 volts, corresponding to a $\frac{\Delta E}{E}$ of about 9%. With these settings, there was little chance of counting accidental coincidences from the 133 and 137 kev transitions which also feed the 482 kev level.

Coincidence Experiment Source

The Hf^{181} activity for the coincidence experiment was produced by irradiating 2 mg of HfO_2 enriched in Hf^{180} in a flux of 2×10^{14} neutrons/cm^2-sec for 2 days. (See Part II B for details of the source production.) The source mount was prepared by cutting a 1/16" thick ring from Plexiglas tubing, 2" o.d., with 1/8" wall thickness. Mylar film, 0.001"

thick, was cemented* to one side of the Plexiglas ring, and drops of an aqueous suspension of the HfO_2 activity were placed at the center of the Mylar circle. After allowing the source to dry, another Mylar film was cemented to the other side of the Plexiglas ring to cover the source. At a point on its circumference, the ring was cemented to the end of a short 1/4" square aluminum support rod. A holding block for the support rod was located midway between the counters and arranged so that the source ring was held coaxial with the counters.

The absolute strength of the source was measured by counting it with a NaI scintillation crystal spectrometer in known geometry. The single channel pulse height analyzer of the spectrometer was set on "integral" and adjusted to accept all pulses above the L x-ray pulses in energy. Using the measured γ-ray relative intensities and internal conversion coefficients of Boehm and Marmier (9), supplemented with the theoretical conversion coefficients of Rose (13), it was possible to determine the absolute strength of the 476, 482 kev γ-radiation. The result is $N_{480} = 1.4 \times 10^6$ counts/min. As an independent check on N_{480}, the coincidence apparatus was set to count the 133.0, 136.9 kev -- 482 kev cascade coincidences. From these measurements the source strength could be deduced. Agreement with the previously mentioned value was obtained.

The results of these coincidence measurements will be presented in Part III A.

---

* Minnesota Mining and Manufacturing Co. adhesive EC 826 was found suitable for bonding Mylar to Plexiglas.

B. 180° Magnetic Beta-Ray Spectrometer

A 180° magnetic beta-ray spectrometer was used to study the low energy electron spectra from the decays of Hf^{181} and W^{181}. This spectrometer has its magnetic field provided by circular, iron-free Helmholtz coils. The electron trajectory is a semi-circular path of 12 cm radius. The construction and operation of this spectrometer and the associated electro-mechanical current stabilizer (regulation to 2 parts in 10,000) have been previously discussed (14) in some detail. Consequently only those features having special bearing on the present experiments will be reviewed here.

The range of the spectrometer is from about 2 to 120 kev electron energy. At these low energies the use of coils to compensate for the earth's magnetic field is especially important. The electron detector is a Geiger counter with a slit-shaped window. For very low energy work the window is covered with one or two layers of thin ($\sim$10 $\mu g/cm^2$) Formvar foil. These foils are prepared by dipping a clean glass plate into a solution of Formvar (4% by weight) in ethylene dichloride and allowing a film to dry on the plate. After freeing the edges, the foil is floated off as the plate is immersed in water.

For typical operation the counter is filled with a mixture of about 15 mm Hg of alcohol vapor and 28 mm Hg of argon. A two layer window will usually hold this pressure quite nicely, but for very low energy work where one layer windows are preferable, it is usually necessary to try several windows before finding one that does not have appreciable leakage.

At very low energies the transmission of the counter window be-

comes of some concern. Although it is quite difficult to make exact measurements of the transmission of such extremely thin foils at very low energies, the assumption of nearly 100% transmission can be justified by several arguments. As a reasonable approximation, the Formvar foil can be considered to be pure carbon. The electron range data of Nelms (15) for carbon, extrapolated to low energies, indicates that the range of a 3 kev electron is approximately 30 $\mu g/cm^2$. Furthermore, the appearances of very low energy conversion lines, for example those of the 3.9 kev transition in the Hf^{181} decay found by Boehm and Marmier (9), give no indication of poor transmission. Although a transmission of unity is assumed in making relative intensity comparisons, it must be recognized that this represents a first approximation. In particular, when comparing the intensity of a lower energy line to that of a higher energy line, the neglect of any energy dependence of the transmission means that the observed intensity ratio, I(lower energy)/I(higher energy), is really a lower limit on the true intensity ratio. Results of Wapstra (16) indicate that counter windows which have not been aluminized may become charged and thus have a higher transmission threshold than otherwise might be expected. This effect would attach more significance to the previously mentioned lower limit considerations.

For the experiments reported here, the slits and windows of the spectrometer were selected so as to give a momentum resolution $\Delta p/p = 0.8\%$. Relative intensities of the conversion lines were usually obtained by dividing the area of the line on a plot of counting rate vs. field current by the current value corresponding to the peak of the line.

In a few instances, where complex neighboring lines of greatly differing strengths made this procedure difficult, the relative peak heights of the lines were simply taken as the relative intensities.

Beta-Ray Spectrometer Sources

The principal radioactive sources employed in the beta spectrometer investigations were the isotopes W^{181} and Hf^{181}. Enriched isotopes of W^{180} and Hf^{180} were obtained from the Oak Ridge National Laboratory.

The W^{180}, in the form of WO_3, was irradiated for about 30 days in a flux of approximately 3×10^{14} neutrons/cm^2-sec in the Materials Testing Reactor (MTR) of the Phillips Petroleum Co., Idaho Falls, Idaho. After allowing the sample to cool several weeks so that the short-lived tungsten isotope impurities had decayed, sources were prepared by vacuum evaporation of the activity onto thin sheets of aluminized mica. A boat or trough to hold and heat the activity was formed out of a 3/8" wide strip of 0.005" (ordinary) tungsten sheet. In order to shape the boat, this sheet had to be brought to red heat and carefully bent while hot. During the evaporation the boat was raised to white heat. The WO_3 [melting point 1473°C(17)] evaporated from the tungsten boat [melting point 3370°C(17)] and coated the mica sheet, which was held a few inches above the boat. Narrow line sources (1 to 2 mm wide, 3 cm long) were cut from the mica sheet and cemented to thin aluminum source mounts. The evaporated layer of activity was just barely visible, consequently the sources were sufficiently thin so as to have negligible self-absorption.

Hf^{181} sources were prepared in a manner similar to the preparation of the W^{181} sources. Hf^{180}, in the form of HfO_2, was irradiated in the MTR for about 10 days at a flux of about 2×10^{14} neutrons/cm^2-sec. Sources were prepared by vacuum evaporation onto aluminized mica sheets. Since the HfO_2 melting point is 2812°C (17), extra precautions were necessary. Bringing the sample to near white heat too rapidly caused it to "dance" out of the boat. Because of the closeness of the melting points of the activity and the boat, slow heating tended to minimize the evaporation of the tungsten boat onto the mica.

C. Ring Focusing Magnetic Beta-Ray Spectrometer

Estimates of the relative internal conversion intensities of the two high energy transitions in the W^{181} decay were obtained from measurements made with the ring focusing beta-ray spectrometer. This iron-free, homogeneous field spectrometer covers an energy spectrum from approximately 30 kev to several Mev electron energy. This instrument has been described elsewhere (18) in detail.

Beta-Ray Spectrometer Sources

The sources used for the ring focusing beta-ray spectrometer measurements were small discs punched from the same coated mica sheets described in Part II B. The mica discs, about 2 mm in diameter, were cemented to small aluminum source mounts.

D. Proportional Counters

For the study of the very low energy electromagnetic spectrum of the W^{181} and Hf^{181} decays, two gas-filled proportional counters were built. These counters are about a foot long and 10 cm in diameter and have side windows of 3 mg/cm^2 mica. One counter is filled with a mixture of 90% argon and 10% methane at a pressure of one atmosphere, and the other with a mixture of 90% xenon and 10% methane at a pressure of about one-third of an atmosphere.

Details of the design, construction, and operation of these counters are given in Appendix I. Information on the resolution, efficiency, and escape peak phenomena which has bearing on the analysis of the experimental data is also given in Appendix I.

Proportional Counter Sources

The W^{181} source used for the proportional counter investigations was accelerator produced* by the reaction $Ta^{181}(p, n)W^{181}$. About 1 mg of the carrier-free activity was mixed with a small amount of aqua regia which was then deposited on a small piece of Plexiglas sheet and dried under a heat lamp. A dot of insulin solution about 1/4" in diameter had previously been placed on the Plexiglas sheet and allowed partially to dry. By this means, a fairly uniform thin source, about 1/4" in diameter, was produced. The source was finally covered with a 0.0004" Mylar film.

Hf^{181} sources for use with the proportional counters were cut from

* Procured from Nuclear Science and Engineering Corp., P.O. Box 10901, Pittsburgh, Pa.

the active coated mica described in Part II B. The mica was cemented to small pieces of Plexiglas sheet and the sources finally covered with 0.0004" Mylar.

Other sources used with the proportional counters for calibration and the study of resolution and escape peak effects were produced and prepared by standard methods similar to those previously discussed.

E. Scintillation Spectrometer

A sodium iodide scintillation crystal spectrometer was used for measuring the relative intensities of various electromagnetic radiations emitted following the decay of W^{181}. The subject of scintillation spectrometry is well known and has recently been extensively reviewed by Mott and Sutton (19). Only the special techniques employed in the present work will be considered here.

Arrangement for Tantalum L/K X-Ray Intensity Ratio Determination

In order to determine the L/K capture ratio in W^{181}, it was necessary to measure the L/K x-ray intensity ratio with relatively high accuracy (at least to within 5%). This measurement was difficult because of the low energy of the L x-rays, about 9 kev, and because of the presence of scattering of both K and L x-rays.

Fig. 2.2 is a schematic view of the detector arrangement employed. A standard high voltage supply, pre-amplifier, and linear amplifier along with a Penco model PA4 100 channel pulse height analyzer, comprise the electronics not shown in the figure. The thin square (2.3 cm x 2.3 cm x 0.55 cm) thallium activated sodium iodide scintillation crystal was not sealed in the usual aluminum "can". This crystal was prepared by polishing all surfaces first on fine emery paper and then on wiping tissue. Methyl alcohol, which dissolves NaI, was the polishing agent. Between polishings the crystal was rinsed in mineral oil, which was also used to cover the crystal when not in use. The crystal was mounted directly on the face of a DuMont 6292 photomultiplier tube. A light coating of mineral oil which remained on the crystal served as an

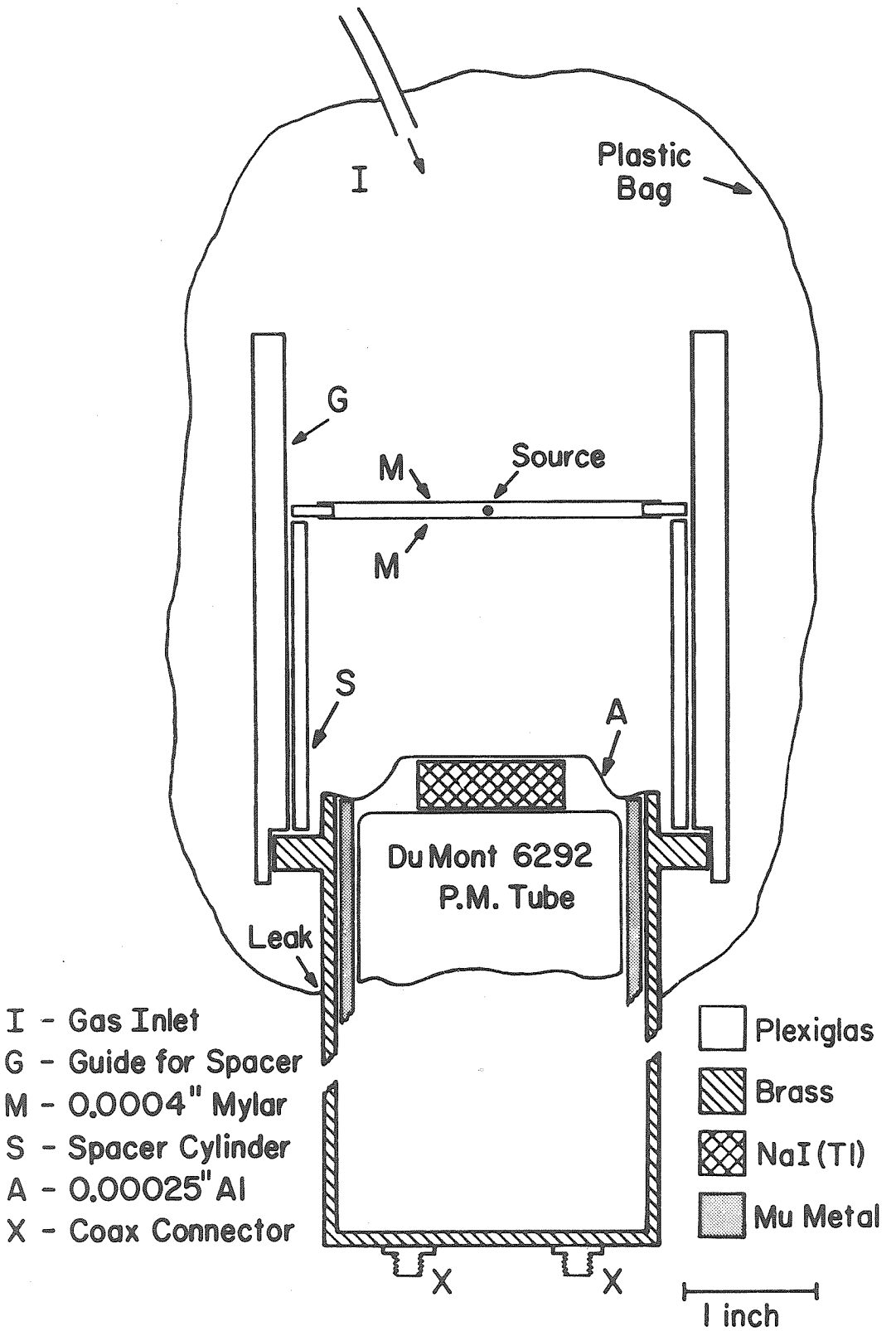

Fig. 2.2. Scintillation counter arrangement for measuring the L/K x-ray intensity ratio from the W^{181} decay.

optical coupling between the crystal and the tube, and also retarded the absorption of moisture by the other surfaces of the crystal.

A 0.00025" aluminum foil covered the face of the crystal and made the photomultiplier assembly light-tight. No reflecting powders were used. Instead, the foil was pressed tightly against the crystal face. In this manner the thickness of the oil layer covering the crystal face was minimized. Fresh polishing of the crystal face before each run was necessary to prevent surface losses (20) of the low energy L x-rays. If the surface were cloudy because of moisture absorption, such surface losses could lower the L/K x-ray ratio by a large factor. Very thin crystal coverings were used to minimize the window absorption correction.

Scintillation Spectrometer Source

The W^{181} source described in Part II D was deposited on 1/4" thick Plexiglas. As shown in Appendix II, the appreciable backscatter of K x-rays from this source could be virtually eliminated by removing the activity from the Plexiglas and redepositing it on a 0.0004" Mylar backing. This new source, which was also covered with 0.0004" Mylar, was used for all the NaI scintillation spectrometer runs. It is indicated in Fig. 2.2.

Scattering Considerations: Counter Geometry

As will be seen in Part III E, a very small percentage change in the L/K x-ray ratio results in a very large percentage change in the L/K capture ratio and capture decay energy calculated from it. Scattering of x-rays from the source mount, the walls of the counter

enclosure*, and the air between the source and the crystal can substantially affect the observed x-ray intensity ratio. In order to investigate the geometry dependent effect of scattering on the L/K x-ray ratio, Plexiglas spacer cylinders, designated S in Fig. 2.2, of various lengths were used to locate the source at different separations from the detector.

Curves of the apparent x-ray ratio as a function of the source-to-crystal separation given in Appendix II show that the L/K ratio increases as the separation decreases. This is interpreted in terms of the increase of L x-ray scattering at close geometry. To further investigate scattering effects, some scintillation spectrometer runs were taken with the counter (source, crystal, and related parts) enclosed in a plastic bag filled with helium. The helium, which was slightly above atmospheric pressure, flowed through the counter surroundings and out tiny leaks where the bag was taped to the counter body. The spacer guide, G, did not make contact with the entire circumference of the counter body; it fitted tightly only on the two protruding tabs shown in the cross section of Fig. 2.2. It was thus easy for the helium to be flushed into the region between the source and crystal.

Results of these measurements are summarized in Part III D.

Arrangement for 136 and 152 Kev Gamma-Ray Intensity Measurements

The scintillation crystal spectrometer was also used to measure

---

* To reduce the background, the counter assembly shown in Fig. 2.2 was housed in a brass cylinder, 3/8" in wall thickness, whose exterior was covered with a 1/16" sheet of tin. Similar brass and tin covering was placed on top of the cylinder. Finally, the whole counter arrangement was located in a lead cave with 2" thick walls.

the relative intensities of the 136 and 152 kev γ-rays, and their combined intensity relative to the Ta K x-rays. For these measurements the thin square NaI crystal of Fig. 2.2 was replaced by a standard commercial 1" diameter x 1" long cylindrical NaI(Tl) scintillation crystal*. The helium bag was not used, since for these measurements scattering effects were not so important and the accuracy requirements not as great.

Because of the strong K x-ray intensity relative to the γ-rays (10), (†), absorbers were employed to reduce the K x-ray counting rate by about a factor of 10 relative to the γ-ray rate. This procedure made negligible the possible pile-up of x-ray pulses to give apparent pulses in the region of the γ-rays.

A spacer cylinder, similar to S in Fig. 2.2, separated the absorber from the crystal, and a second spacer cylinder separated the source from the absorber. By using different length spacer cylinders, various source-absorber and absorber-crystal separations could be obtained.

The experimental results are described in Part III G.

---

* Harshaw Chemical Co. crystal model 4D4.

† See also the result of Eq. (20), p. 67.

PART III

RESULTS

The results of the various measurements will now be presented and discussed in terms of the establishment of a new level at 6.25 kev in Ta^{181}. The W^{181} decay energy and branchings will also be determined.

A. Coincidence Experiment: 476, 482 Kev Transitions in Hf^{181} Decay

Although Debrunner et al. (8) reported finding no coincidences between the 476 and 482 kev transitions in the Hf^{181} decay, this coincidence experiment has been repeated because the result is very crucial to the arguments that follow. The closeness in energy of the 476 and 482 kev transitions means that special precautions are in order. Since no details of the previous experiment were published (8), an additional check on the result is worthwhile from these considerations as well.

Because the energy separation of the γ-rays was too small to be resolved by the NaI(Tl) scintillation crystals of the coincidence apparatus*, the experiment was accomplished in the following manner. The two single channel pulse height analyzers were set for an energy of about 480 kev with a 9% channel width. Coincidences were counted and compared with what was to be expected on the basis of the reported (9) relative intensity of the 476 kev transition, making allowance for random coincidences.

The lifetime of the 482 kev level has been measured (5) to be about

---

* See Part II A for details of the coincidence apparatus.

1×10^{-8} sec. Thus the fast coincidence resolving time of $2\tau_f = 4.4 \times 10^{-8}$ sec was sufficient to reduce random coincidences as much as practical, but was not too fast for the intermediate state lifetime. As a check on the experiment, and to allow for any possible error in the lifetime or resolving time, coincidences were also measured with only the slow resolving time of $2\tau_s = 4\mu$ sec (i.e. with the fast input to the triple coincidence analyzer switched off). Naturally, the expected random coincidence rate was higher in this case.

The random rate has been calculated on the basis of the two singles rates and the resolving time. The expected coincidence rate from the 476 kev intensity has been calculated using the source strength of Part II A, and the detector efficiencies determined from experimental data. The results of the experiment and calculations are listed in Table I. From these data it can be seen that the 476 and 482 kev transitions in the Hf^{181} decay are not in coincidence.

Table I

476 - 482 Kev Cascade Coincidence Experiment Results

Resolving Time	Total Run Time min	Observed Coincidences* N_c^{ob}	Calculated Random Coincidences* N_r	True Coincidences* $N_c^{tr} = N_c^{ob} - N_r$	Expected Coincidences* N_c^{exp}
$2\tau_f$	300	0.077 ± .016	0.101 ± .006	< 0.01	4.11
$2\tau_s$	5	9.80 ± .14	9.04	0.76	4.06
$2\tau_s$	125.5	9.66 ± .31	9.16	0.50	4.11

* Coincidences are given in counts per minute.

This result rules out the proposed (9) 958 kev level in Ta^{181} (see Fig. 1.1). However, in order to explain the 476 kev transition, a previously unreported Ta^{181} level must exist somewhere. A search for a weak low energy transition might provide the clue. In particular, one good possibility would be a 6 kev transition, implying a new level at 476 or 6 kev. A weak 6 kev transition might easily have escaped detection in previous investigations. In addition, a level at 6 kev might be especially difficult to detect if spin and parity considerations allow this level to be populated by only the weak 476 kev transition.

B. Low Energy Electron Spectra in Ta^{181}

Measurements with the 180° β-ray spectrometer were performed on Hf^{181} sources to determine whether or not transitions could be found that would help fit the 476 kev transition into the Ta^{181} level scheme. The low energy region, especially near 6 kev, was carefully investigated with a very thin window on the Geiger counter.

Although the background due to the beta continuum and Auger electron groups is quite large, there seems to be positive evidence for a transition of about 6 kev in this decay. A tracing of a typical chart recorder curve for Hf^{181} is shown in Fig. 3.1(c). The energy regions below 5 kev and above 9 kev in this figure actually represent "pictorial averages" of the data from a large number of different spectrometer runs. This averaging, which is rather qualitative*, is necessary because of the poor signal-to-noise ratio. To a certain extent, the averaged parts of Fig. 3.1(c) represent an upper limit for spectral lines. The region in the figure marked "6 Kev Conversion Group" is where the M-shell conversion lines of such a transition would be expected. The location where a 6 kev $N_{I, II, III}$ line would be expected is indicated as well. Conversion electrons corresponding to the previously reported (9) 3.9 kev transition in the Hf^{181} decay also appear in Fig. 3.1(c).

---

* The averaging was accomplished by first finding the average Hρ position (current value at the midpoint) for each peak or suggestion of a peak, using all available data. To estimate the relative intensities, smoothed tracings of several of the best chart recorder curves were compared by overlaying the curves on a light box. A tracing of the overlay composite, with the peaks located at the previously determined average positions, was then used in the preparation of the final curve of Fig. 3.1(c). The wiggles in the averaged regions of this curve are intended to indicate fluctuations appropriate to the combined results of about four or five individual runs.

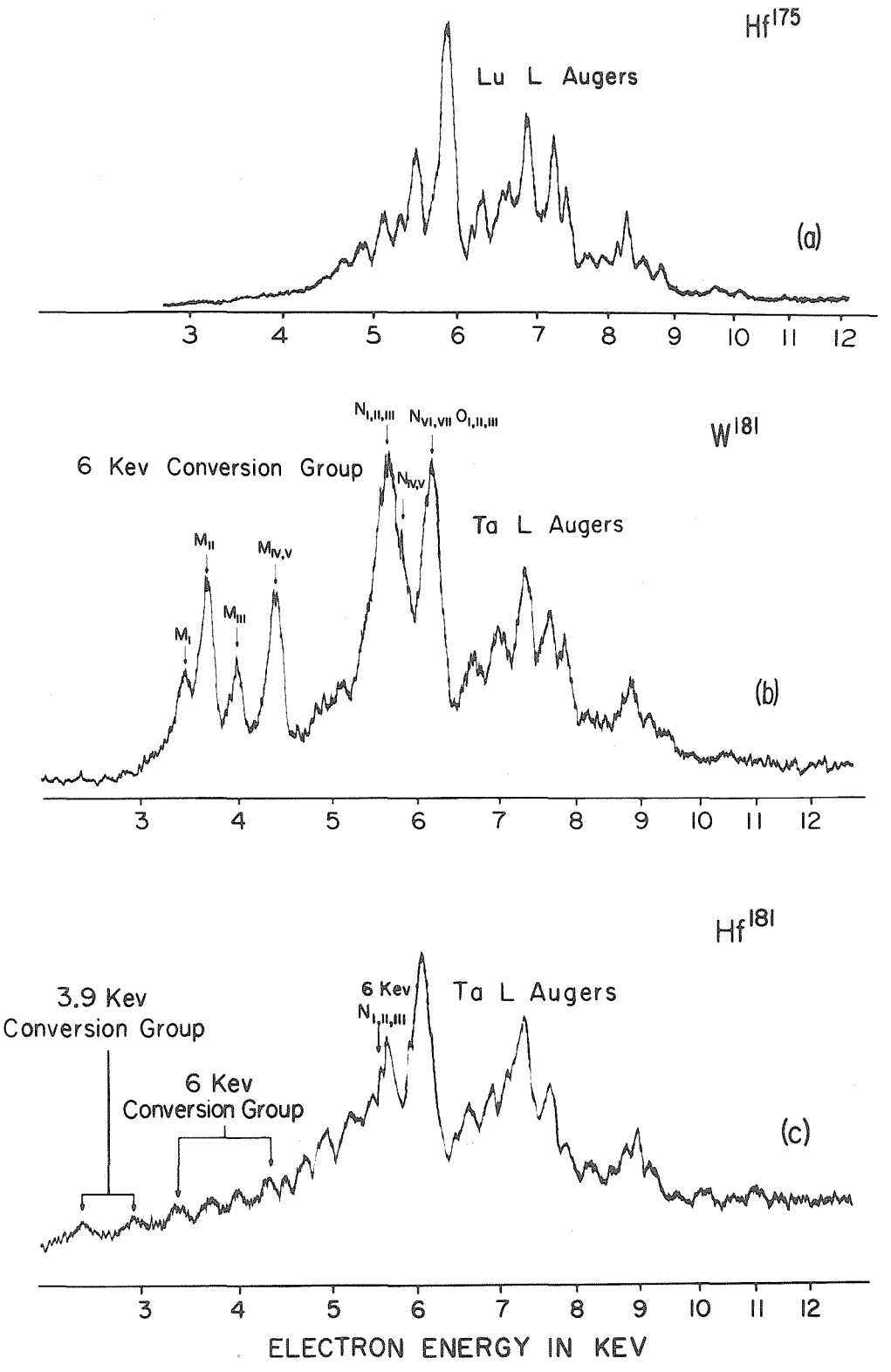

Fig. 3.1. 180^{o} β-ray spectrometer curves from the decays of (a) Hf^{175}, (b) W^{181}, and (c) Hf^{181}. The prominent peaks between about 6 kev and 9 kev are L Auger electron groups. Low energy conversion electron groups are present in (b) and (c). Curve (b) in particular exhibits pronounced M-shell conversion lines of a 6.25 kev transition.

Fig. 3.1(a) is the low energy electron spectrum of Lu^{175} excited by the electron capture decay of Hf^{175}. The prominent lines are the lutecium L Auger electron transitions. Lu^{175} is known (21) not to have any low energy conversion electrons. By comparing Figs. 3.1(a) and (c) it can be seen that the "bumps" at about 4 kev in the Hf^{181} curve can not be interpreted as low energy Auger electrons, and therefore must be conversion lines. Further discussion of these curves will be given shortly.

As has been previously mentioned, a 6 kev transition in Ta^{181} suggests a level at 6 kev. If this is the case, then such a level might well be excited in the W^{181} decay. To check this possibility, the 180° β-ray spectrometer was also used to study W^{181} sources. Fig. 3.1(b) shows the electron spectrum from this decay. The Auger electrons from Hf^{175}, W^{181}, and Hf^{181} show marked similarities as would be expected, since Lu^{175} and Ta^{181} are close neighbors in Z and A. The outstanding feature of Fig. 3.1(b) is the presence of four strong electron lines near 4 kev. There are no lines in Fig. 3.1(a) to correspond to this prominent group in (b), and therefore these lines must be conversion electron lines*.

The presence of four lines close to each other suggests an M-shell conversion group†. The energies of these lines were obtained by averaging the energy values from a number of spectrometer runs. The peaks occur at 3.5, 3.8, 4.1 and 4.4 kev. These energies, when

---

* These low energy conversion lines in the W^{181} decay were found by Dr. Felix Boehm of this laboratory, to whom the author is indebted for the curves shown in Figs. 3.1(a) and (b).

† The M_{IV} and M_{V} lines would not be resolved with this instrument.

combined with the M-shell binding energies of Hill, Church, and Mihelich (22), yield four values for the transition energy that agree with each other within probable error. A weighted average of these energies gives the result:

$$E_{transition} = 6.25 \pm 0.3 \text{ kev} \quad .$$

The stated error takes into account the statistical error in the measurement and the precision of the calibration of the instrument, which at this energy is the dominant factor.

In Fig. 3.1(b) the 6 kev M conversion lines are marked with arrows. In addition, arrows indicate where $N_{I, II, III}$, $N_{IV, V}$, and $N_{VI, VII}O_{I, II, III}$ conversion groups are to be expected. By comparison with the Lu L Augers, it is possible to estimate the N- and O-shell contribution to the total conversion intensity. Combining the results from several runs, the final value for the relative internal conversion intensity in the W^{181} decay is

$$\frac{I_{6\ MNO}}{I_{L\ Augers}} \geq 0.51 \pm 0.05 \quad . \qquad (1)$$

This result is given as a lower limit because of possible counter window attenuation of the lower energy conversion lines relative to the Augers. The window effect, as indicated in Part II B, is probably insignificant.

If the Hf^{181} decay spectrum of Fig. 3.1(c) is now compared to Fig. 3.1(b), it can be seen that the four "bumps" near 4 kev in (c) have a one-to-one correspondence to the M conversion lines of (b). The relative intensities in (c) are not the same as in (b), but this is not surprising because there is some overlap of the 6 kev group in (c) with

the N and O lines of the 3.9 kev conversion group. [However, it is not possible to argue that all of the spectrum labeled "6 Kev Conversion Group" in (c) is due to the 3.9 kev transition. Certainly the bump at about 4.3 kev can not belong to a 3.9 kev conversion group.] Moreover, the previously mentioned "pictorial averaging" process and the poor signal-to-noise ratio of (c) may help account for the discrepant intensity ratios. It is possible, nevertheless, to make a rough estimate of the relative intensity for the 6 kev M-shell internal conversion in the Hf^{181} decay. The result is

$$\frac{I_{6\ M}}{I_{L\ Augers}} \leq 0.07 \quad . \tag{2}$$

The result is given as an upper limit because of possible contribution from the 3.9 kev transition, and because of possible bias in making the "pictorial average".

It is of interest to check if the 6 kev intensity of Eq. (2) is in accord with the hypothesis that the 6 kev transition is fed by (or feeds) only the 476 kev transition. Boehm and Marmier's (9) value for the 476 kev total transition intensity of 0.82% has been used to estimate* the expected 6 kev conversion intensity relative to the L Auger intensity under this cascade assumption. Taking into account the approximations made in the calculations, the result is in agreement with Eq. (2). Therefore the cascade assumption is quite plausible.

Although the 6 kev transition in the W^{181} decay would seem to be

---

* Multipolarities, intensities, experimental conversion coefficients, and a simplified version of the decay scheme were taken from reference 9. Theoretical conversion coefficients were obtained from reference 13. Average transition probabilities for x-ray and Auger processes, along with average x-ray fluorescence yields were taken from reference 23. The 6 kev transition M-shell conversion coefficient was estimated from the experimental total conversion coefficient given in Part III F combined with results from Appendix III, Part C.

the same transition weakly excited in the Hf^{181} decay, it may be argued that the former transition is the result of heavier tungsten isotope impurities in the source. The W^{181} source also contained some other long-lived tungsten isotopes, despite the fact that the source material had been enriched in W^{180} by a factor of about 40 over the natural abundance. Of particular concern was the possibility of double neutron capture by W^{186} * (11% abundance in the enriched W^{180} sample). The resulting W^{188} activity with its 70 day half-life might have been responsible for the 6 kev transition. To check this possibility, the W^{181} data were compared with the data from a source prepared by neutron bombardment of (97%) enriched W^{186}. The measurement of the relative intensity of the prominent 155 kev Os line (from the $W^{188} \rightarrow Re^{188} \rightarrow Os^{188}$ decay chain) in both tungsten sources showed that W^{188} contamination of the W^{181} source was negligible. Any W^{188} activity present would have been at least a factor of 100 weaker than the W^{181} activity. Thus the L Auger electrons from the W^{181} source were principally the result of the 145 day W^{181} activity. The intensity of the 6 kev conversion lines was checked periodically over a 5 month interval and was found to decay at the same rate as the Ta L Auger lines. Therefore it was concluded that the 6 kev activity belonged to the W^{181} decay. As will be seen later, this conclusion was confirmed by proportional counter detection of 6 kev γ-rays in the decay of W^{181} accelerator-produced from Ta^{181} (99.99% natural abundance). In this case, there were no other long-lived tungsten isotopes present.

---

* Double capture might easily occur because W^{186} has a large capture cross section of about 30 barns, and the product W^{187} has an even larger cross section of about 90 barns.

M-Subshell Conversion Line Ratios

An indication of the multipolarity of the 6 kev transition is given by the M-subshell conversion ratios. Table II presents E1 and M1 theoretical subshell conversion ratios for a 6.25 kev transition in tantalum along with the observed conversion ratios from the W^{181} decay. Theoretical conversion coefficients were obtained by interpolating between the M-subshell coefficients tabulated by Rose (13) to obtain coefficients for Z = 73, which were then extrapolated down to 6.25 kev (k = 0.0122). The agreement between the observed ratios and theoretical E1 ratios is reasonably good. The M1 ratios are definitely not in agreement with experiment, and for higher multipolarities there is pronounced disagreement. Ratios calculated for multipolarity mixtures also fail to yield agreement with experiment.

Table II

M-Subshell Conversion Ratios for a 6.25 Kev Transition in Ta

Multipolarity	Subshell Conversion Ratio		
	M_I/M_{III}	M_{II}/M_{III}	$M_{IV,\,V}/M_{III}$
E1 (theoretical)	0.57	1.20	3.9
M1 (theoretical)	66.4	6.9	0.53
observed	0.85	1.79	1.76

As will be seen later, other arguments also indicate that this transition is E1. It is therefore of interest to consider various reasons why there is not better agreement between the observed conversion ratios and the theoretical ones. Since Rose's M-shell conversion coefficients are calculated for a point nucleus without screening, the absolute values

may well not be quite valid. However, screening effects should tend to cancel out in the ratios. On the other hand, extrapolation to very low energy may introduce some uncertainty in the coefficients, although estimates of extrapolation error can not readily be made. A possible explanation of the discrepancy can be given on the basis of the so-called anomalous E1 conversion coefficients.

Asaro and co-workers (24) have pointed out that E1 transitions in heavy element odd-A isotopes sometimes have anomalous conversion coefficients. In particular, the L_{III} experimental coefficients usually agree with the theoretical ones, but the L_I and especially the L_{II} experimental coefficients may be considerably larger than the theoretical ones. These authors relate the anomaly of the conversion coefficients to the retardation of the transition lifetime over the single particle lifetime estimate. They also give some M-shell data that indicate, in general, that the M_{III} theoretical and experimental coefficients agree, and that experimental M_I and M_{II} are high and $M_{IV,V}$ is low relative to the corresponding theoretical coefficients. These are just the directions of the discrepancies in the data of Table II ! The Asaro data are for A around 230, which is not too far from A = 181.* In addition, the magnitudes of the 6 kev data deviations are in agreement with what might be expected from the Asaro data. It is thus reasonable to attribute the differences between the theoretical E1 and observed M-subshell conversion ratios to the anomalous conversion coefficient effect.

---

* Nuclei with A near 230 and A near 181 are known to have large deformations. (See Part I.) It is not unreasonable that E1 lifetimes might be retarded for strongly deformed nuclei. Asaro et al. (24) give references to theoretical papers in which conversion coefficient and retardation effects are more fully discussed.

6 Kev Transition Lifetime Estimate from Anomalous Conversion Coefficient Considerations

Under the assumption that the entire deviation between the observed and theoretical E1 conversion ratios of Table II is due to anomalous conversion, it is possible to estimate the lifetime retardation and thus the γ-ray half-life for the 6 kev transition. The quantitative analysis by Asaro et al. (24) of the relationship between the L-shell conversion anomaly and the lifetime retardation can be extended to the M-shell. In analogy with their "total anomaly factor", f, for the L-shell, an M-shell "total anomaly factor", f_M, can be defined as

$$f_M = \left\{ \left| \alpha_{M\,I}(\text{exp}) - \alpha_{M\,I}(\text{th}) \right| + \left| \alpha_{M\,II}(\text{exp}) - \alpha_{M\,II}(\text{th}) \right| + \left| \ldots \alpha_{M\,III} \ldots \right| + \left| \ldots \alpha_{M\,IV,V} \ldots \right| \right\} \Big/ \sum_i \alpha_{M\,i}(\text{th}) \quad , \qquad (3)$$

where $\alpha_{M\,i}(\text{exp, th})$ is the M_i-subshell experimental (exp) or theoretical E1 (th) conversion coefficient. Following the Asaro L-shell procedure, $\alpha_{M\,III}(\text{exp})$ is equated to $\alpha_{M\,III}(\text{th})$. If both numerator and denominator of Eq. (3) are now divided by $\alpha_{M\,III}$, the result is

$$f_M = \left\{ \left| \left(\frac{M_I}{M_{III}}\right)_{exp} - \left(\frac{M_I}{M_{III}}\right)_{th} \right| + \left| \left(\frac{M_{II}}{M_{III}}\right)_{exp} - \left(\frac{M_{II}}{M_{III}}\right)_{th} \right| + \left| \left(\frac{M_{IV,V}}{M_{III}}\right)_{exp} - \left(\frac{M_{IV,V}}{M_{III}}\right)_{th} \right| \right\} \Big/ \sum_i \left(\frac{M_i}{M_{III}}\right)_{th} \quad , \qquad (3')$$

where the conversion coefficient ratios are denoted (M_I/M_{III}), etc. The previous (24) definition of the retardation is again used:

$$R = \frac{\text{experimental partial photon half-life}}{\text{theoretical single proton half-life}} \quad . \qquad (4)$$

Asaro et al. (24) made a log-log plot of f_L vs. R for a number of E1 transitions. The resulting curve is a straight line over most of the data interval, although there is considerable scattering of the points. Their M-shell conversion data, which were not shown plotted, have been used to calculate f_M for several transitions. Table III summarizes the results, which are shown plotted in Fig. 3.2. The one point far off the curve is the Ac^{227} point. This large deviation is most likely due to the possibility mentioned in note (c) of Table III. The f_M value for the 6 kev transition in Ta^{181} computed from the data of Table II is also given in Table III.

Table III

M-Shell Anomaly Factor for Odd-A E1 Transitions

Nucleus	Transition Energy (kev)	Anomaly Factor f_M	Retardation R
Np^{237} (a)	59.6	0.88	3.1×10^5
Pa^{231} (a)	84.2	10.5 (b)	2.8×10^6
Pa^{231} (a)	25.7	0.145	4.5×10^4
Pa^{233} (a)	29.3	0.115	7.2×10^4
Ac^{227} (a)	27.5	0.275 (c)	3.3×10^4
Ta^{181} (d)	6.25	0.45	---

Notes: (a) Data from reference 24.

(b) $M_{IV,V}$ subshell data not included.

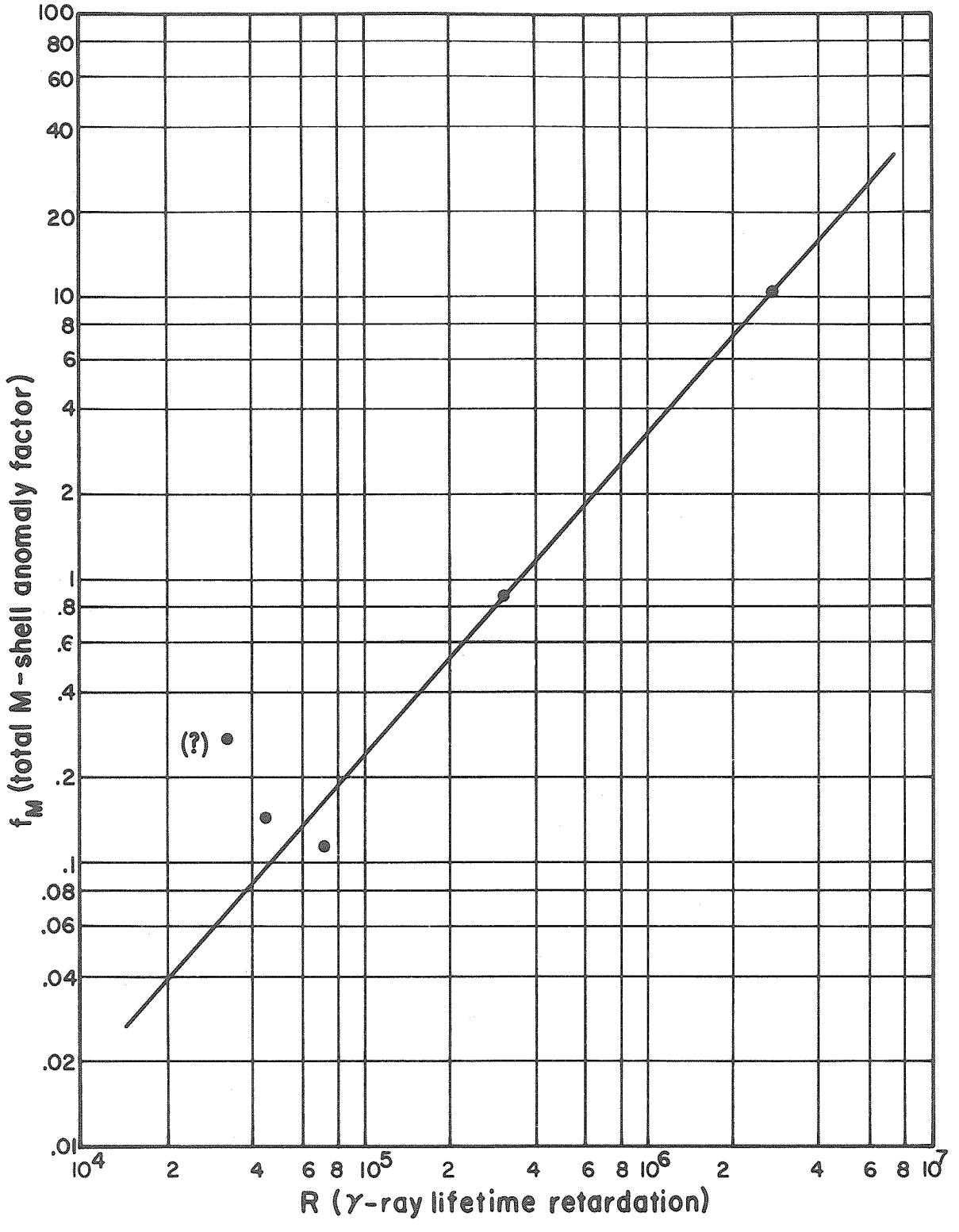

Fig. 3.2. Conversion coefficient anomaly factor for the M-shell [Eq. (3')] as a function of the E1 gamma-ray lifetime retardation for high-Z, odd A-nuclei. The solid line is the "best fit" to the experimental data.

(c) This transition may have a small M2 admixture, in which case the lifetime analysis would not be valid. See reference 24 for details.

(d) Data from Table II.

Using the value of f_M for the 6 kev transition given in Table III and the curve of Fig. 3.2, the retardation of the 6 kev lifetime is estimated to be $\sim 1.7 \times 10^5$, which is in accord with what might be expected*. When this value of R is combined with the theoretical single proton half-life for the 6 kev transition, $t_{sp} = 5.9 \times 10^{-10}$ sec, calculated from the Moszkowski (25) formula†, the following estimate of the actual γ-ray transition half-life is obtained:

$$t_\gamma = \sim 1 \times 10^{-4} \text{ sec} \quad . \tag{5}$$

Auger Transition Relative Intensities

The relative intensities of the K Auger and L Auger electron transitions following the W^{181} decay have been determined from 180° β-spectrometer measurements. This result has bearing on internal conversion coefficient determinations to be discussed later. The average intensity ratio from three runs is

$$\frac{I_{KA}}{I_{LA}} = 0.056 \pm 0.006 \quad .$$

---

* Table 6.32 of reference 23 indicates that 10^5 is a typical E1 retardation factor. Also see the discussion in Part IV C where other experimental and theoretical retardation data are given.

† As in reference 24, the statistical factor is taken as unity.

C. Proportional Counter Measurements

If the 6 kev transition in Ta^{181} is pure E1, as the electron spectrum measurements indicate, the estimated total conversion coefficient (α_T = 81 from Table A VII, Appendix III, Part C) and the 6 kev conversion intensity of Eq. (1) imply that some observable γ-ray intensity should be present in the W^{181} decay. Moreover, if the intensity of the 6 kev γ-ray could be measured relative to the accompanying x-rays, it would be possible to determine the absolute conversion coefficient. This, in turn, would clarify the multipolarity assignment. A study was therefore undertaken to see if the unconverted 6 kev γ-rays could be detected.

Because of their relatively high resolution and moderately high efficiency for low energy photons, gas-filled proportional counters were used to investigate the low energy electromagnetic spectra. Fig. 3.3 shows three spectra taken with the xenon proportional counter. Fig. 3.3(a) shows the W L x-ray group* and escape peak from a Ta^{182} source, which β-decays to W^{182}. This decay has been studied by many workers (5) and no transitions in the 6 kev region have been reported. Fig. 3.3(b) shows the Ta L x-ray group† and escape peak from a Hf^{181} source, and Fig. 3.3(c) shows the same spectral region for a W^{181} source. The neighboring Ta^{182} spectrum is presented for comparison purposes. In each case, arrows mark the locations of the L_α, L_β, and L_γ x-ray

*The W L x-ray group is composed of L_α, L_β, and L_γ subgroups which have average energies of 8.4, 9.8, and 11.4 kev respectively.

†The Ta L x-ray group is composed of L_α, L_β, and L_γ subgroups which have average energies of 8.1, 9.4, and 11.0 kev respectively.

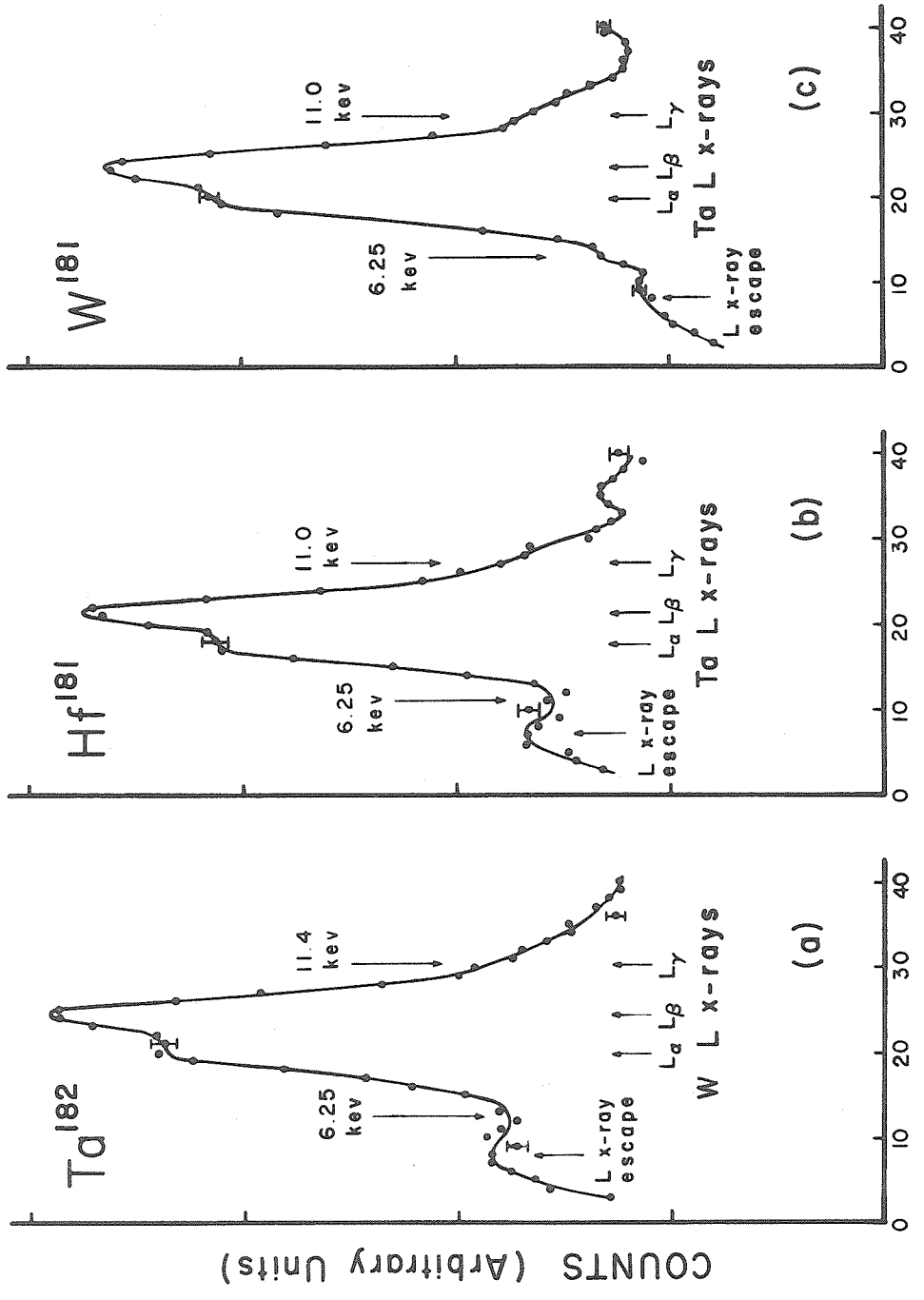

Fig. 3.3. Low energy electromagnetic spectra taken with the xenon proportional counter. The prominent peaks are the L x-rays from the decays of (a) Ta^{182}, (b) Hf^{181}, and (c) W^{181}. The L x-ray escape peak appears at about channel 10. The valley at about 6 kev in (a) and (b) is absent in (c), indicating the presence of a ~6 kev γ-ray.

groups, and the L x-ray escape peak. The latter is due to the escape of xenon L x-rays from the counter. An arrow also marks the location of 6.25 kev in each spectrum. Figs. 3.3(a) and (b) are seen to have distinct valleys in the 6 kev region, whereas this valley is missing in Fig. 3.3(c).

The conclusions from these curves are that γ-rays of about 6 kev energy are certainly present in the decay of W^{181}, and that their intensity is rather weak compared to the Ta L x-rays. Since this W^{181} source, unlike that used for the β-ray spectrometer measurements, was accelerator produced, there was no difficulty with the presence of other tungsten isotope impurities. It can thus be concluded that the 6 kev transition definitely belongs to the W^{181} activity. The lack of evidence in Fig. 3.3(b) for a 6 kev transition is not surprising in view of the β-spectrometer results which showed that the 6 kev conversion relative intensity in the Hf^{181} decay was much weaker than that in the W^{181} decay.

The same three sources studied with the xenon counter were also studied with an argon proportional counter. Because of the improved resolution of this counter over the xenon counter, it is possible to draw quantitative conclusions from the results. Fig. 3.4 shows typical argon counter spectra. The heavy lines indicate the experimental data, corrected only for external and scattered background. The higher resolution of this counter almost separates the L_α and L_β x-ray groups. In addition, argon K x-ray escape peaks, $L_\alpha e$ and $L_\beta e$, are evident for the prominent L groups. The L_γ x-ray group is not well resolved. As with the xenon counter results, there is a clear indication of a contribution near 6 kev in the W^{181} data.

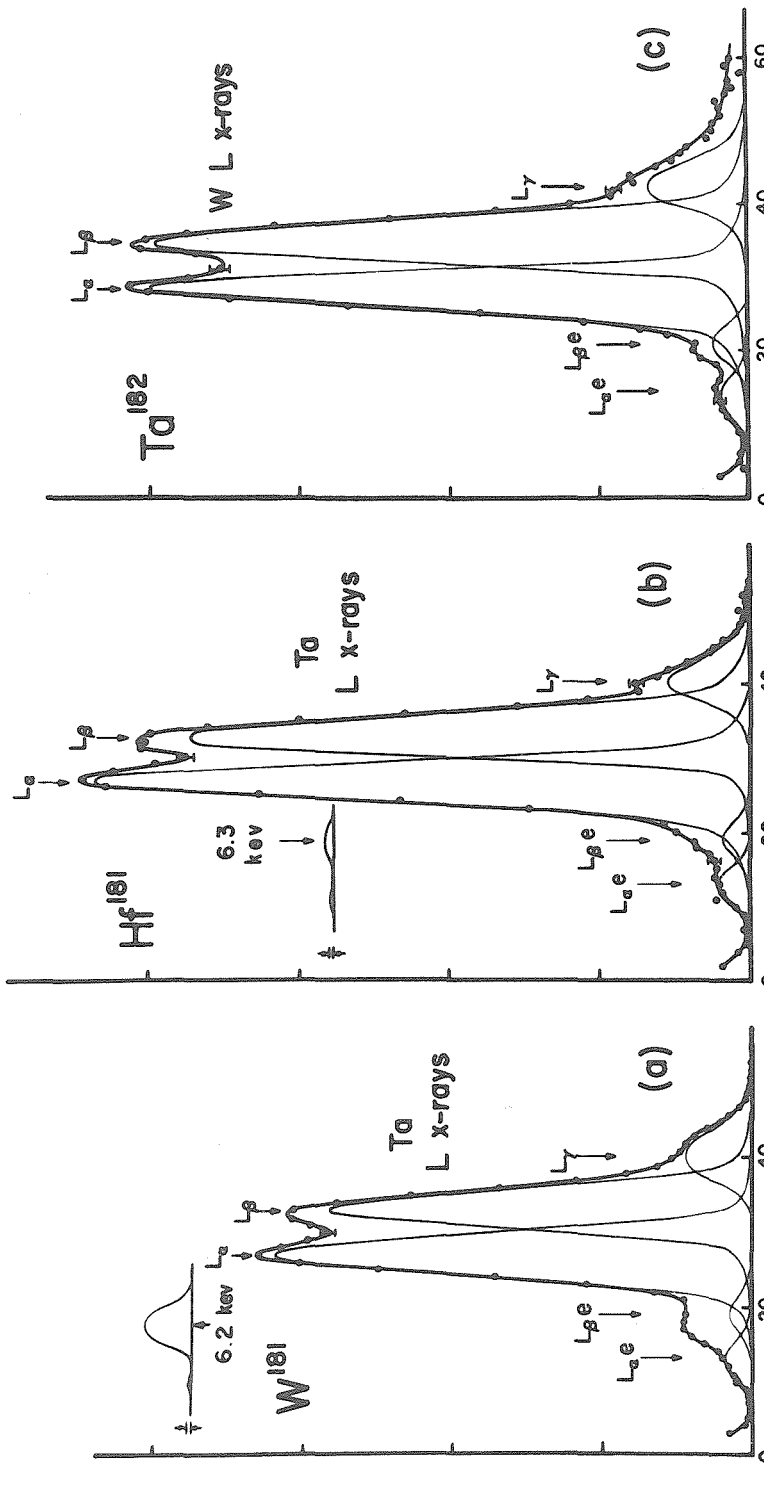

Fig. 3.4. Typical L x-ray spectra taken with the argon proportional counter using (a) W^{181}, (b) Hf^{181}, and (c) Ta^{182} as sources. The experimental data have been decomposed to exhibit a 6 kev transition in the decays of W^{181} and Hf^{181}.

The efficiency, resolution, and escape peak behavior of these counters have been separately investigated and the results are reported in Appendix I. The manner in which this information was applied to the raw data to determine the 6 kev intensity will now be outlined. The three L x-ray groups for each curve have been fitted with Gaussian curves of appropriate width. Empirical escape ratios (ratio of escape peak to main peak) were then used to construct Gaussian escape peak curves of suitable intensity and width. The 6 kev intensity was found by graphically subtracting the calculated Gaussians from the experimental data. This process was iterated, with slight intensity changes, until the calculated curves made a good fit with the experimental data and a reasonably symmetric difference curve resulted in the region of 6.25 kev. This difference curve is indicated in the insets in Figs. 3.4(a) and (b). The escape peak from the L_γ x-rays was taken into account in the calculations, although, for simplicity, it is not shown in Fig. 3.4. Finally, the decomposed data were corrected for counter efficiency in order to get true intensities. The small contribution above L_αe on the inset difference curves represents a small error which is principally due to the background correction. Its size, which is indicated in the figure, gives some measure of the error in the 6 kev intensity obtained by this means.

As a check on the above procedure, which will be referred to as method 1, the relative intensity of the 6 kev γ-ray was independently determined by two different means. One of these checks, which will be called method 2, involved the use of differential absorbers of aluminum. The attenuation coefficient for the x-ray escape contribution at 6 kev is

the same as for the primary energy, 9.4 kev; the attenuation coefficient for the γ-ray component in this region, however, is that for the true energy, 6.25 kev. Rough measures of the various intensities were obtained from argon counter runs (i) with no absorber, (ii) with a 0.001" Al absorber, and (iii) with a 0.003" Al absorber. These data, when combined with the counter efficiencies (from Appendix I) and absorber attenuation coefficients (26), yielded the 6 kev transition intensity. It is to be noted that with method 2, no separate determination of the escape ratio was necessary. Method 2 was only applied to W^{181}.

Method 3 consisted in normalizing the Hf^{181} and W^{181} data so that the L x-rays would have the same apparent intensity as the L x-rays from Ta^{182}. By subtracting the Ta^{182} escape peak from the normalized data, estimates for the 6 kev γ-ray contribution were obtained. Iteration of the process with inclusion of appropriate counter efficiencies allowed the determination of the true relative intensities. The data used for method 3 analysis were separate from those used for method 1.

The intensities of the 6 kev γ-ray relative to the total L x-ray group determined by the three methods are summarized in Table IV. The errors for the individual measurements allow for statistical effects and for uncertainties in background and efficiency corrections. These errors also reflect the reliability of the different values. The weights used for averaging are the inverse variances, and the error stated with the average is the standard deviation estimated by internal

consistency*.

Table IV

Argon Proportional Counter Measurements of the 6 Kev γ-Ray Intensity

Method	$I_{6\gamma}/I_{LX}$ for W^{181} decay	$I_{6\gamma}/I_{LX}$ for Hf^{181} decay
1 (a)	0.047 ± 0.010	0.0065 ± 0.0036
1 (b)	0.046 ± 0.012	
2 (c)	0.051 ±0.024	
3 (b)	0.044 ±0.016	0.010 ± 0.008
weighted average	0.046 ± 0.007	0.007 ± 0.003

Notes: (a) Data taken with 100 channel analyzer set for 0.5 volt channels.

(b) Data taken with 100 channel analyzer set for 1 volt channels.

(c) Data taken by hand runs with single channel pulse height analyzer set for a 1 volt channel.

The Hf^{181} intensity value should really be considered as an upper limit, because the 6 kev intensity in Hf^{181} is so small, that a certain amount of bias was introduced in analyzing the data. This intensity value has been checked, in a manner similar to the check on the Hf^{181} 6 kev conversion intensity (see footnote p. 30), to see if it is consistent with the 6 kev transition being in cascade with the 476 kev transition. The result is in agreement with the cascade hypothesis.

---

* The standard deviation for external consistency is approximately 0.001 for both averages.

Incidental to the measurement of the 6 kev intensity, the relative intensities of the L x-ray groups were also determined. These results are presented in Table V.

Table V

Relative Intensities of L X-Rays Measured with the Argon Counter

Method	W^{181} Decay		Hf^{181} Decay	
	$I_{L\beta}/I_{L\alpha}$	$I_{L\gamma}/I_{L\alpha}$	$I_{L\beta}/I_{L\alpha}$	$I_{L\gamma}/I_{L\alpha}$
1 (a)	0.91	0.20	0.98	0.16
1 (b)	1.04	0.20		
2 (c)	1.05	0.14		

Notes: See notes for Table IV.

At this point it is appropriate to consider two factors that have bearing on the intensity measurements. In the analysis of the data of Fig. 3.4 and related results, it has been assumed 1) that there was no self-absorption of the low energy radiation in the source, and 2) that the observed x-rays were entirely from the daughter atoms of the decay. If the source material were thick enough, parent atom x-rays might be produced by fluorescence excitation and self-absorption might also occur. Both the Hf^{181} and Ta^{182} sources were prepared by vacuum evaporation onto mica. This means that they were certainly thin enough so that neither of these processes would occur to any extent. The W^{181} source was not vacuum evaporated, so that these considerations are applicable to it. Using the scintillation counter arrangement described in Part II E, the L/K x-ray intensity ratio was determined for the pro-

portional counter source and for an old vacuum evaporated W^{181} source. From these measurements it could be concluded that there was negligible self-absorption in the W^{181}. From the observed fluorescence excitation of parent atom x-rays in a very thick source* and the estimated thickness of the W^{181} proportional counter source, it was possible to also conclude that there was negligible parent x-ray production in the latter source.

W^{181} L/K X-Ray Intensity Ratio

As will be seen later, the W^{181} L/K x-ray intensity ratio is of importance for the determination of the 6 kev conversion coefficient and the W^{181} electron capture decay energy. In principle, this ratio can be determined from xenon proportional counter measurements. Fig. A 1.10 in Appendix I shows the xenon counter x-ray spectrum for the W^{181} source. When allowance is made for scattering, background, counter efficiency, and escape phenomena, this curve yields the following value for the L/K x-ray intensity ratio in W^{181}:

$$I_{LX}/I_{KX} = 0.20 \pm 0.06.$$

This large (30%) error is necessary because of the many sizeable corrections required for the raw data. The most serious corrections, from the point of view of introducing error in the result, are the efficiency correction and the scattering correction. The counter efficiency for the L x-ray group differs from that for the K_β x-ray by a factor of 7.

---

* Relative intensities of parent and daughter x-rays have been obtained from the curved-crystal γ-ray spectrometer data of other members of the group (27), who used a neutron activated 0.01" diameter tantalum wire for a source.

Analytical corrections for scattering are almost impossible, although (as shown in Appendix II) scattering can be reduced by remounting the source. Since the L/K x-ray ratio is needed to high precision, the result above must be taken as a first-order approximation. An improved value can be obtained with the scintillation counter, for which the corrections are not nearly so large and for which the scattering can be substantially reduced.

Incidental to the xenon counter measurement of the L/K x-ray ratio, the ratio of the K_α to the K_β x-ray intensities was also obtained. Taking into account the necessary corrections, the value measured for this quantity is

$$I_{K\alpha}/I_{K\beta} = 2.97.$$

This result is in crude agreement with the value $I_{K\alpha}/I_{K\beta} = 3.76$ from Table 7.2-3 of reference 23. Scattering and efficiency corrections probably account for the difference.

D. Scintillation Spectrometer Measurement of W^{181} L/K X-Ray Ratio

The details of the means by which the intensity ratio of the L and K x-rays in the W^{181} decay has been determined to a high precision are given in Appendix II. The salient features of the method will be reviewed here. By remounting the W^{181} activity on a thin Mylar backing, the backscattering of the K x-rays was virtually removed. By covering the NaI crystal with just an extremely thin aluminum foil, the energy efficiency corrections for both L and K x-rays were made very small, thereby causing the uncertainty introduced by these corrections to be extremely small. By studying the apparent L/K x-ray ratio as a function of counting geometry and the medium between the source and crystal, it was possible to eliminate most of the scattering from the counter surroundings. Finally, the L/K x-ray ratio was corrected for small coincidence losses, which occurred if an L x-ray entered the crystal at the same time as a K x-ray.

Typical of the raw data is Fig. A 2. 1 (b) of Appendix II. The observed peaks are the L x-rays, the K x-ray escape peak, and the K x-rays. The final result of these measurements, taking into account all of the various corrections, is

$$\frac{I_{LX}}{I_{KX}} = 0.264 \pm 0.013 \quad . \tag{6}$$

The stated (5%) error allows for uncertainty in the corrections and decomposition of the L peak from the K escape peak, as well as for uncertainty in the raw intensity measurements*.

---

* Throughout this work, raw intensity areas have been determined by weighing cut-out tracings of the curves with an analytical balance. High quality (uniform) tracing paper was used. The errors in this process have been determined to be less than 1%.

E. W^{181} L/K Capture Ratio and Decay Energy

The coincidence experiment of Part III A and the occurrence of the 6 kev transition in W^{181} argue strongly for a Ta^{181} level at 6 kev. Other arguments in Part IV will establish the spin and parity of this new level to be 9/2−. (From what has been shown so far, the probable E1 nature of the 6 kev transition certainly makes this assignment plausible.) If these yet to be established results are tentatively accepted, it is possible to make certain conclusions about the W^{181} decay energy.

If Ta^{181} has a level at 6 kev, it is clear from energy considerations that W^{181} can decay by electron capture to both the 6 kev level and to the ground state. Furthermore, both L-shell and K-shell electron capture can occur to both levels. With a few simplifying assumptions, it is possible to calculate the L/K capture branching ratio from the L/K x-ray intensity ratio. From the branching ratio, the capture decay energy can be determined.

To assume that the capture to the states at 136 kev and above may be neglected is quite straightforward. Previous work (10) has shown that the branching to these states is of the order of 10^{-3} times weaker than the branching to the ground state (i. e. to the ground state and 6 kev state). Measurements reported in Part III G are also in agreement with a very weak high energy branching.

Some simplification results by assuming at this point that the transitions to the 6 kev state and ground state are both either allowed or first-forbidden, non-unique. Later discussion will show that these transitions are, indeed, either one or the other of these types, and thus this assumption is really no restriction at all. The level assignments

of Fig. 1.1 and the 9/2− assignment for the 6 kev level also make this clear.

Under these assumptions, the only way K-shell holes are produced in tantalum daughter nuclei is by K-capture taking place. L-shell holes can be produced either by L-capture or by the filling of K-shell vacancies. Let P_K be the probability of K-capture occurring and P_L the probability of L-capture occurring. Then the relative K x-ray intensity, I_K, is

$$I_K = P_K \omega_K \quad ,$$

where ω_K is the K-shell fluorescence yield. The relative L x-ray intensity, I_L, is

$$I_L = P_L \omega_{LL} + P_K \omega_{LK} \quad ,$$

where ω_{LL} is the average L-shell fluorescence yield for vacancies produced directly by L-capture and ω_{LK} is the average L-shell fluorescence yield for vacancies produced through K-capture. Then it follows that

$$\frac{P_L}{P_K} = \frac{1}{\omega_{LL}} \left[\frac{I_L}{I_K} \omega_K - \omega_{LK} \right] \quad . \tag{7}$$

P_L/P_K is just the L/K capture ratio and I_L/I_K is the x-ray intensity ratio, which has been measured.

In order to evaluate the capture ratio from Eq. (7), knowledge of the fluorescence yields is required. For this purpose ω_K(Ta) is taken from the tables of Wapstra et al. (23). ω_{LL} and ω_{LK} must be computed from the partial fluorescence yields for the L-subshells, $\omega_{L\,I}$, $\omega_{L\,II}$, and $\omega_{L\,III}$. For a process P,

$$\omega_{LP} = \sum_{i=1}^{3} u_{Pi}\omega_{Li} \quad , \tag{8}$$

where u_{Pi} is the chance that process P produces a vacancy in the L_i-subshell. Unfortunately, the L-shell partial fluorescence yields are rather poorly known. The problem of experimentally measuring $\omega_{L\,I}$ and $\omega_{L\,II}$ is particularly difficult, and the results of different workers are not in agreement. The subject of L-shell fluorescence yields is treated in Burhop's (28) book, in which the work prior to 1951 is reviewed. Laskar (29) has surveyed some recent results as well as some of the older work, and has made a careful analysis of the data. His values for $\omega_{L\,i}$ have been plotted and extrapolated to Z = 73. These results are listed in Table VI, along with other (30), (31) experimental yields for tantalum*. The average of these values, which is used in the

---

* Quite recently, Robinson and Fink (32) published a review article on experimental electron capture results in which they report a new measurement of tantalum L-subshell fluorescence yields. These new yield values, $\omega_{L\,III} = 0.23 \pm 0.02$ and $\omega_{L\,II} = 0.23 \pm 0.04$, are the unpublished results of C. E. Roos. Robinson and Fink (32) also attribute a value $\omega_{L\,I} = 0.28 \pm 0.07$ to Roos, but a recent private communication from C. E. Roos (33) indicates that there is an error in this presentation. The value 0.28 should have been labeled $\bar{\omega}_L$, the total or average yield for all the L-subshells together. Roos (33) stated that these measurements were made at the same time and by essentially the same method as his K-shell fluorescence yield measurements (34).

In any case, there seems to be some question about these yield values. Previous measurements of the L-subshell fluorescence yields show that $\omega_{L\,III}$ is, generally speaking, higher than $\omega_{L\,I}$ (see, for example, Table VI in the text and Fig. 7.51 of reference 23). This is also reflected in the curve of the total or average L-fluorescence yield as a function of atomic number (see Fig. 5 of reference 32). The sharp increase in this curve at around Z = 73 is attributed to the occurrence of Coster-Kronig transitions of the type $L_I - L_{III}M_{IV,V}$, which shift L_I vacancies to the L_{III}-subshell, where the partial fluorescence yield is greater. Thus it is rather difficult to understand how Roos's average yield (or for that matter his L_I yield) can be higher than his L_{III} and L_{II} yields. It is for this reason that the new Roos data in reference 32 are

calculation of ω_{LL} and ω_{LK}, is also tabulated. The errors in these yields may be as large as 10%.

Table VI

L-Shell Partial Fluorescence Yields for Tantalum

Reference	$\omega_{L\,I}$	$\omega_{L\,II}$	$\omega_{L\,III}$
Laskar (29)	0.153	0.283	0.191
Kinsey (30)	0.17	0.31	(0.18)
Küstner and Arends (31)	(0.284)	(0.326)	0.191
Average (a)	0.162	0.297	0.191

Note: (a) The values in parentheses have not been included in the average. Kinsey's value for $\omega_{L\,III}$ is rejected because, as he and other workers have noted, it is probably 10% too low. The $\omega_{L\,I}$ and $\omega_{L\,II}$ values of Küstner and Arends are rejected on the basis of arguments given in Chapt. 7.5 of reference 23.

The u_{Ki} (Z = 73) are determined from the graphs of Fig. 7.52 in the Nuclear Spectroscopy Tables of Wapstra et al. (23). The errors are said to be of the order of 0.01. Ratios of the u_{Li} (Z = 74) are obtained from graphs of ratios of electron radial wave functions, evaluated at

---

not included in Table VI.

If these L_{II} and L_{III} data were included, the average $\omega_{L\,II}$ would then become 0.274 instead of 0.297, and the average $\omega_{L\,III}$ would become 0.204 instead of 0.191. These changes have only a small effect on the L/K capture ratio [0.355 instead of 0.359 -- see Eq. (9)] and decay energy determination [178 kev instead of 176 kev -- see Eq. (12)].

the nuclear radius, published by Brysk and Rose (35).* $u_{L\,III}$ is taken to be zero, and the u_{Li} are normalized by the condition $\sum u_{Li} = 1$. Table VII summarizes the u_{Pi} values used in calculating L-shell fluorescence yields from Eq. (8). The resultant L-yields, along with the K-yield (23), are given in Table VIII.

Table VII

Probabilities for Vacancy Production in the Ta L-Subshells

Means of Excitation	Vacancy Probability for		
	L_I	L_{II}	L_{III}
K-hole filling (u_{Ki})	0.030	0.288	0.513
L-capture process (u_{Li})	0.943	0.057	0

Table VIII

Fluorescence Yields for Tantalum

Fluorescence Yield	Value
ω_K	0.943
ω_{LK}	0.188
ω_{LL}	0.170

* The assumption of only allowed or first-forbidden, non-unique transitions enters here in the choice of wave functions and permits L_{III}-subshell capture to be neglected. Differences in the neutrino energy emitted in capture from the different L-subshells are neglected, as are neutrino energy differences for capture to the ground state and to the 6 kev state.

Eq. (7) can now be evaluated, using the L/K x-ray ratio of Eq. (6) and the fluorescence yields of Table VIII. The resultant L/K capture ratio is

$$P_L/P_K = 0.359 \pm 0.070 \quad . \tag{9}$$

The stated error only takes into account the uncertainty in the x-ray intensity measurement. The L-shell fluorescence yields enter into Eq. (7) in such a way that P_L/P_K is very sensitive to the yield values. A 10% change in the value of ω_{LK} produces a 30% change in the value of P_L/P_K.* Because of the uncertainties in the errors associated with the adopted values of the ω_{Li}'s and the u_{Ki}'s, and because of the complex way in which these errors affect P_L/P_K, it is difficult to state a truly realistic error for this quantity. The capture ratio value of Eq. (9) must be regarded as the best estimate that can be made on the basis of presently available fluorescence yields.

Decay Energy from Orbital Capture Considerations

The orbital capture decay formulation of Brysk and Rose (35) may be used to compute the capture decay energy. Using their notation, the L/K capture ratio is related to the energies of the neutrinos emitted in capture by the equation†

$$\frac{P_L}{P_K} = \frac{q_{LI}^2}{q_K^2} \cdot \frac{g_{LI}^2}{g_K^2} \left(1 + \frac{f_{LII}^2}{g_{LI}^2}\right) \quad . \tag{10}$$

---

* It should also be remarked that the way in which the x-ray ratio occurs in a difference term in Eq. (7) causes the resultant capture ratio to be very sensitive to changes in the x-ray ratio. Because of this effect it was necessary to determine I_L/I_K to a high precision.

† See the footnote at the bottom of p. 53.

The g's and f are radial wave functions evaluated at the nuclear surface, and the q's are the neutrino energies:

$$q_K = Q_{EC} - B_K \tag{11}$$

and similarly for q_{LI}. Q_{EC} is the decay energy (the atomic energy difference between parent and daughter) and B_K is the (positive) K-shell binding energy. The B's are determined from reference 23, while graphs of the wave function ratios are given in reference 35. The previously calculated L/K capture ratio, when combined with Eq. (10), yields the following capture decay energy:

$$Q_{EC} = 176 \begin{matrix} + 44 \\ - 22 \end{matrix} \text{ kev} \quad . \tag{12}$$

Again the stated error limits* take into account only the uncertainty in the x-ray intensity measurements. Errors in the fluorescence yields would substantially alter the result. The neglect of the difference between the neutrino energy for capture to the ground state and capture to the 6 kev state could only introduce a small error ($< \sim 3$ kev) in the result compared to the stated errors in Eq. (12).

This decay energy value is not in agreement with the value 92 kev (± 10%) determined by Bisi, Terrani, and Zappa (7), who used a similar method. Their x-ray intensity ratio of $I_L/I_K = 0.39 \pm 0.01$, which is not in agreement with the result (0.264) of Eq. (6), was measured with an argon proportional counter. Possible scattering and difficulty in determining the argon counter efficiency for such widely separated energies probably explains why their value is too high. Their L/K capture ratio of 1.54 differs from the result of Eq. (9) because they

---

* The error limits are asymmetric because Q_{EC} increases extremely rapidly with decreasing I_L/I_K.

used substantially different L-shell fluorescence yields from those listed in Table VIII, as well as a different x-ray intensity ratio.

The value Q_{EC} = 176 kev is, however, in good accord with the decay energy arguments of Debrunner et al. (10), (36). From γ-ray - x-ray coincidence experiments, they concluded that L-capture but no K-capture feeds the 136 and 152 kev transitions, and therefore that the decay energy must lie between 160 and 205 kev.

If, contrary to the assumption made in the foregoing, it is assumed that all of the capture decay occurs through a first-forbidden, unique transition (ΔI = 2, yes), then the x-ray intensity ratio of Eq. (6) and the decay formulation of Eq. (10) are no longer valid. The results of Brysk and Rose (35) may be used to reformulate this problem for first-forbidden, unique transitions. In this case the calculation gives Q_{EC} = 422 kev. Arguments can then be made that show that classification of the capture transition to the 6 kev level as first-forbidden, unique (or any of the higher orders of forbiddeness) implies a contradiction to the 205 kev upper limit for the W^{181} decay energy of Debrunner et al. (10). Thus this transition must be allowed or first-forbidden, non-unique as originally assumed.

There are two possible checks on the value of the decay energy. One would be to use the mass difference between W^{181} and Ta^{181}. Unfortunately, no mass values for W^{181} have been published at this time. The other check would be the measurement of the internal bremsstrahlung spectrum end-point. If a decay energy of 176 kev is assumed, then from Eq. (11) the maximum K-capture neutrino energy, $q_{\nu\,max}$, (and hence the maximum photon energy) is 106 kev. The following formula can be derived (37) for the total internal bremsstrahlung (IB) intensity relative

to the K x-rays:

$$\frac{I_{IB}}{I_{KX}} = \sim \frac{1}{\omega_K} \cdot \frac{\alpha}{12\pi} \left(\frac{q_{\nu max}}{511 \text{ kev}} \right)^2 .$$

From this it can be seen that the IB spectrum would have an intensity of 8.8×10^{-6} relative to the K x-rays. It can also be shown (37) that the IB photon spectrum has an expected maximum at $\sim 1/3\, q_{\nu max} =$ 35 kev. Since the IB spectrum end-point is approximately mid-way between the K x-rays and the 136, 152 kev γ-rays, it would be very difficult to measure this spectrum without the use of coincidence techniques (IB - K x-ray coincidences). However, the very weak IB intensity means that this would be an extremely difficult experiment, if not an impossible one.

F. 6 Kev Transition Conversion Coefficient and Branching

From the measured intensity ratios of the 6 kev γ-rays to the x-rays and the 6 kev conversion electrons to the Auger electrons, it is possible to determine the internal conversion coefficient of the 6 kev transition and the branching to the 6 kev level. Fig. 3.5 is a simplified decay scheme that is useful in considering these problems. The weak ($\sim x\,10^{-3}$) branching to the 152 and 136 kev transitions is neglected.

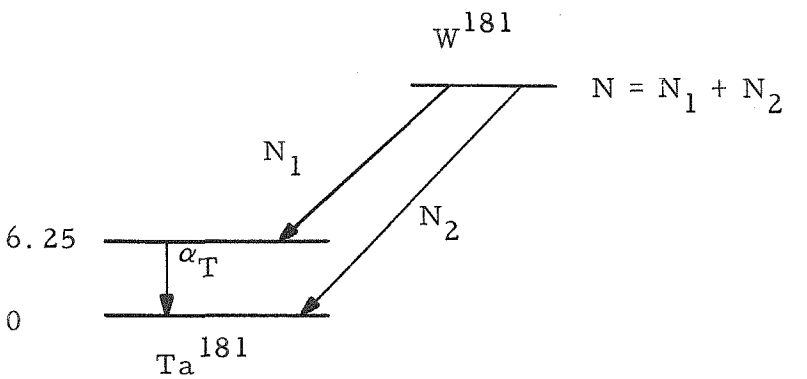

Fig. 3.5. Simplified W^{181} decay scheme.

Let N_1 transitions lead to the 6 kev level and N_2 to the ground state. Then the total number of transitions is $N = N_1 + N_2$. For these two capture transitions let N_K/N = the fraction of the total captures that are from the K-shell, and N_L/N = the fraction of total captures from the L-shell. [$(N_L/N)/(N_K/N_L)=P_L/P_K$ of Part III E.] On the grounds of the assumptions of Part III E, it can be shown that each of these fractions is the same for both capture branches.

If α_T is the 6 kev transition total internal conversion coefficient, then the 6 kev γ-ray intensity is

$$I_{6\gamma} = N_1 \frac{1}{1 + \alpha_T} \quad ,$$

and the 6 kev conversion intensity is

$$I_{6E} = N_1 \frac{\alpha_T}{1 + \alpha_T} \quad .$$

The total K x-ray intensity is

$$I_{KX} = (N_1 + N_2) \frac{N_K}{N} \omega_K = N_K \omega_K \quad ,$$

and the total K Auger intensity is

$$I_{KA} = N_K (1 - \omega_K) \quad .$$

The total L x-ray intensity is

$$I_{LX} = N_L \omega_{LL} + N_K \omega_{LK} \quad ,$$

and the total L Auger intensity is

$$I_{LA} = N_L (1 - \omega_{LL}) + N_K a_{LK} \quad .$$

ω_K, ω_{LL}, and ω_{LK} are defined and tabulated in Part III E. a_{LK}, the L Auger yield from the filling of K-shell vacancies, is defined as

$$a_{LK} = \sum_{i=1}^{3} u_{Ki} (1 - \omega_{Li}) \quad .$$

Using the data of Tables VI and VII, the value for this Auger yield is found to be

$$a_{LK} = 0.643 \quad . \tag{13}$$

The previous intensity relations may be used to derive the following equations for α_T:

$$\alpha_T = \frac{I_{6E}}{I_{LA}} \cdot \frac{I_{LA}}{I_{KA}} \cdot \frac{1}{\frac{I_{6\gamma}}{I_{LX}} \cdot \frac{I_{LX}}{I_{KX}}} \left(\frac{1}{\omega_K} - 1 \right) \tag{14a}$$

$$\alpha_T = \frac{I_{6E}}{I_{LA}} \cdot \frac{1}{\frac{I_{6\gamma}}{I_{LX}}} \cdot \frac{\frac{P_L}{P_K}(1-\omega_{LL}) + a_{LK}}{\frac{P_L}{P_K}\omega_{LL} + \omega_{LK}} \quad . \tag{14b}$$

In a similar manner, two relations may be derived for the ratio of ground state capture to 6 kev state capture:

$$\frac{N_2}{N_1} = \frac{1}{\frac{I_{6\gamma}}{I_{LX}} \cdot \frac{I_{LX}}{I_{KX}}} \cdot \frac{1}{\frac{N_K}{N}(1+\alpha_T)\omega_K} - 1 \tag{15a}$$

$$\frac{N_2}{N_1} = \frac{\alpha_T}{(1+\alpha_T)} \cdot \frac{1}{\frac{I_{6E}}{I_{LA}}} \cdot \frac{1}{\frac{N_L}{N}(1-\omega_{LL}) + \frac{N_K}{N} a_{LK}} - 1 \quad . \tag{15b}$$

N_K/N and N_L/N can be evaluated from the L/K capture ratio of Eq. (9) and the ratio of M + N + ... -capture to L-capture given in Table 5.41 of reference 23. The results are

$$N_K/N = 0.689 \qquad \text{and} \qquad N_L/N = 0.247 \quad . \tag{16}$$

To evaluate Eqs. (14) and (15), the conversion electron and Auger intensities are taken from Part III B, the 6 kev γ-ray intensity from Part III C, and the x-ray ratio is taken from Part III D.

The results of the calculations of the 6 kev internal conversion coefficient yield

$$\alpha_T = 45.0 \tag{14a'}$$

$$\text{and} \quad \alpha_T = 41.9 \tag{14b'}$$

The first value is based on the conversion intensity relative to the K Augers, while the second value is based on the conversion intensity

relative to the L Augers. The fairly close agreement (within 7%) between the two values indicates an over-all consistency, and, in particular, indicates that the calculations of ω_{LL}, ω_{LK}, and a_{LK} are reasonably good. Combining Eqs. (14a') and (14b'), the final result is

$$\alpha_T \geq 44 \pm 7 \quad . \tag{14c}$$

This value is stated as a lower limit because the observed conversion intensity was given as a lower limit. (See comments p. 29 .)

The above value of α_T may now be used to evaluate Eq. (15). Proceeding as before, the following values are obtained:

$$N_2/N_1 = 1.82 \tag{15a'}$$

and

$$N_2/N_1 = 1.96 \quad . \tag{15b'}$$

The average is $N_2/N_1 = 1.89$. This ratio may be used to calculate the percentage branchings for the two lower capture transitions:

$$N_1/N = 35 \pm 10\% \quad \text{and} \quad N_2/N = 65 \pm 10\% \quad . \tag{15c}$$

If α_T of Eq. (14c) is now compared with the theoretical conversion coefficients for a 6.25 kev transition in tantalum as listed in Table A VII of Appendix III, Part C, it can be seen that the experimental value is in best agreement with the E1 value ($\alpha_T = 81$). Although the E1 value is about a factor of two larger than the experimental value, as Rose (38) has pointed out, the M-shell coefficients may be high by as much as a factor of two because of neglect of screening in the theoretical calculations. Then, too, considerable error may be introduced in extrapolating these coefficients down to 6 kev. In view of these considerations a very small M2 admixture is possible, but M1 (+ E2) and higher multipolarities are certainly excluded. Furthermore, the nature of the lower

limit of Eq. (14c) tends to imply closer agreement between the theoretical E1 and experimental coefficients. The window absorption effect, however, at very most, could reduce α(expt) by about 30%. Thus it is not possible to argue for the higher multipolarities on these grounds.

It might be remarked that if this E1 transition has anomalous conversion coefficients, as the data of Table II indicate, some discrepancy between the theoretical and experimental coefficients would be expected. Since experimental M_I and M_{II} conversion is high and $M_{IV,V}$ conversion is low relative to the theoretical conversion, the final effect of the anomaly on the total M-shell conversion is not readily apparent. The fact that $\alpha_{M\,IV,V}$ is quite a bit larger than $\alpha_{M\,I,II}$ (13) means that the anomalous conversion coefficient effect would probably make α_M(expt) low compared to α_M(th).

In summary, it is seen, both from the absolute total conversion coefficients and from the M-subshell conversion ratios, that the 6 kev transition in Ta^{181} must be electric dipole.

G. Study of the 136 and 152 Kev Transitions

For a better understanding of the Ta^{181} level scheme, the previously reported (6), (10) very weak 136 and 152 kev transitions in the W^{181} decay were re-investigated. Considerable information was obtained by studying both the conversion electron and γ-ray spectra of these transitions.

With the source strengths available, the luminosity of the 180° β-spectrometer was only sufficient for the K conversion lines of these transitions to be barely distinguished from the background. Upon combining the results of several runs*, it was possible to estimate the relative intensities of K conversion for these two transitions and to set a limit on their total intensity relative to the K Auger transitions. The results are:

$$I_{152\,K}/I_{136\,K} = \sim 2 \pm 1 \qquad (17a)$$

$$I_{136,\,152\,K}/I_{K\ Augers} \leq \sim 1/60 \quad . \qquad (18a)$$

The ring focusing β-ray spectrometer, which has a high luminosity, was also used to investigate the 136 and 152 kev transitions. Even the data* from this instrument had a poor signal-to-noise ratio, although they were considerably better than the 180° spectrometer data. The averaged results of several W^{181} runs from the ring focusing spectrometer gave:

$$I_{152\,K}/I_{136\,K} = 1.7 \pm 0.4 \qquad (17b)$$

$$I_{136,\,152\,K}/I_{K\ Augers} \leq \sim 1/25 \quad . \qquad (18b)$$

---

* The author is indebted to Dr. Felix Boehm of this laboratory for these raw data.

The results of Eqs. (17a) and (17b) can be combined to yield

$$I_{152\,K}/I_{136\,K} = 1.74 \pm 0.4 \quad . \tag{17c}$$

136, 152 Kev Gamma-Ray Intensities

A standard sodium iodide scintillation crystal spectrometer was used to determine the relative intensities of the 136 and 152 kev γ-rays. Since the high energy γ-rays are extremely weak compared to the K x-rays in the W^{181} decay, it was necessary to use graded filters to attenuate the x-rays. Without filters, the signal-to-noise ratio for the γ-rays was very poor. A series of filters with decreasing atomic number was employed so that the fluorescence x-rays from the first filter would be strongly attenuated, and thus make negligible contribution to the low energy region of the Ta K x-ray pulse distribution.

Fig. 3.6 shows the data from a typical run. The filters for this run were 0.018" Sn + 0.003" Mo + 0.005" Cu + 0.003" Al. The lower curves are the raw experimental data. The upper inset curve shows the high energy region after background and scattering corrections. In this inset, the points are the raw data and the bold curve is the sum of the two Gaussians which represent the two γ-rays. The widths of the Gaussians were determined in the same way that the proportional counter line widths were determined (see Appendix I). For the present experiment, the percentage width (full width at half-maximum) is given by

$$w_{1/2} = 140 \frac{1}{\sqrt{E}} \ \% \quad ,$$

where E is the energy in kev units. The Gaussians are centered at 136 and 152 kev respectively, as determined by an independent energy calibration of the spectrometer. The heights of the Gaussians are adjusted

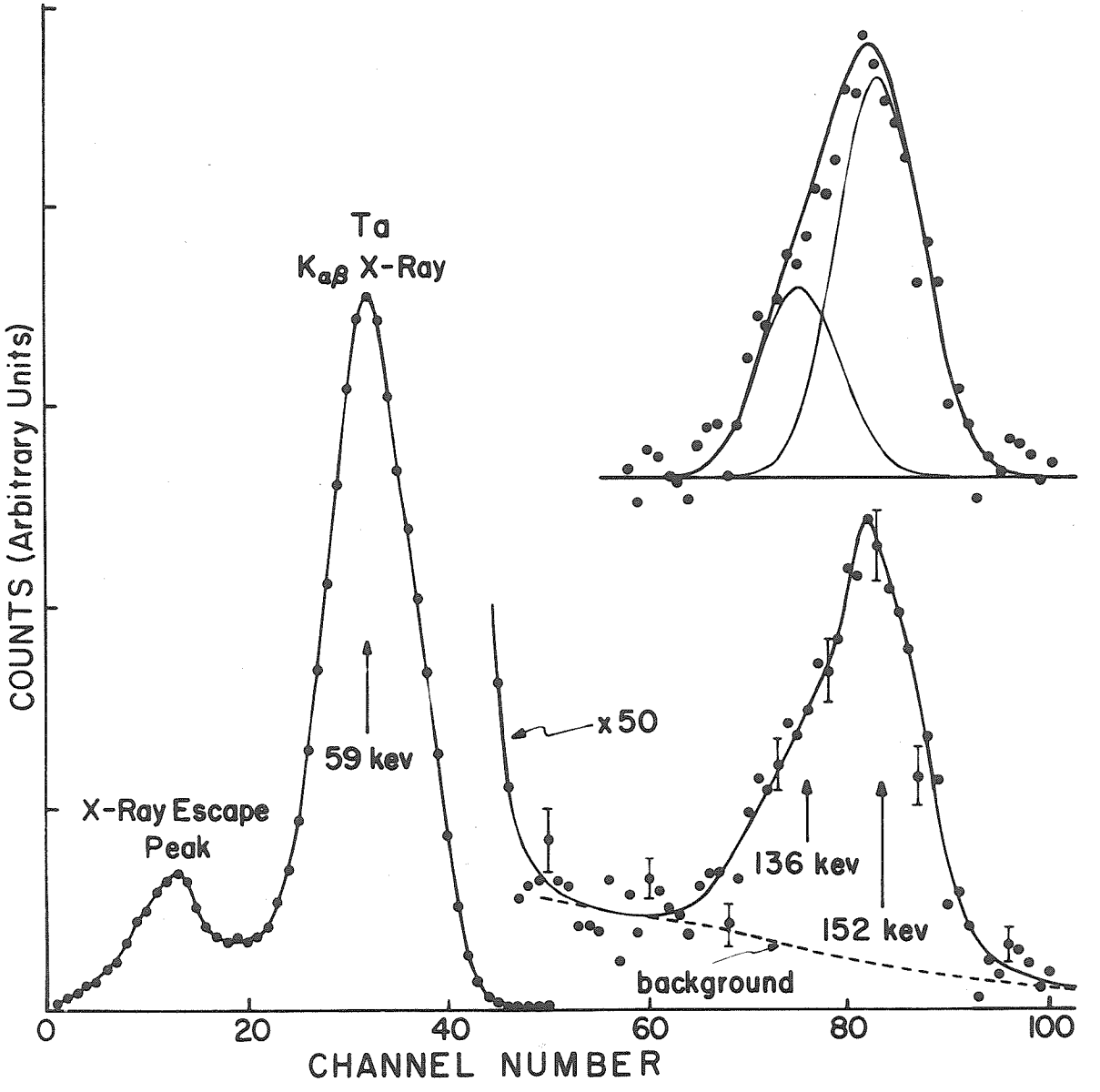

Fig. 3.6. NaI(Tl) scintillation spectrum from the W^{181} source showing the combined peak due to the 136 and 152 kev γ-ray transitions. Filters of Sn, Mo, Cu, and Al have been used to attenuate the intense K x-rays. The inset shows the experimental points (with background and scattering corrections) fitted with Gaussian curves.

until a "best fit" is obtained. The ratio of areas of the Gaussian curves gives the raw intensity ratio of the γ-rays. Several such runs were taken with different filters and in different geometry. Table IX summarizes the experimental conditions and findings and gives the corrected intensity ratio as well. The true intensity ratio is obtained by correcting* the raw intensity ratio for γ-ray absorption in the filters and aluminum crystal covering, and for transmission of the γ-rays through the crystal.

Table IX

Relative Intensity Measurements of the 136 and 152 Kev γ-Rays

Run	1	2	3	4	5
Filters					
Dy_2O_3					0.34 g/cm^2
Sn	0.018"	0.018"	0.018"	0.018"	0.018"
Mo			0.003"	0.003"	
Cu	0.005"	0.003"	0.005"	0.005"	
Al			0.003"	0.003"	
Source to filter distance	1/4"	1/8"	3"	1"	1/4"
Filter to crystal distance	3 1/4"	2"	3"	1 1/2"	4"
Raw I_{152}/I_{136}	1.72	2.12	1.72	2.17	1.95
True I_{152}/I_{136}	1.63	2.01	1.61	2.03	1.66

Averaging the true intensity values with equal weights, the final

---

* The attenuation coefficients of reference 26 were used in making these corrections.

result is

$$I_{152\gamma}/I_{136\gamma} = 1.80 \pm 0.3 \quad . \tag{19}$$

The ~15% estimated uncertainty allows for the statistical counting error and for error from the various corrections and decompositions. A calculation has shown that there is negligible "pile-up" of the K x-ray pulses in the high energy region. (This would not be the case if the filters were not used.) Furthermore, Compton scattering of the 152 kev γ-ray in the filter and crystal has been estimated to be less than 2%, hence this effect does not appreciably enhance the apparent 136 kev intensity.

An estimate of the strength of the high energy transitions can be made by comparing the composite 136, 152 kev γ-ray intensity to the K x-ray intensity. This was done for runs 1 through 4 of Table IX, and in addition for a run with no filters. Data from the run without filters were used to obtain the ratio of the K x-ray escape peak to the main x-ray peak, $I_{KX}e/I_{KX} = 0.143$. The filtered x-ray intensities were corrected for escape by means of this ratio. The direct experimental escape peak intensity (for example see Fig. 3.6) was not used because of the possibility of fluorescence x-rays from the filters contributing to the observed intensity in the escape region.* The results of these intensity measurements are given in Table X. The raw intensities were corrected for absorption in the filters etc. by the same method used with the Table IX data. A weighted average of the data yields the final result

$$I_{136,\,152\gamma}/I_{KX} = (1.2 \pm 0.3) \times 10^{-3} \quad . \tag{20}$$

---

* Run 5 of Table IX was not used for the γ-ray/x-ray intensity ratio measurement because of the presence of rather strong dysprosium fluorescence x-rays.

All values except the run 6 value were given a weight of 1. The run 6 value was given a weight of 1/2, since there is considerable uncertainty in the γ-ray intensity measurement when no filters are used. The estimated error allows for systematic as well as for statistical uncertainties.

Table X

Relative Intensity of the 136, 152 Kev γ-Rays to the K X-Rays

Run	1	2	3	4	6
Filters	(a)	(a)	(a)	(a)	none
Raw $I_{136,152}/I_{KX} \times 10^2$	1.37	1.14	1.17	1.56	0.0603
True $I_{136,152}/I_{KX} \times 10^3$	1.52	1.35	0.962	1.28	0.593

Note: (a) Same filters as for the corresponding run number in Table IX.

Branching Results

From these intensity measurements it is possible to determine the branching to the 136 and 152 kev transitions. For this purpose the abbreviated decay scheme of Fig. 3.7 is useful. For simplicity it is

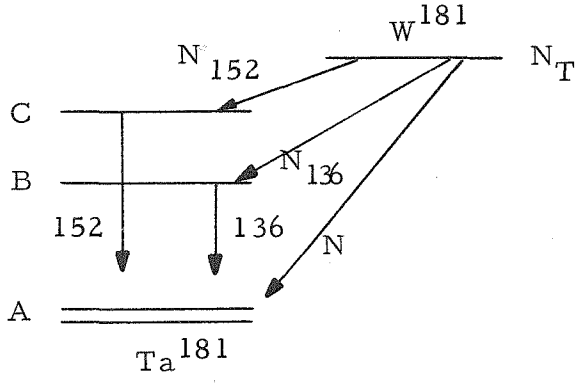

Fig. 3.7. Simplified W^{181} decay scheme.

assumed that no transition CB occurs, and that only transitions CA and BA occur from the upper levels. This assumption will be justified in Part IV C, where spins and multipolarities are discussed. If this assumption is not quite valid, then instead of determining the 152 kev branching, N_{152}, a lower limit is determined for this branching (and conversely for N_{136}). N_{152}/N_{136} can be calculated both from the γ-ray ratio and from the conversion electron ratio. The following formulas relate these quantities and the internal conversion coefficients:

$$\frac{N_{152}}{N_{136}} = \frac{I_{152\,\gamma}\ [1+\alpha_T(152)]}{I_{136\,\gamma}\ [1+\alpha_T(136)]} \tag{21a}$$

$$\frac{N_{152}}{N_{136}} = \frac{I_{152\,K}\ [1+\alpha_T(152)]\ \alpha_K(136)}{I_{136\,K}\ [1+\alpha_T(136)]\ \alpha_K(152)} \quad . \tag{21b}$$

Taking the conversion coefficients* from Appendix III, Parts A and B, and the intensity ratios from Eq. (17c) and Eq. (19), the resulting branching ratios are

$$\left(\frac{N_{152}}{N_{136}}\right)_\gamma = 1.55 \quad \text{and} \quad \left(\frac{N_{152}}{N_{136}}\right)_K = 1.80 \quad .$$

The weighted average of these values is

$$N_{152}/N_{136} = 1.6 \pm 0.3 \quad , \tag{22}$$

where the γ-value is given a weight 3 and the K-value a weight 1. The

---

* It is assumed that the 152 kev transition is pure M1 -- possibility 1) of Table A VI, Appendix III. Since α_K and α_T are each roughly the same for the three possible multipolarity choices, it can be seen that the wrong choice can only affect the branching calculations by about 15% at most.

γ-value is favored because the γ-intensity ratio is more accurately determined than the conversion ratio, and because Eq. (21a) is much less sensitive to small errors in the conversion coefficients than is Eq. (21b). From Eq. (22), the percentage branchings (of the total high energy transitions only) are

$$p_{136} = 38\% \quad \text{and} \quad p_{152} = 62\% \quad .$$

Let the combined branching to the upper two states be $N_u = N_{136} + N_{152}$. The ratio between N_u and N, the combined branching to the lower two states, is then

$$\frac{N_u}{N} = \frac{I_\gamma}{I_{KX}} \cdot \frac{N_K}{N} \cdot \frac{\omega_K}{p_{136}\,[\,1+\alpha_T(136)]^{-1} + p_{152}\,[\,1+\alpha_T(152)]^{-1}} \quad , \quad (23)$$

where I_γ / I_{KX} is the combined 136, 152 kev γ-ray intensity relative to the K x-rays, and N_K/N is the ratio of K-capture to total capture for the lower states given in Eq. (16). The preceding data, along with the γ-ray to x-ray ratio of Eq. (20) and ω_K of Table VII were used to evaluate N_u/N. The result of the calculation is

$$N_u/N = 1.98 \times 10^{-3} \quad .$$

From this value it follows that the total low-level branching is

$$N/N_T = 0.998 \quad .$$

All of the branchings, expressed as percentages of the total W^{181} decay, are listed in Table XI. The results of Eq. (15c) have been used in evaluating N_6 and N_0.

Table XI

Percentage Branchings in the W^{181} Decay

Level (a)	Branching %	Estimated error % (±)
$N_{136, 152}$	0.20	0.05
$N_{0, 6}$	99.8	0.1
N_{152}	0.12	0.03
N_{136}	0.075	0.018
N_6	34.9	10
N_0	64.9	10

Note: (a) Levels are designated by the energy of the depopulating γ-ray.

It is of interest to compare these branching results with the work of Debrunner et al. (10). The ratio of N_{152}/N_{136} from Eq. (22) is in close agreement with their value. The absolute values of N_{152} and N_{136} agree with the previous (10) values within the stated error, but the agreement is not particularly close (as in the case of the ratios). This small discrepancy may be due to a difference in the 136, 152 kev γ-ray intensity relative to the K x-rays caused by scattering or filter correction error. Unfortunately, Debrunner et al. did not publish their value for this intensity ratio.

H. Log ft Values

In order to understand the W^{181} decay better, it is important to know the comparative half-lives or ft values for the capture transitions to Ta^{181}. For this purpose the often used nomograph of Moszkowski (39) is not suitable, because L-capture is not taken into account and because the electron binding energies are neglected. Hoff and Rasmussen (40) give formulas for calculating f for allowed transitions. They state that these allowed f's can be applied to other types of transitions as well when comparisons are made with ft values for β-decay. These formulas are

$$f_K = \frac{\pi}{2} g_K^2 q_K^2 \tag{24a}$$

$$f_{L\,I} = \frac{\pi}{2} g_{L\,I}^2 q_{L\,I}^2 \tag{24b}$$

$$f_{L\,II} = \frac{\pi}{2} f_{L\,II}^2 q_{L\,II}^2 \tag{24c}$$

$$f_{L\,III} = 0 \tag{24d}$$

The g^2 (f^2) are the "large" ("small") components of the radial Dirac electron wave functions squared, evaluated at the nuclear surface. The q's are the capture-neutrino energies in $m_o c^2$ units.

To calculate the log ft values, the wave functions are taken from graphs in reference 35, and Eqs. (11) and (12) are used to obtain the q's. The W^{181} half-life is known (5) to be 145 days = 1.25×10^7 sec. The partial half-lives for the various transitions can be computed with the

aid of the branchings of Table XI. A correction* must be applied to the 152, 136 kev branchings to account for M + N + . . . -shell capture. Table XII shows the results of the ft calculations. The stated errors with log ft for 0 and 6 kev take into account the uncertainty in both the decay energy and branching. The errors in log ft for transitions to the higher levels only allow for decay energy uncertainty. For these cases the errors are extremely large because the corresponding q's depend strongly on the decay energy. The agreement between the log ft values for K and L capture to the 0 and 6 kev states is very good and thus represents a check on the branching measurements. Calculations are made for both 152 and 158 kev levels, since the 152 kev transition may terminate either at the ground state or the 6 kev state. This ambiguity will be eliminated shortly.

Table XII

Log ft Values for the W^{181} Decay

Transition to level at	f_K	f_L	$\log(ft)_K$	$\log(ft)_L$
0 kev	0.177	6.36×10^{-2}	$6.70^{+0.3}_{-0.2}$	$6.70^{+0.2}_{-0.1}$
6 kev	0.158	5.91×10^{-2}	$6.92^{+0.4}_{-0.2}$	$6.93^{+0.3}_{-0.1}$
136 kev	--	1.85×10^{-3}	--	7.59 ± 1
152 kev	--	3.37×10^{-4}	--	6.64 ± 1.5
158 kev	--	8.41×10^{-5}	--	6.04 ± 2

* See Chapt. 5.4 of reference 23.

PART IV

DISCUSSION

The results of the measurements will now be interpreted in terms of a level scheme for Ta^{181}. Although the present experiments alone allow several choices of levels and spins, it will be seen that a unique level scheme can be determined with the aid of data from previous experiments combined with nuclear model considerations.

A. Level Considerations from Experiment

The Ta^{181} level scheme reported by Debrunner et al. (8) must be modified to include the 6 kev transition. As has been previously mentioned, the data require a level at 6.25 kev. The Ta^{181} ground state is well known (5) to have spin 7/2+. The E1 character of the 6 kev transition then requires that the 6 kev level have spin 5/2, 7/2, or 9/2 and negative parity. Since the branchings to the 6 kev level and ground state from the 9/2+ W^{181} ground state* are roughly comparable, spin 5/2 is ruled out. If this were not the case, the capture transition to the 5/2 level would be first-forbidden, unique, contrary to the results of Parts III E and H. The 152 kev transition may lead from a 152 kev level to the ground state, or there is also the possibility that it may lead

---

* Here, and in the following discussion, the W^{181} ground state is taken as 9/2+, in agreement with the work of Gallagher et al. (41) on the Re^{181} decay. Previously Debrunner et al. (10) suggested a 7/2- assignment for this level, but recent considerations of Mottelson and Nilsson (4) show that the 9/2+ assignment should be correct. Bureau and Hammer (42) also concluded that this level should be 9/2+, which is in accord with the results of the present work.

from a 158 kev level to the 6 kev level.

If the K/L conversion ratio of Cork et al. (6) is used to conclude that the 152 kev transition is pure M1 or M1 with a small E2 admixture (see Appendix III B), then several possible level schemes can be constructed. These are indicated in Fig. 4.1. Spin 5/2 for the 158-152 kev

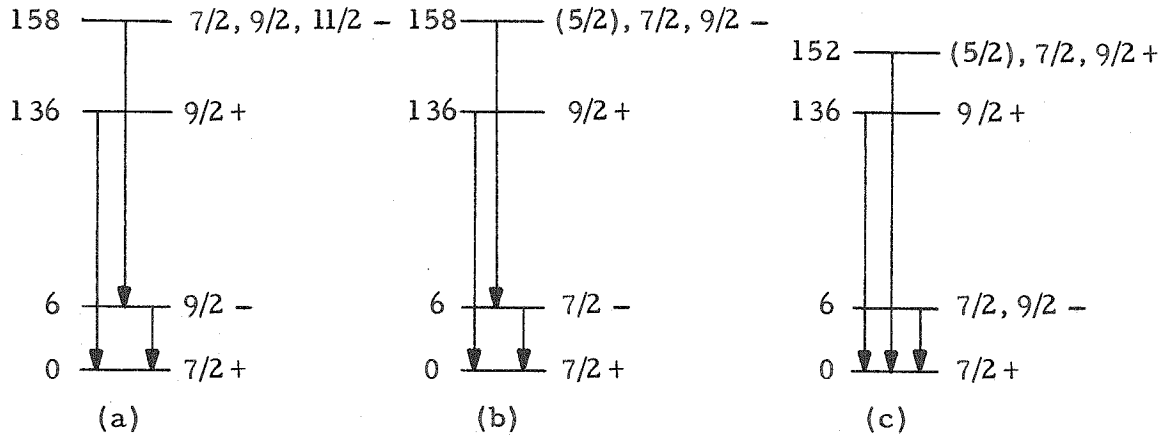

Fig. 4.1. Possible level schemes for Ta^{181}, assuming the 152 kev transition is M1 (+E2).

level is ruled out in view of the relative intensity of the L-capture from the 9/2+ W^{181} ground state to this level as compared to capture to the 9/2+ 136 kev level. For the same parity change, a $\Delta I = 2$ transition would be considerably less favored than a $\Delta I = 0, 1$ transition.

If, contrary to what has been assumed above, the 152 kev transition is assumed to be a multipolarity mixture of E1 + M2*, then several other level schemes are feasible. These are shown in Fig. 4.2. The 5/2 spins are ruled out on the same grounds as before.

---

* The multipolarity assignment of this transition is discussed in detail in Appendix III B. Pure M1 or M1 + E2 is strongly favored, although from conversion coefficient measurements alone E1 + M2 can not be ruled out, especially if the K/L conversion ratio of Cork et al. (6) is subject to question. Additional information on the conversion of the 152 kev transition would be very useful.

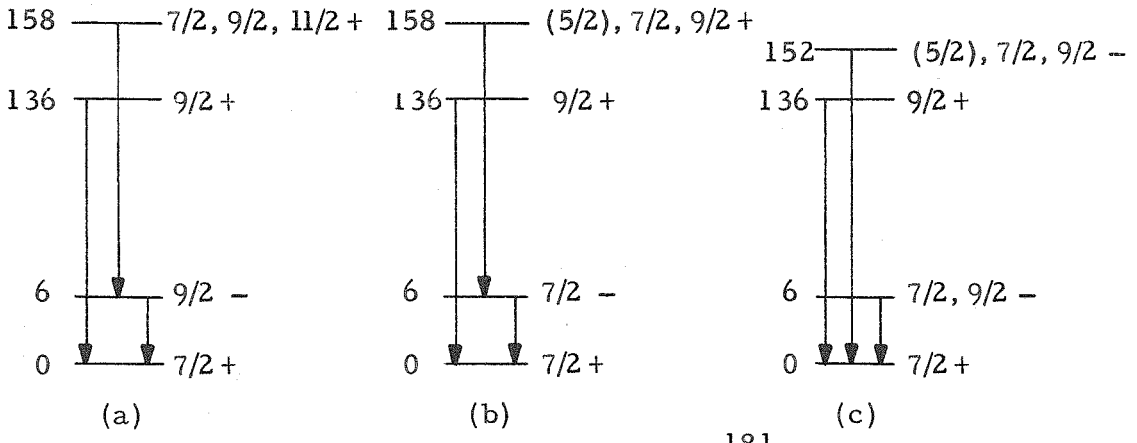

Fig. 4.2. Possible level schemes for Ta^{181}, assuming the 152 kev transition is E1 + M2.

On the basis of the branchings and log ft values alone, it is difficult to exclude any of the other possibilities of Figs. 4.1 and 4.2 because of the so-called asymptotic quantum number selection rules (43), (4). Selection rule effects can cause shifts in the expected ft values of factors of ten or more. However, information about the 476 kev transition can be used to rule out the 7/2- possibility for the 6 kev level. From the coincidence experiment results of Part III A it is concluded that the 476 kev transition feeds the 6 kev level. Using their internal conversion coefficient data (α_K = 0.06 and α_K/α_L = 4.3), Boehm and Marmier (9) tentatively assigned the 476 kev transition as M2. (On the basis of the conversion data alone, other possible assignments for this transition might be E1 + M2 or M1.) These authors' conversion and intensity data and the measured (5) 1.1 x 10^{-8} sec lifetime of the 5/2+ 482 kev level require the 476 kev transition γ-ray half-life to be ~7 x 10^{-7} sec. This lifetime indicates that the 476 kev transition must be M2 (with possible E3 admixture), since the single particle M2 lifetime

is $\sim 2 \times 10^{-8}$ sec (25). If a typical M2 retardation* of R = 100 is applied to the single particle estimate, it can be seen that a close agreement with the observed γ-lifetime is obtained. No admixture of E1 consistent with the conversion data, even allowing for a retardation* of 10^5, would permit such a long lifetime [$t_{sp}(E1) = \sim 10^{-15}$ sec]. Similar lifetime considerations exclude this transition from being classified as M1 [$t_{sp}(M1) = \sim 10^{-13}$ sec]. With the 476 kev transition assigned as M2, the 6 kev level must be 9/2-. With this choice of spin and parity, the M2 transition would be classified as unhindered -- in agreement with the observed lifetime.

---

* See Table 6. 32 of reference 23 for typical single particle lifetime retardations.

B. Level Considerations from Theory

The choice of 9/2− for the 6 kev level is in excellent accord with the nuclear model considerations of Nilsson (1), (4). The 9/2− [514] intrinsic level is expected (4) to be one of the low-lying excited states in Ta^{181}. Furthermore, the asymptotic quantum number selection rules (43), which are summarized in convenient form in reference 4, indicate that the W^{181} capture decay to the Ta^{181} ground state is classified as allowed, hindered, while the capture transition to the 6 kev level is classified as first-forbidden, unhindered. The log ft values of Table XII are in complete agreement with these classifications.

With the 6 kev level assigned as an intrinsic state, the question naturally arises as to whether or not the 152 kev transition occurs between an 11/2− rotational level at 158 kev and the 6 kev level. This possibility is shown in Fig. 4.1(a). The unified model (2) gives the following rotational level spacings:

$$E_{rot} = E_o + \frac{\hbar^2}{2\mathcal{I}} I(I+1) \quad . \tag{25}$$

This equation, which is good to first order (neglecting rotational-vibrational interaction), has an additional term for the case of a rotational band characterized by the quantum number K = 1/2. (References 2 and 4 should be consulted for definitions and terminology of the various quantities discussed here.) Eq. (25) can be used to predict where the first rotational level of the 9/2− intrinsic state would be expected.

In order to predict rotational levels with Eq. (25), some knowledge of the behavior of the nuclear moment of inertia, $\mathcal{I}$, in going from one

rotational band to another is necessary. Very few experimental data about this behavior are available, however the following approach represents a good first-approximation. Let C denote the coefficient from Eq. (25), $C = \hbar^2/2\mathcal{I}$. The ratio of C for the first excited state band to C for the ground state band has been computed for Lu^{175} and Re^{183}, which are nuclei analogous* to Ta^{181}. The average ratio is 0.95. For the ground state K = 7/2+ rotational band in Ta^{181}, the value of C is 15.14 kev. From this value and the above average ratio, it is estimated that the K = 9/2− band in Ta^{181} has C = ~14.4 kev. Eq. (25) then gives $E_{rot}(1^{st})$ = ~158 kev or a first rotational level at ~164 kev.

Since L-capture from W^{181} to the predicted rotational level is energetically possible, an 11/2− rotational level at 158 kev seems very likely. The ft value for such a transition (first-forbidden, unhindered) should be roughly comparable to the ft value for the (allowed, hindered) capture transition to the 9/2+ 136 kev level. Table XII shows that, within the stated error, the experimental ft values are indeed comparable.

The preceding arguments make an 11/2− 158 kev level plausible. In Appendix IV detailed arguments are presented that show that this choice is unique. The selection rules combined with observations from the W^{181} and Hf^{181} decays exclude all the other possibilities of Figs. 4.1 and 4.2.

In agreement with the log ft values of Table XII, the transitions to the K = 7/2+ rotational band are allowed, hindered, while the

---

* These are two odd-proton nuclei, close to W^{181} in A, for which the ground state has even parity, and for which 9/2⁻[514] is the first excited intrinsic state.

transitions to the K = 9/2− band are first-forbidden, unhindered. That the ft value for the transition to the 9/2+ first rotational level is larger than the ft value for the 7/2+ ground state transition, has also been observed (4) in the similar decay of Yb^{177}. Indeed, theory (44) predicts the ft values to be in the ratio*

$$\frac{ft\left(\frac{9}{2}+ \rightarrow \frac{9}{2}+\right)}{ft\left(\frac{9}{2}+ \rightarrow \frac{7}{2}+\right)} = \frac{\left\langle \frac{9}{2}\ 1\ \frac{9}{2}\ -1 \,\middle|\, \frac{9}{2}\ 1\ \frac{7}{2}\ \frac{7}{2}\right\rangle^2}{\left\langle \frac{9}{2}\ 1\ \frac{9}{2}\ -1 \,\middle|\, \frac{9}{2}\ 1\ \frac{9}{2}\ \frac{7}{2}\right\rangle^2} = 4.30 \quad . \qquad (26)$$

This ratio corresponds to a $\Delta(\log ft) = 0.63$. The difference in the experimental log ft's from Table XII (= 0.90) agrees with this theoretical value within the stated experimental errors. The corresponding ft ratio for the capture transitions to the K = 9/2− band has not been calculated, since for forbidden transitions it is not possible to make a unique choice of interaction matrix elements.

---

* In obtaining Eq. (26) it is assumed that the Fermi interaction contribution to the 9/2→9/2 transition is negligible. The fact that this is usually the case in transitions of this type has been verified by experiment (45), and is reasonable from isotopic spin selection rule considerations. The Clebsch-Gordan coefficients are evaluated with the aid of Table 9.71 of reference 23.

C. Conclusions

The complete level scheme of Ta^{181}, including a new decay scheme for W^{181} proposed on the grounds of this work, is shown in Fig. 4.3. This level scheme is entirely consistent with all experimental evidence and also is in accord with theoretical considerations. Information in the figure not directly obtained in the course of the present investigations has been taken from the literature (5). The features of special significance in this level scheme are 1) the appearance of a new 9/2− intrinsic level at 6.25 kev above the 7/2+ ground state, 2) the re-assignment of the previously suggested (10) 152 kev level as an 11/2− rotational level at 158 kev, and finally 3) the absence of the proposed (9) level at 958 kev. A 1/2− [541] level at 958 kev would be rather unusual from Nilsson model (1), (4) considerations since this would require a level from above* magic number 82 to compete with levels from below* magic number 82. The relocation of the 476 kev transition eliminates this predicament.

The 22 kev transition between the 11/2− and 9/2+ level has not been observed. In view of the proposed level arrangement, it is extremely unlikely that this transition could be detected because of intensity considerations. The Weisskopf estimate of the 22 kev E1 transition probability is roughly comparable to the 152 kev M1 transition probability. From selection rules (4), however, the E1 transition is classified as hindered, while the M1 is classified as unhindered. Thus the 22 kev transition should be retarded by a factor of at least 10^3 relative to the

---

* Level ordering on the low deformation approximation (shell model limit).

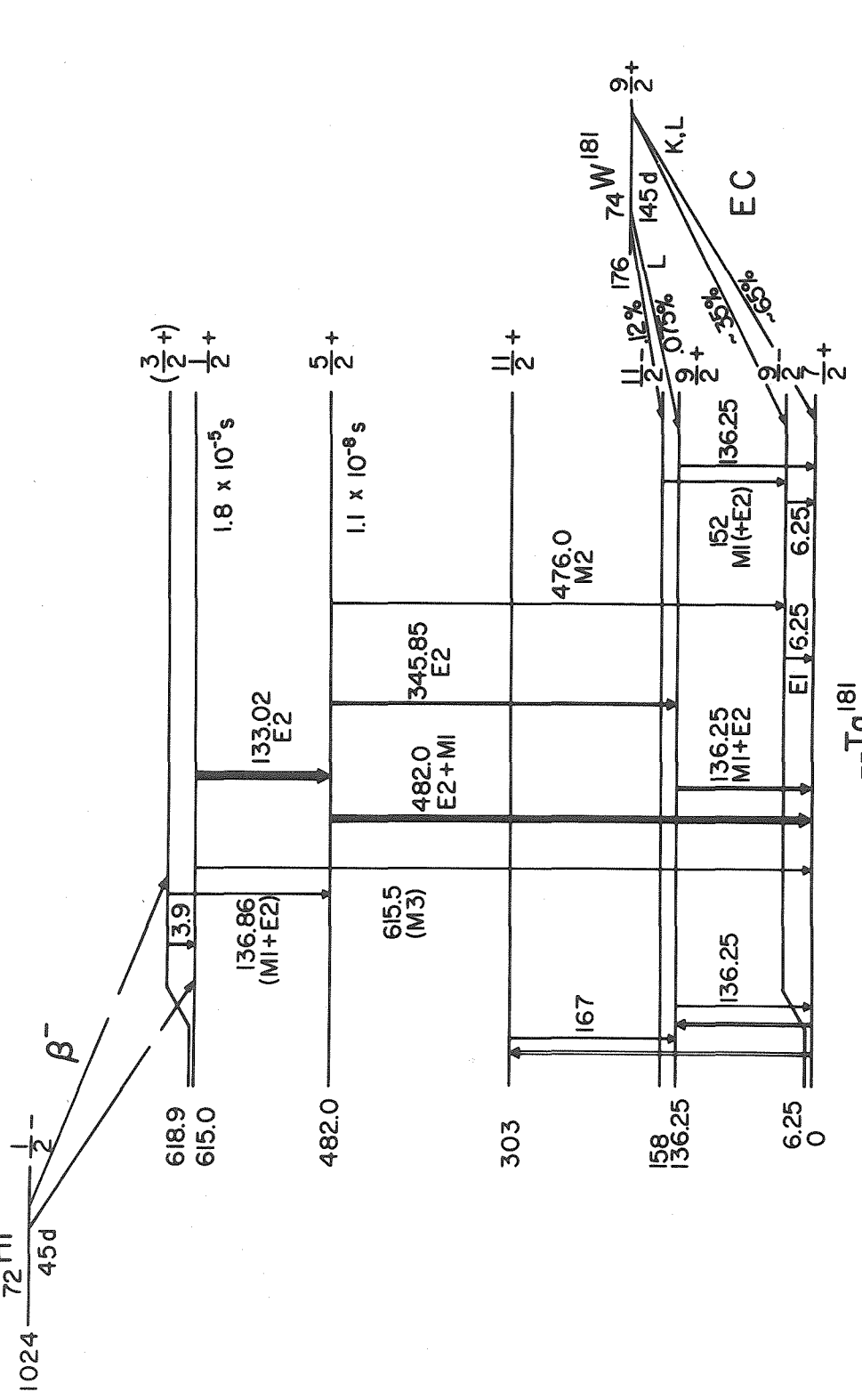

Fig. 4.3. Complete Ta^{181} level scheme showing the 9/2 – 6.25 kev level. The 152 kev transition is placed between the new 11/2 – 158 kev rotational level and the 6 kev level. All assignments are consistent with both theory and experiment.

152 kev one. Consequently, if present at all, the 22 kev transition would be extremely weak. This means that the neglect of this transition in determining the branching to the 158 and 136 kev levels is valid and that the approach of Part III G is correct.

On the basis of the unified model, Chase and Wilets (46) have calculated that the 396 kev E1 9/2− [514] → 7/2+[404] transition in Lu^{175} is retarded by a factor of 7×10^5 compared to the single particle estimate. Since this transition occurs between the same Nilsson states as the 6 kev transition, it is interesting to note that this theoretical retardation is in rough agreement with the anomalous conversion coefficient estimate of the 6 kev E1 retardation, $R_6 \approx 2 \times 10^5$ (see Part III B). On the other hand, it should be pointed out that the retardation of the 396 kev Lu^{175} γ-ray can be determined from the experimental lifetime of the 396 kev level, $t_{1/2} = 3.4 \times 10^{-9}$ sec, measured by Vartapétian (47) and the γ-ray and conversion intensities of Hatch et al. (48). The result is $R_{396} = 4.3 \times 10^6$ -- a factor of 6 larger than Chase and Wilets' (46) estimate. It is not possible to attribute this difference to a large error in the γ-ray lifetime, since Runge et al. (49) remeasured this lifetime and obtained essentially the same results as Vartapétian (47). From these considerations it follows that the 6 kev γ-ray lifetime estimate of Eq. (5), $t_\gamma \approx 1 \times 10^{-4}$ sec, probably represents the true lifetime within a factor of about 10. Any deviation from this estimate would be expected to be in the direction of a longer lifetime.

Fig. 4.4 is a pictorial plot of the intrinsic states of several odd-Z nuclei near Ta^{181}. * The left-hand scale gives the approximate energy ordering of the Nilsson (4) single particle levels for odd-Z nuclei with a deformation $\delta = 0.23$. Level proton occupancy numbers are also given. The intrinsic level schematics are arranged with increasing A and Z. Large deformation asymptotic quantum numbers designate the various intrinsic levels. Ground states are matched in energy to the corresponding levels on the left scale. Most of the level assignments are taken from Mottelson and Nilsson (4). The Lu^{173} level assignments may be interchanged, but at present no clear choice can be made. The Re^{187} data are from the studies of others (50) in this laboratory.

Some interesting exceptions to the orderly filling of the Nilsson levels are shown in Fig. 4.4. The tantalum odd-A isotopes are expected to have 5/2+ ground states, but 7/2+ ground states are observed. Likewise, rhenium odd-A isotopes are expected to have 9/2− ground states, but 5/2+ are observed. Ground states of iridium odd-A isotopes fill the 3/2+ level which is at a considerably higher total excitation energy than the previously mentioned intrinsic levels. The curious result is that the 9/2− level does not seem to occur as a ground state, although in Ta^{179} and Ta^{181} it is almost a "degenerate ground state". In view of this, information on the intrinsic levels in Ta^{183} and Ta^{185} might be most interesting. Pairing energy effects are probably the cause of these deviations from the Nilsson predictions.

---

* A similar intrinsic level representation has been given previously by Hatch et al. (48).

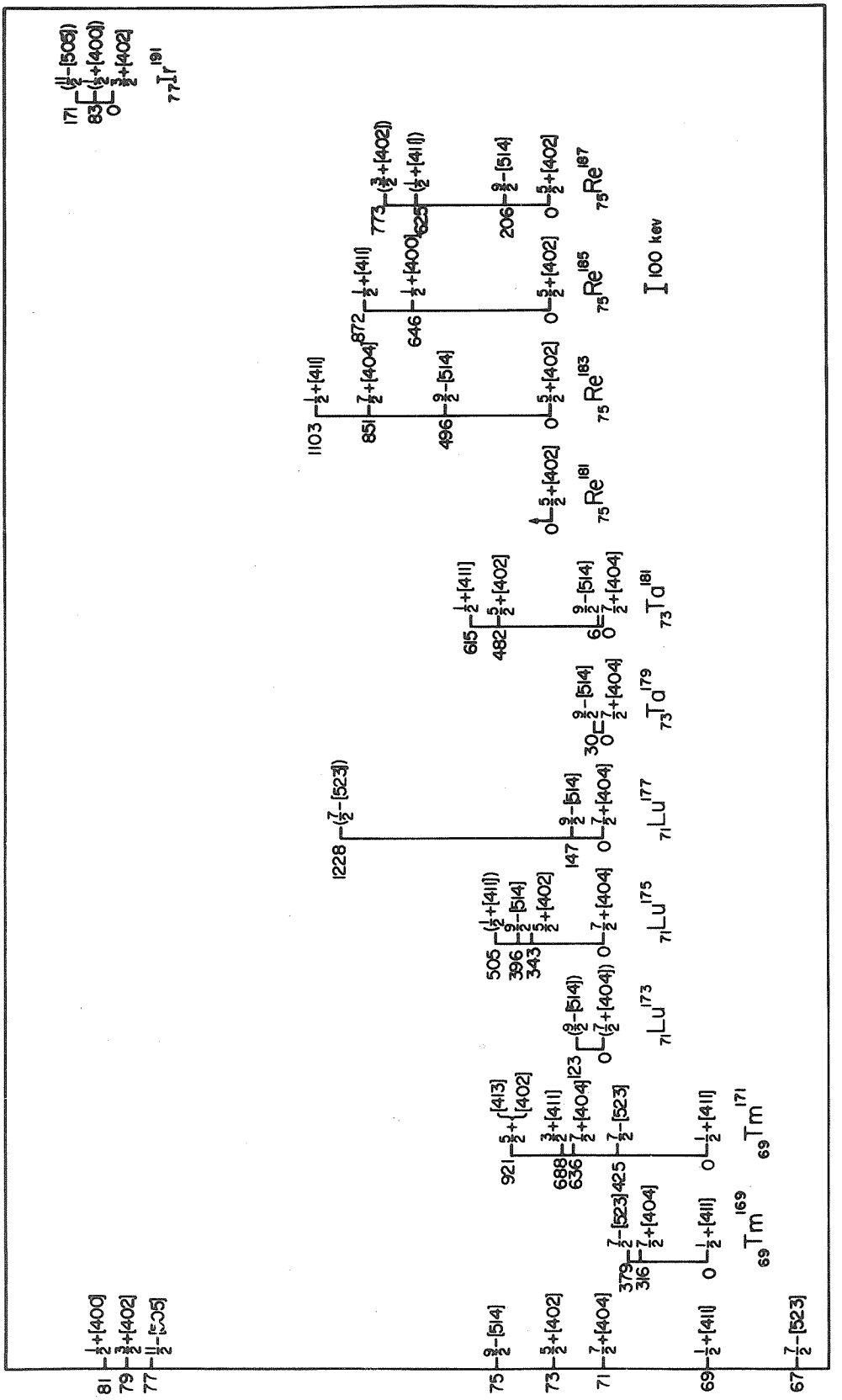

Fig. 4.4. Intrinsic levels in some odd-A nuclei near A = 181. The left scale gives level proton occupancy number along with level energy ordering obtained from the Nilsson diagram assuming a deformation of $\delta = 0.23$. Each level is denoted by its energy, spin, parity, and asymptotic quantum numbers, $[N\, n_z\, \Lambda]$. Ground states are matched in energy to the corresponding Nilsson prediction.

In summary, the 9/2− [514] assignment for the 6 kev level in Ta^{181} is extremely plausible from the level systematics of neighboring nuclei. In Fig. 4.4, from Lu^{175} to Ta^{181}, the 9/2 − level is seen to move closer to the 7/2+ ground state with increasing A. The new level clarifies the W^{181} decay and explains the weak 476 kev transition in the Hf^{181} decay. It is especially interesting that the 9/2− 6 kev level is one of the lowest lying intrinsic states presently known. (The only lower lying intrinsic state is the unusual 1/2+ 0.08 kev level in U^{235} -- see reference 4.) All experimental findings are consistent with the unified model (1), (2). The W^{181} capture decay energy determined in this work, Q_{EC} = 176 kev, is one of the few electron capture decay energies (32) that has been inferred from the experimental L/K capture ratio. Finally, it can be pointed out that extremely low energy nuclear spectroscopy can be a valuable tool for exploring nuclear structure.

APPENDIX I

PROPORTIONAL COUNTERS

For the study of the low energy electromagnetic spectra in the W^{181} and Hf^{181} decays, two gas-filled proportional counters were built. Details of the design, construction, and operation of these counters will now be given.

Proportional counters of various types have been used in nuclear spectroscopy for well over ten years. The books of Korff (51) and Rossi and Staub (52) give quite general treatments of this subject. In particular, they consider such questions as gain, linearity, resolution, and efficiency in relation to the geometry of the counter, the operating voltage, the filling gas mixture and pressure, and other variables. A recent review of West (53) deals with many points of practical importance in the operation of proportional counters for spectroscopy and includes an extensive bibliography. Other comprehensive discussions of proportional counters have been presented by Curran (54).

Design and Construction

The design of the present proportional counters is similar to that used by Wu and co-workers (55). Two identical counters were constructed -- one of which was filled with argon and the other with xenon. Each counter envelope was formed from 100 mm o.d. Pyrex 7740 tubing. First one end of the tubing was sealed by drawing the glass down to a hemisphere. A hole 1" in diameter was then made in the wall

of the tubing for the window. The lip of the hole was ground smooth to form a surface for cementing the window in place. Following this, the cathode was made from 2S-O (99.4% pure) aluminum sheet, 0.025" thick (22 gauge), 12" x 10", as shown in Fig. A 1.1(a).

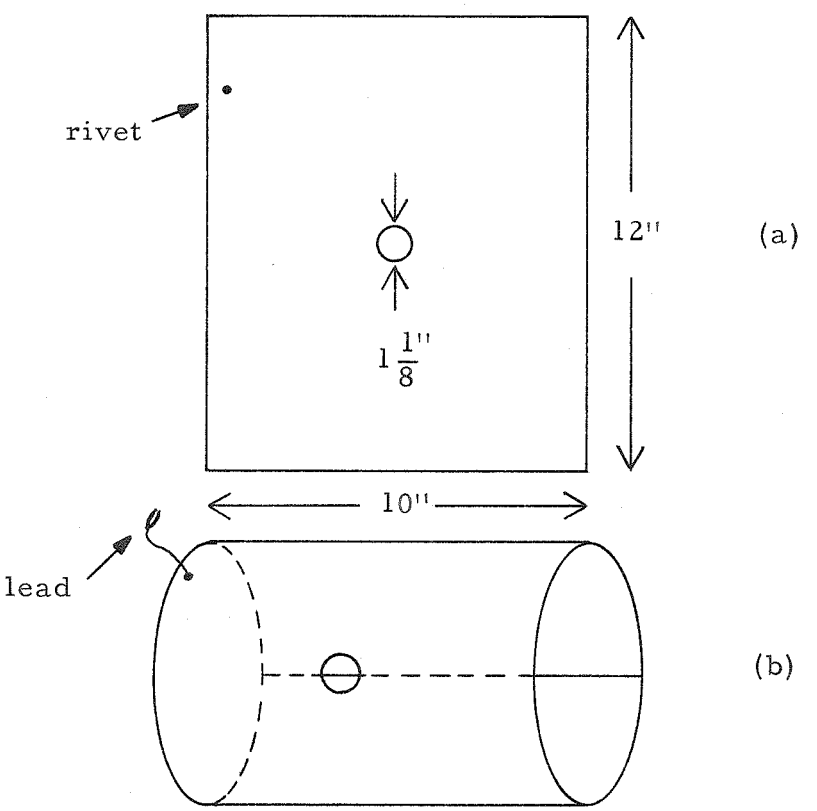

Fig. A 1.1. Cathode construction (material: 22 gauge 2 S-O aluminum).

A 1 1/8" hole was placed at the center with a chassis punch. A small hole was drilled near the edge of the long side and a small brass rivet fastened in the hole to form a soldering lug. The sheet was then formed into a "springy" cylinder 10" long by carefully rolling it around a piece of 4" diameter round stock. A

flexible lead with a small alligator clip at one end was finally soldered to the brass rivet as shown in Fig. A 1. 1(b).

After completing the cathode, the "bottle" and the cathode were carefully cleaned successively with distilled water, reagent grade acetone, carbon tetrachloride, and absolute alcohol. The cathode was then fitted into the bottle, the holes being aligned at that time. A short side arm for the cathode lead was provided and a short length of heavy tungsten wire was sealed into the side arm. At this point the alligator clip was used to attach the cathode to the tungsten wire seal. Next the other end of the bottle was drawn down and closed as indicated in Fig. A 1. 2. The over-all length of the bottle was about 14 1/2 inches.

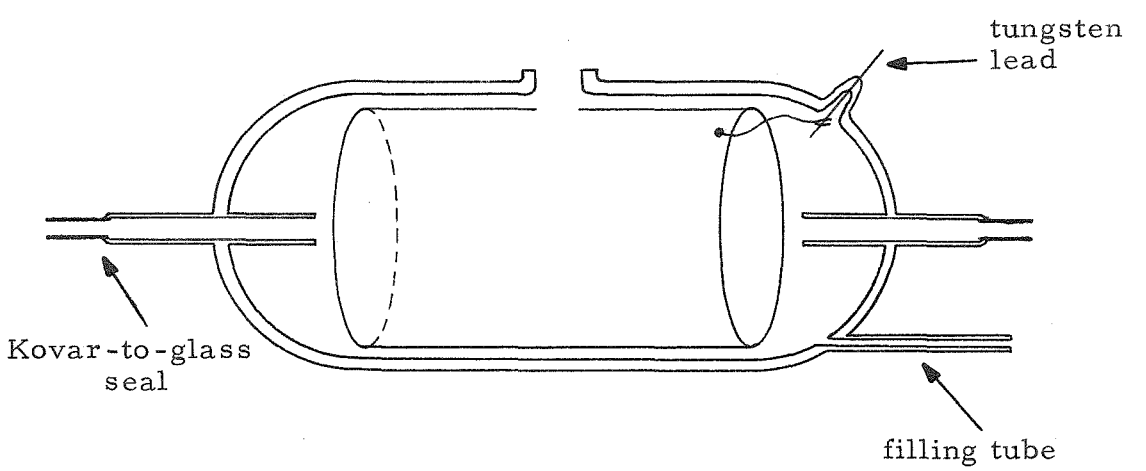

Fig. A 1. 2. Preliminary counter assembly - - aluminum cathode sealed in Pyrex counter "bottle".

Two Kovar-to-glass seals were prepared to accomodate the anode assembly. 1/8" Kovar tubing was sealed to Pyrex tubing, taking care

that no uranium glass was used in the seal. With the counter tube mounted in the glass lathe, the Kovar seals were attached to the ends of the tube, allowing the glass tubing to protrude a few inches into either end of the bottle for a guard tube. Great care was taken to see that the two tubes were coaxial with each other and with the glass cylinder. Finally the filling tube was added.

The anode was constructed by fastening a 0.003" tungsten wire between two brass holders. The holders, shown in Fig. A 1.3, were made by turning down one end of a 3/32" brass rod which was then drilled to provide a 0.007" diameter hole. To attach the wire to the holders, each end of the wire was inserted into one of the 0.007" holes. The

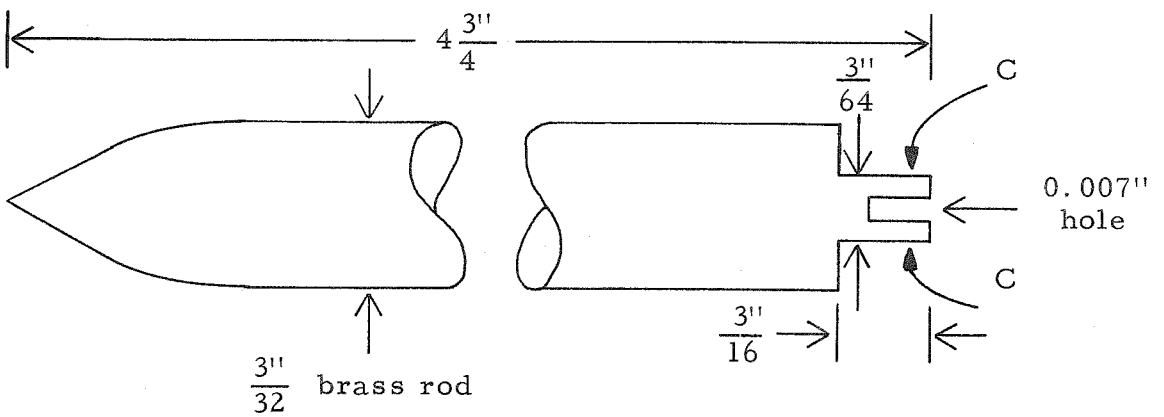

Fig. A 1.3. Anode holder detail.

wire was secured in place by crimping the holders at point C indicated in Fig. A 1.3. The opposite ends of the holders were pointed for ease in threading the anode assembly through the Kovar-to-glass seals. The anode was finished by soldering the brass holders to the Kovar seals, taking care to get a vacuum tight joint. In soldering the second holder,

the anode assembly was put under tension so as to keep the wire straight. A final careful cleaning followed.

To complete the counter, a 3 mg/cm^2 mica window was cemented to the window flange with Epibond 100*, a heat cured epoxy resin. The whole counter was first carefully heated in an oven to 148°C. The Epibond, which had been cast into sticks by gentle heating, was applied to the warm window flange. The counter was returned to the oven for 15 minutes to allow the resin to become thoroughly soft. The window was then put in place and lightly pressed down to the flange. Finally the whole assembly was baked at 148°C for 4 1/2 hours to cure the resin. Fig. A 1.4 shows the final assembled counter.

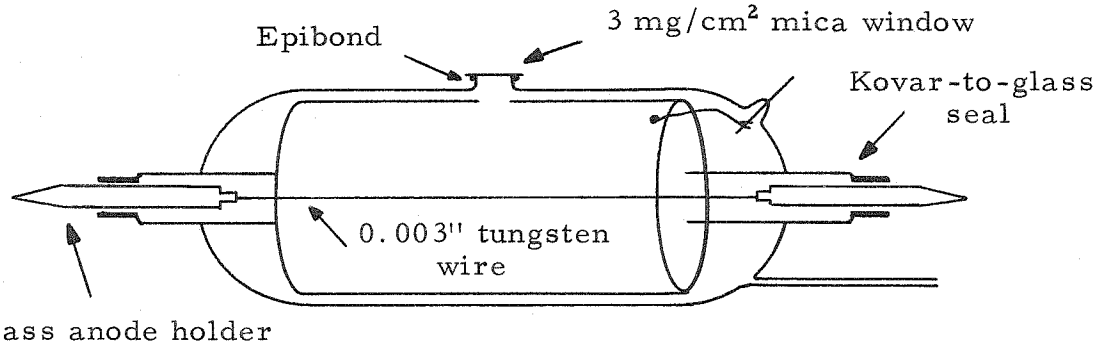

Fig. A 1.4. Proportional counter -- final assembly.

Counter Filling

The argon counter was filled with a commercially prepared mixture of 90% argon and 10% methane which was available† in a high pressure tank. The xenon counter was filled with the gas from a one liter Pyrex

---

* Supplied by Furane Plastics, Inc., 4516 Brazil St., Los Angeles 39, California.

† Supplied by Matheson Company, Inc., East Rutherford, N.J.

flask* and methane* was added until the pressure in the system was increased by about 10%.

The gas handling system was conventional, and contained an oil diffusion pump with forepump, liquid air cold trap, high vacuum gauge, low vacuum gauge, and appropriate valves for controlling the gases and counter. The system was made of copper tubing with bellows-type packless valves† and had a sylphon bellows joined to a Kovar-to-glass seal to allow for flexibility in connecting the glass counter to the metal system.

Evacuation and filling had to be accomplished very slowly to prevent the thin window from getting too much strain. First the counter and filling systems were brought to high vacuum ($\sim 4 \times 10^{-6}$ mm of Hg) and kept at high vacuum for about 2 to 3 weeks to allow the system to outgas as much as was practical. During this period the anode filament was heated to red heat with a Variac for a short while to further its outgassing. After outgassing, the pump was closed off and the counter filled. The counter was then sealed off permanently from the system at a constriction previously made in the filling tube. The argon counter was filled to a total pressure of one atmosphere, while the final pressure in the xenon counter turned out to be 0.39 atmosphere.

It might be remarked at this point that these counters have been in intermittent operation over a period of more than 3 years with the same

---

* Supplied by Matheson Company, Inc., East Rutherford, N.J.

† Supplied by Hoke, Inc., Englewood, N.J.

gas filling without any apparent loss of efficiency or resolution. Because of the care given to the outgassing of the counters it was possible to permanently seal them and remove them from the gas handling system. If several counters with different gases and pressures are constructed in this manner, one obtains a number of advantages over both the flow type and refillable non-flow type proportional counters also in common use.

Operation

To provide electrostatic as well as background radiation shielding, the counter is housed in a large iron box. With this arrangement the background was usually quite low.

The circuit employed is shown in Fig. A 1.5. The anode is at ground potential and the cathode is connected to a negative super-stabilized high voltage supply. A filter consisting of two 0.25 μf, 3000 volt condensers and a small r.f. choke was found necessary to suppress the high frequency ripple found in some power supplies used. For the operation of the counter as a spectrometer the following

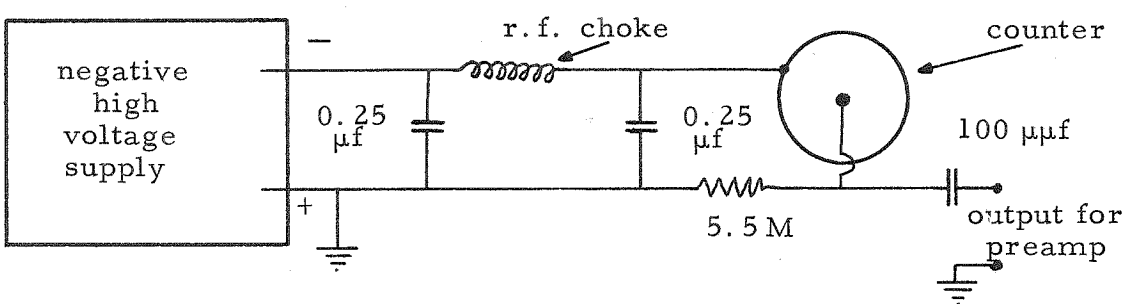

Fig. A 1.5. Proportional counter voltage supply circuit.

electronic components were employed: a modified Hamner model N401 high voltage supply and either 1) a Baird-Atomic model 219 preamplifier, model 218 linear amplifier, model 510 single channel pulse height analyzer, and model 131A glow tube scaler; or 2) a Franklin model 349 preamplifier, model 348 linear amplifier, and a Penco model PA-4 100 channel pulse height analyzer. The argon counter was found to operate satisfactorily at 2300 to 2800 volts, while the xenon counter was usually operated at 1800 to 1900 volts, although the exact selection of voltage depends somewhat on the nature of the problem being studied.

In the usual operation it was necessary to prevent electrons from the source (β-rays and conversion electrons) from entering the counter. This was accomplished by requiring the radiation entering the counter to pass through the gap of a strong permanent magnet. The magnet pole pieces were capped with Plexiglas to reduce bremsstrahlung production. To make relative intensity measurements of high and low energy radiation, it was found necessary to shield the counter as shown in Fig. A 1.6 because of the differential penetration of the glass walls by the different energy photons.

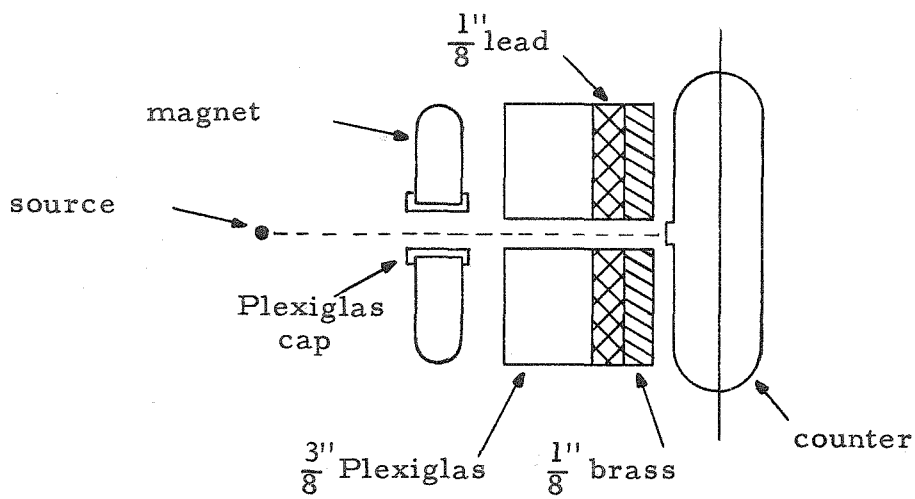

Fig. A 1.6. Arrangement for counter collimation and shielding.

Escape Peak

An important consideration in the operation of most proportional counters is the occurrence of an escape peak at an energy equal to the transition energy less the energy of the x-ray (usually K) of the filling gas. For the argon counter the escape peak is ordinarily much smaller than the main peak, while for the xenon counter the K escape peak may be quite a bit larger than the main peak. This is principally due to the fact that the K x-ray fluorescence yield (23) of xenon (0.870) is much larger than that of argon (0.081). Usually with the xenon counter two K escape peaks are seen -- the more intense one resulting from the escape of xenon K_α x-rays and the less intense one resulting from the escape of K_β x-rays. In addition, L x-ray escape peaks may occur, but are resolved only in the xenon counter for lines of low energy compared to the xenon K binding energy. Some of these escape features will be pointed out in the section on results where typical spectra are presented.

Although generally a nuisance, the escape peak may be of unique value. Two neighboring lines, unresolved in the main peaks, may be resolved in the escape peak, since the energy separation is the same though the lines now effectively occur at lower energy.

Exact analysis of the escape behavior is difficult. West (53) indicates approximate methods and estimates the escape fraction (which will be denoted P_e, the fraction of the total pulses appearing in the escape peak) for a 5 cm diameter counter filled with different gases at different pressures.

Attempts were made to calculate the escape fraction for both of the counters. The approach was similar to that employed (56) in calculating the escape fraction for scintillation crystals. For proportional counters, however, the "infinite slab of infinite thickness" approximation that is useful with scintillation crystals is no longer valid. A more realistic approach is to approximate the counter by means of an infinte slab of thickness equal to the counter diameter. A further improvement is obtained by employing a very approximate correction to the "slab counter" results to make them more nearly correspond to the case of a cylindrical counter. Still the agreement between the calculations and experiment leaves much to be desired, as can be seen from Fig. A 1.7. Here the escape ratio f_e ($= \frac{P_e}{1 - P_e}$, the ratio of the escape peak to the main peak) is plotted as a function of the incident photon energy for the argon counter. The experimental points are obtained by comparing the area of the escape peak to that of the main peak for various spectra taken with the counter. The calculated values are for the "slab counter with cylindrical correction" approximation*.

---

* Approximating the counter by an infinite slab of thickness equal to the counter diameter yields the following formula:

$$P_e = \frac{1}{2}\omega p_K \left\{ 1 - \frac{\mu_x}{\mu_\gamma} \ln\left(1 + \frac{\mu_\gamma}{\mu_x}\right) - e^{-(\mu_x + \mu_\gamma)T} + \frac{\mu_x}{\mu_\gamma} \mathrm{Ei}\left[-(\mu_x + \mu_\gamma)T\right] \right.$$
$$- \left(\frac{\mu_x}{\mu_\gamma} + \mu_x T\right) e^{-\mu_\gamma T} \mathrm{Ei}(-\mu_x T) - e^{-\mu_\gamma T}\left[1 + \frac{\mu_x}{\mu_\gamma} \ln\left|1 - \frac{\mu_\gamma}{\mu_x}\right|\right]$$
$$\left. + e^{-\mu_x T} + \frac{\mu_x}{\mu_\gamma} e^{-\mu_\gamma T} \mathrm{Ei}\left[-(\mu_x - \mu_\gamma)T\right] + \left(\mu_x T - \frac{\mu_x}{\mu_\gamma}\right) \mathrm{Ei}(-\mu_x T) \right\}$$
$$\times \left[1 + \mu_x R\, e^{+\mu_x R}\, \mathrm{Ei}(-\mu_x R)\right]^{-1} , \qquad \text{(A 1)}$$

(Footnote continued on p. 98 .)

ARGON COUNTER

ESCAPE RATIO

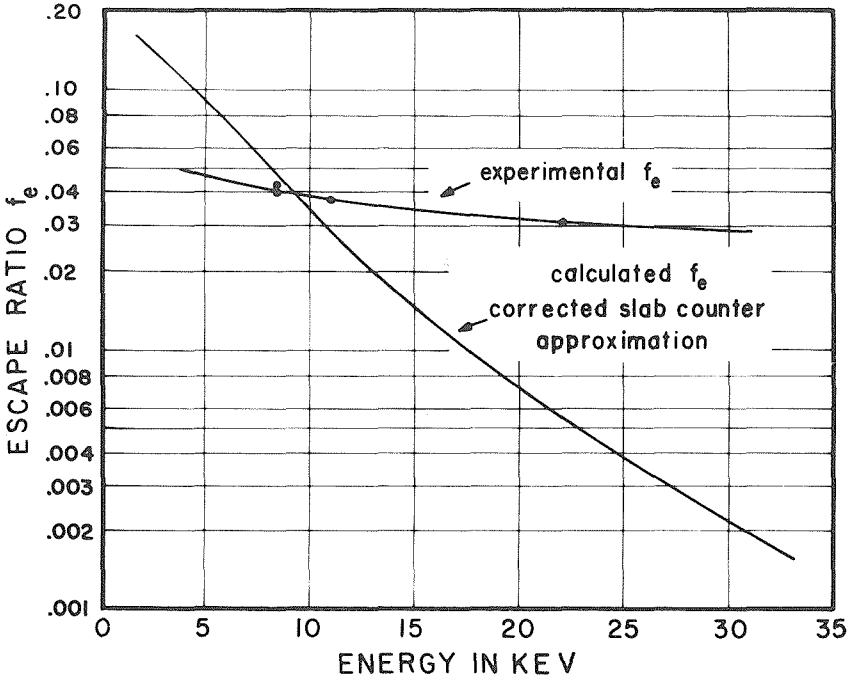

Fig. A1.7. Escape ratio, f_e, for the argon counter. "Slab counter" approximation calculation is compared to experimental evaluation.

XENON COUNTER

RESOLUTION

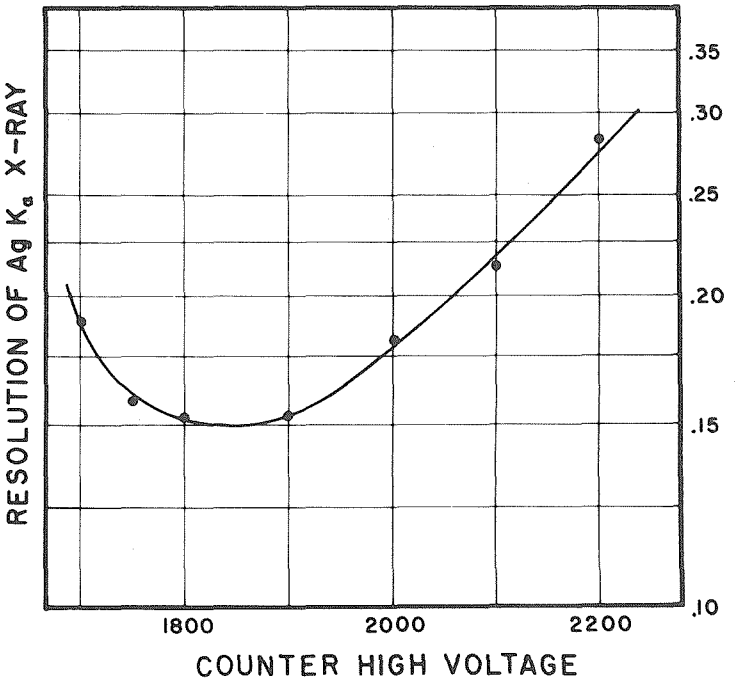

Fig. A1.8. Dependence of the effective resolution of the xenon counter on the voltage applied to the tube.

If we try a better approximation -- a spherical counter of radius equal to the cylindrical counter radius -- we obtain the following integral:

$$P_e = \frac{1}{2}\mu_\gamma \omega p_K \int_0^{2R}\int_0^{\pi} \exp\left\{-\mu_\gamma x - \mu_x \left[-(R-x)\cos\theta + \sqrt{(R-x)^2\cos^2\theta - x(x-2R)}\right]\right\} \sin\theta \, d\theta \, dx \quad , \qquad (A\,2)$$

where P_e is the escape fraction (fraction of total pulses in escape peak)

R is the counter radius in cm

μ_γ is the absorption coefficient for the incident radiation in cm^{-1}

μ_x is the absorption coefficient for the escaping x-rays in cm^{-1}

ω is the appropriate (usually K) x-ray fluorescence yield

p_K is a small correction factor to account for the relative probability of photoelectric excitation in the different shells and is treated by West (53). The numerical integration of Eq. (A 2) would be quite involved, and it was felt that this would not be worthwhile since this equation too represents an approximation. For those uses of the counter where the evaluation of the escape peak is essential, the most straightforward approach is to measure this effect experimentally and extrapolate the results to the region of interest as indicated in Fig. A 1.7.

Resolution

With proportional counters, for a given set of operating conditions,

---

where T = 2R is the thickness of the slab (10 cm) and the other symbols have the same meaning as in Eq. (A 2) to follow in the text. Ei(−x) is a type of exponential integral defined and tabulated in Jahnke and Emde, reference 57. The term in {} brackets is the result of the true slab approximation, and the multiplicative term at the end is the quasi-cylindrical correction factor. The first two terms in the {} brackets represent the infinite slab of infinite thickness in agreement with results of reference 56, as can be seen by letting T in Eq. (A 1) approach infinity.

the resolution (relative full width at half-maximum), $w_{1/2}$, varies approximately as the inverse square root of the energy. This relationship, which holds over the usual energy region of application of the counters, may be expressed as follows:

$$w_{1/2} = \frac{\Delta E}{E} = k \frac{1}{\sqrt{E}} \quad , \qquad \text{(A 3)}$$

where E is the energy in kev. For the argon counter k is about 0.45 $(\text{kev})^{1/2}$ when the counter is run at 2760 volts and is fairly constant over the region from 6 kev to 30 kev. For the xenon counter run at 1850 volts, a typical value of k in Eq. (A 3) is about 0.70 $(\text{kev})^{1/2}$. Thus under the above conditions, the resolution of the 22 kev silver K x-rays from Cd^{109} * is about 10% for the argon counter and 15% for the xenon counter. For typical operation of sodium iodide scintillation crystals†, the corresponding value of k is 2 to 4 times larger than the values quoted for the gas proportional counters.

Empirically it is found that the relative half-width of the counters is dependent on the voltage applied to the tube. Consequently if one wishes to optimize the resolution some consideration must be given to the choice of operating voltage. The dependence of the resolution on the voltage applied to the xenon counter is shown in Fig. A 1.8 (p. 97).

---

* For checking the resolution of the proportional counters, as well as for making energy calibrations, a Cd^{109} source is particularly convenient. This isotope electron capture decays to Ag^{109} emitting only the strong silver K_α x-rays at 22.1 kev (weighted average of $K_{\alpha 1}$ and $K_{\alpha 2}$) and the weak K_β's at 25.0 kev in addition to the 87.5 kev γ-ray that is usually not detected in the proportional counters.

† A rectangular NaI(Tl) crystal 1" x 1" x 1/4" thick gives k equal to about 1.75 $(\text{kev})^{1/2}$ in the energy region 20 to 200 kev with 840 volts applied to a DuMont 6292 photomultiplier tube. Also see, for example, reference 58.

Here $w_{1/2}$ for the 22 kev silver x-rays from Cd^{109} is plotted as a function of the applied voltage. For each point the amplifier gain was changed so that the peak always occurred at the same channel. At very low voltages the amplifier has to be run at very high gain and this can contribute to the width of the pulse distribution. At very high voltages there is probably a multiplication (tube gain) broadening. An analogous effect of the multiplication on the resolution is observed (58) in the operation of scintillation crystals used with photomultiplier tubes. From Fig. A 1.8 it is seen that 1850 volts on the xenon counter is quite satisfactory from the standpoint of resolution.

Efficiency

In order to measure relative intensities with the counters, knowledge of the efficiency is essential. The efficiencies have not been measured experimentally as it would be burdensome to do this with sufficient accuracy over a large energy interval. Since the calculations are relatively straightforward, efficiencies have been calculated for both counters and these are found to be adequate for most purposes. One must take into account the absorption in the air path, the counter window, and in any absorbers present. In addition, allowance must be made for the stopping power of the counter gas, which is very sensitive to the Z of the gas and to the pressure. For monochromatic radiation a first approximation to the relative efficiency, ϵ , is given by

$$\epsilon = e^{-\Sigma \mu_i x_i} \left(1 - e^{-\mu_g x_g}\right) \quad , \qquad (A\,4)$$

where the μ_i's are the attenuation coefficients* of the various absorbing

* Obtained directly or by interpolation from reference 26.

materials (air, counter window, etc.) and the x_i are the corresponding thicknesses. μ_g is the photoelectric absorption coefficient for the filling gas and x_g is the corresponding path length.

The above treatment can be improved by evaluating the effect of the angular spread of the incident radiation through the absorbers and counter gas. Bisi and Zappa (59) have formulated this problem and have made numerical evaluations for two different geometries. Their results, interpolated to approximate the usual geometry for the present work, have been used in the calculation of the relative efficiencies for the counters. In Fig. A 1.9 relative efficiencies for the argon and xenon counters are plotted as a function of energy. It should be emphasized that these curves are for monochromatic radiation and to obtain the efficiency function for a continuum they must be folded into the resolution profile. Resolution broadening would then smooth out the sharp K edge jump in the xenon counter curve.

Typical Results

To illustrate the characteristics of these proportional counters several typical spectra will now be considered. Xenon and argon counter spectra from the decays of W^{181}, Hf^{181}, and Ta^{182} have already been presented in Figs. 3.3 and 3.4. Escape peaks for the L x-rays are evident in all these curves. The detailed discussion of these results has been given in Part III C.

Fig. A 1.10 shows spectra taken with the xenon counter for a W^{181} source. The Ta K_α x-ray group, designated K_α, at 57.1 kev is on the far right. The K_β group is off scale. The backscattered K_α radiation is denoted $K_\alpha s$. The Ta K_β escape peak which is due to the escape of

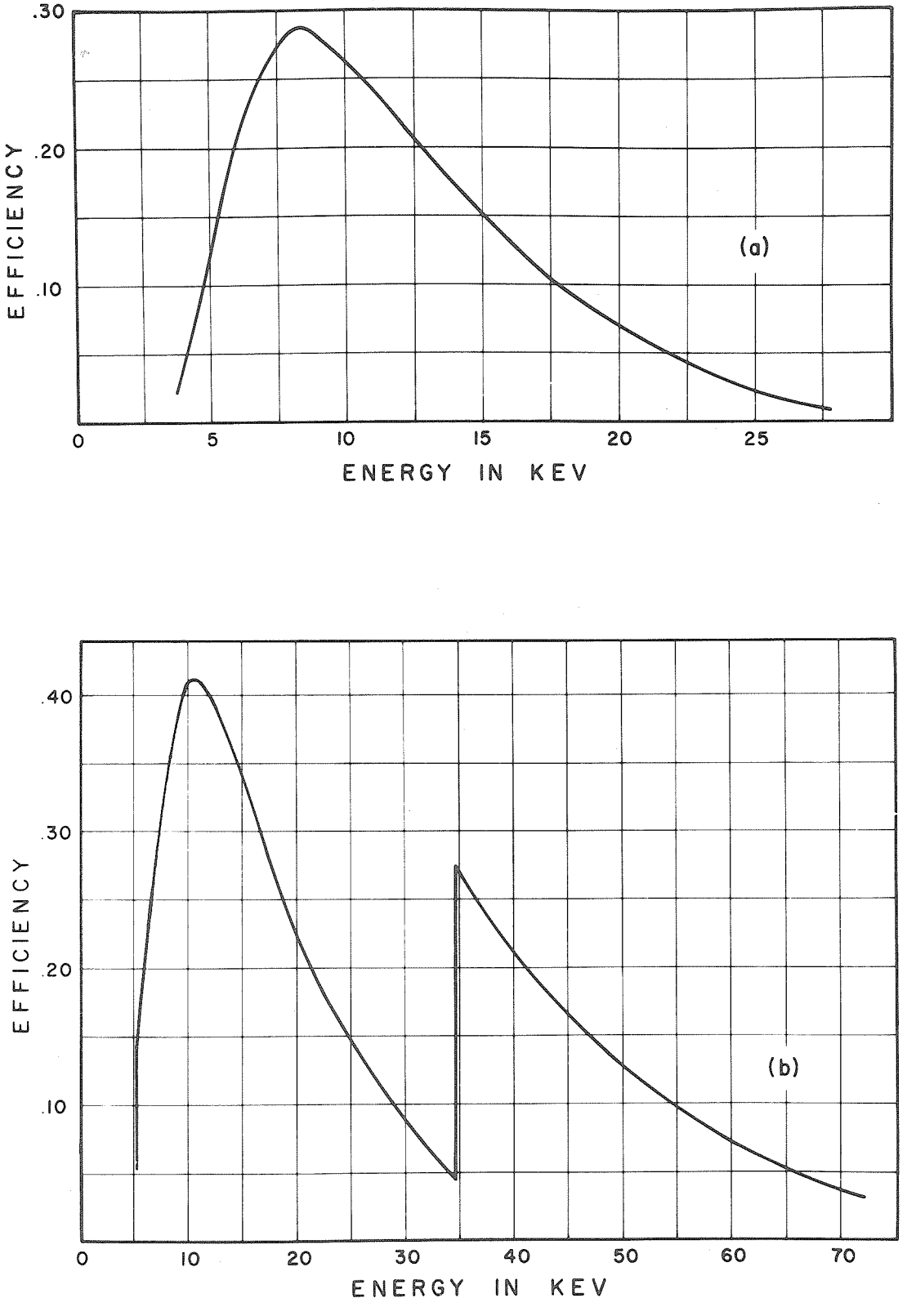

Fig. A 1.9. Relative efficiency for monochromatic radiation of (a) the argon proportional counter and (b) the xenon proportional counter.

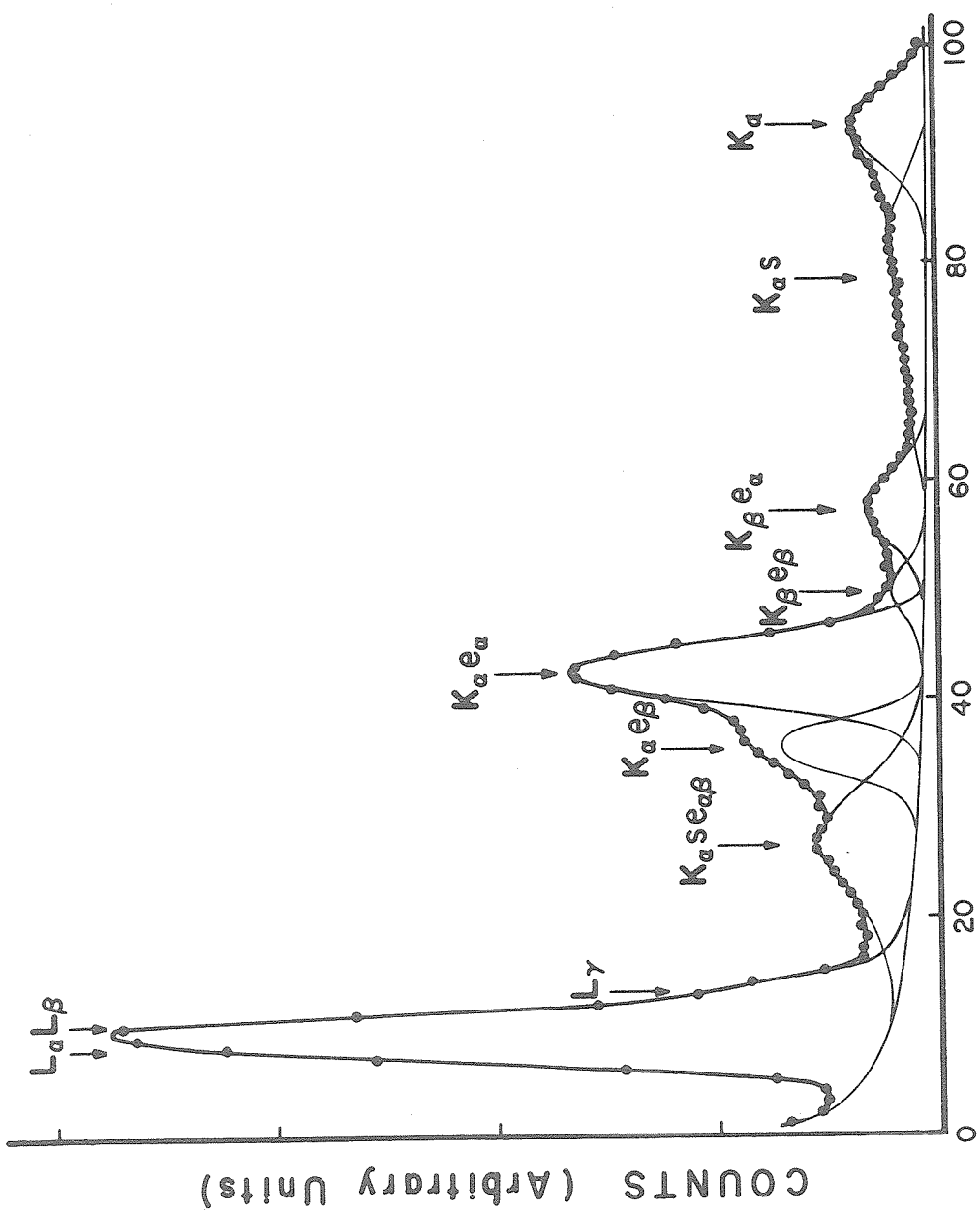

Fig. A 1.10. Xenon proportional counter spectrum showing the Ta K and L x-rays and associated escape and backscattered peaks. W^{181} is used as the source.

xenon K_α x-rays is denoted $K_\beta e_\alpha$, and that which is due to the escape of the xenon K_β x-rays is denoted $K_\beta e_\beta$. Similar notation is used for the Ta K_α escape peaks and the backscattered K_α escape peak. The backscattered peaks are unusually large because of the thick Plexiglas backing for this source mount. (See discussion in Appendix II.) On the extreme left is the Ta L x-ray group at 8.7 kev. At this particular instrument setting the L sub-groups are not resolved, but under appropriate conditions they can be barely resolved with the xenon counter. The curve shows the experimental data for which efficiency corrections have not been made.

Finally, Fig. A 1.11 shows the argon counter spectrum of Cd^{109} on the left and that of Se^{75} on the right. In Fig. A 1.11(a) the prominent peak is the silver K_α x-ray at 22.1 kev. The broadening on the left of the main peak is the escape peak and the small bump to the right is the K_β x-ray group. In Fig. A 1.11(b) the prominent peak is the arsenic $K_{\alpha\beta}$ (unresolved) x-ray group at 10.7 kev and the small peak to the left is the escape peak. Curves such as these were used in the study of the counter resolution and escape behavior.

In summary, it can be seen that the sealed-off type gas proportional counters described here are particularly useful for the study of x-rays and low energy γ-rays. They are relatively easy to construct and, by using different filling gases and pressures, they can be operated satisfactorily over a sizeable range of energy. At low energies, their higher resolution gives them a definite advantage over scintillation crystals.

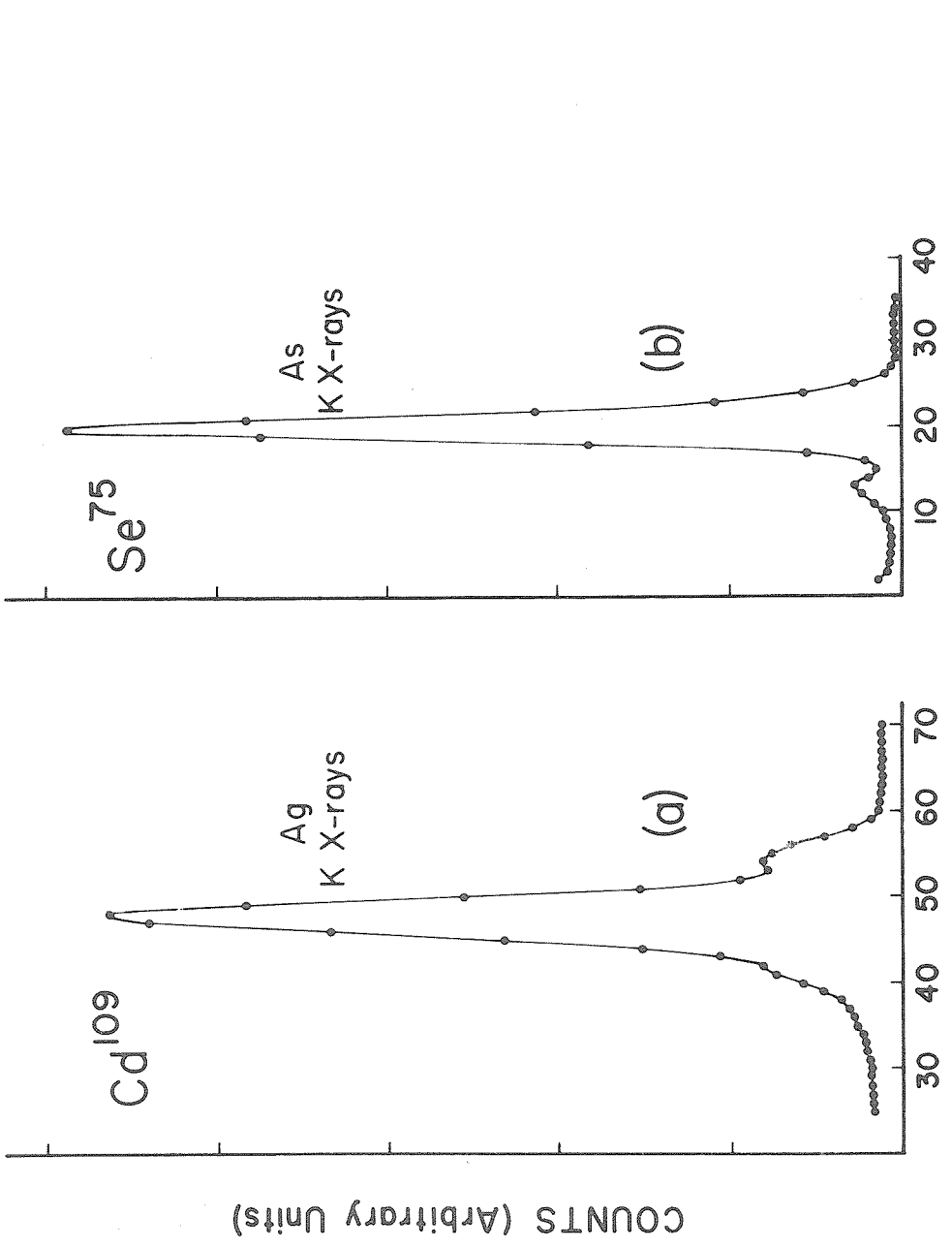

Fig. A1.11. K x-rays and escape peaks observed with the argon proportional counter using (a) Cd^{109} and (b) Se^{75} as sources.

APPENDIX II

W^{181} DECAY L/K X-RAY INTENSITY RATIO

The measurement of the L/K x-ray intensity ratio for the W^{181} decay to the accuracy required for the capture ratio determination (Part III E) proved to be experimentally difficult. The prominence of the backscattered K x-rays in the xenon proportional counter spectrum (see Fig. A 1.10, Appendix I) indicated that the source mounting should be improved. This was done as described in Part II E. Furthermore, the great difference in the xenon counter efficiency for the K x-rays and the L x-rays [see Fig. A 1.9(b), Appendix I] meant that the efficiency correction might introduce considerable error in the intensity ratio. To avoid efficiency correction difficulties, a NaI(Tl) scintillation crystal, covered only by a thin aluminum foil (see Part II E), was used to measure the x-ray intensity ratio.

Fig. A 2.1(a) shows a scintillation crystal spectrum obtained from the old proportional counter source (0.25" Plexiglas backing) with the scintillation crystal covered only by a 0.0012" aluminum foil. The dashed curve is the reflection of the right-hand side of the Ta K x-ray profile about the center of the peak. The asymmetry (the experimental points lie higher on the low energy side of the peak) indicates the presence of considerable backscattering. The small bump to the left of the escape peak (at about channel 23) also indicates this. The energy separation of the direct K x-ray from the backscattered K x-ray, ΔE, is the same for both the main peak and the escape peak. But since E, the energy, is much smaller for the escape peak than for the main peak,

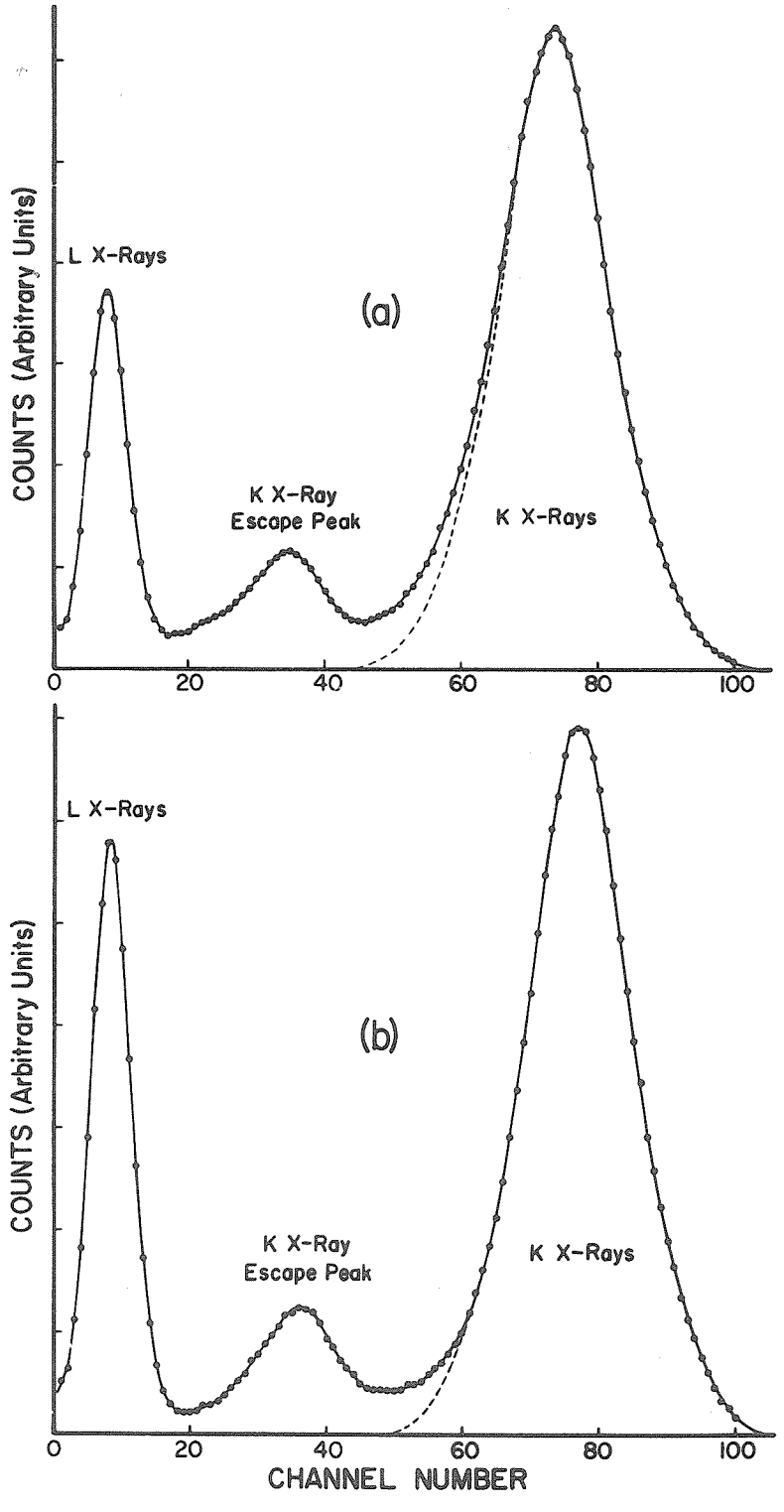

Fig. A 2.1. X-ray spectrum from W^{181} decay observed with the NaI scintillation spectrometer showing the effects of source backing and crystal covering: (a) 1/4" Plexiglas backing, 0.0012" Al foil covering; (b) 0.0004" Mylar backing, 0.00025" Al foil covering.

the relative separation, $\Delta E/E$, of the backscattered x-ray from the direct x-ray is greater in the escape region.

Fig. A 2. 1(b) shows a typical scintillation crystal spectrum obtained from the new remounted source (0.0004" Mylar backing) with the scintillation crystal covered only by a 0.00025" aluminum foil. Both curves (a) and (b) were taken in approximately the same geometry, so the sizeable difference in relative intensity of the L x-rays (compared to the K x-rays) can be explained in terms of the thickness of the crystal coverings*. In addition, comparison of the experimental K x-ray curve to the dashed reflected profile in (b) shows that there is very little if any backscatter.† The escape peak in Fig. A 2. 1(b) also indicates this.

Curves such as Fig. A 2. 1(b) taken in different source-crystal geometries show different apparent L/K x-ray ratios. To investigate this effect, several runs were taken with varying source-crystal separations. In addition to taking measurements in air, measurements were also made with the source and crystal surrounded by a helium atmosphere. (See Part II E for details of the helium chamber arrangement.) Fig. A 2. 2 shows the results of these measurements. The lowest curve is the raw (uncorrected) intensity ratio data for the runs in

---

* The correction factor for absorption of the L x-rays (relative to the K x-rays) in the crystal covering is 1.43 for (a) and 1.07 for (b).

† The fact that the observed K x-ray pulse distribution corresponds to two unresolved x-ray groups, K_α and K_β separated by about 9 kev in energy, has not been taken into account. The contribution of the K_β group to the reflected profile would tend to make the apparent backscattering slightly greater for both (a) and (b). However, Fig. A 2. 1 is intended to give only a qualitative picture of the backscattering behavior.

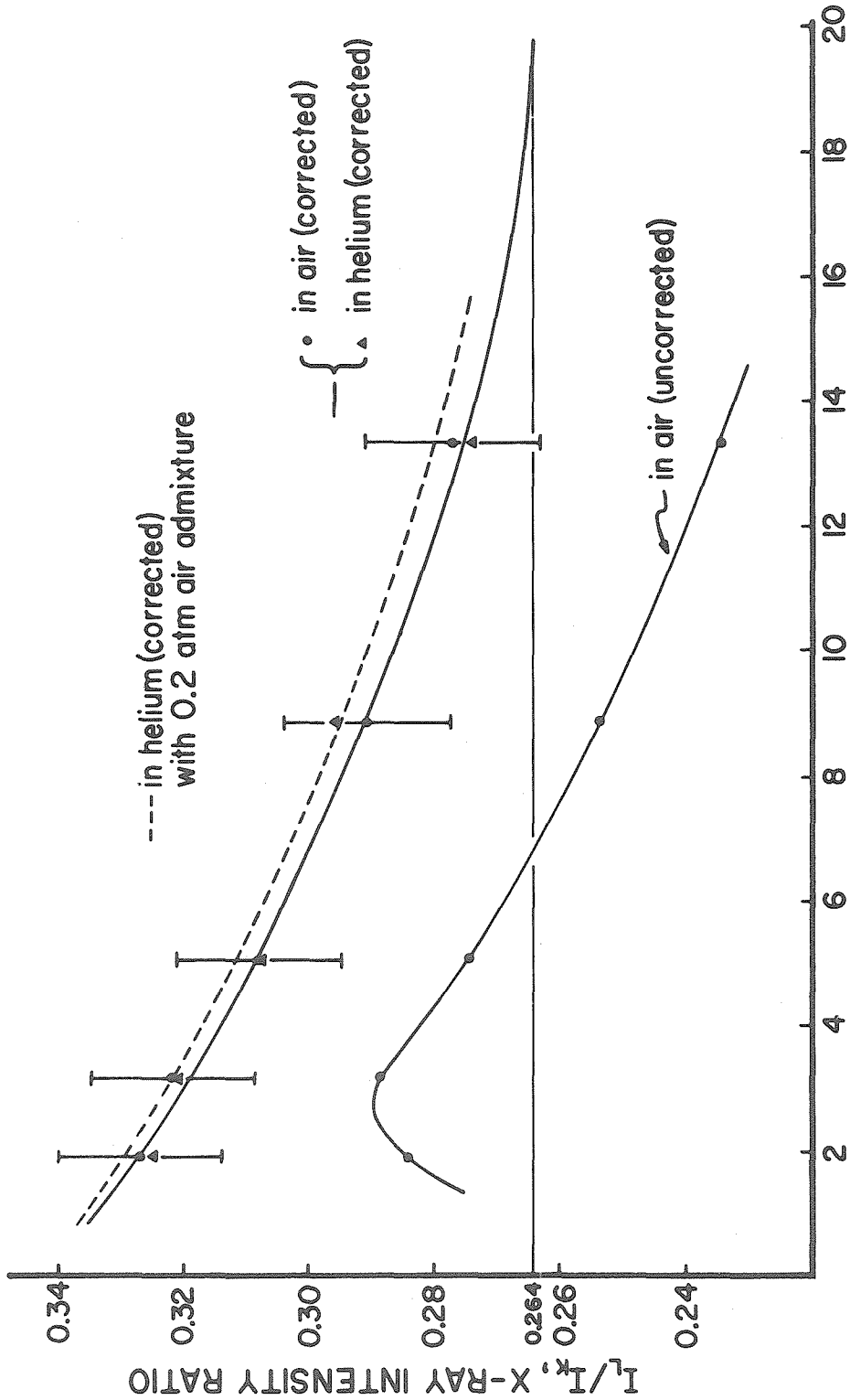

Fig. A 2. 2. L/K x-ray intensity ratio for the W^{181} decay as a function of the source-crystal separation. The lower curve is the uncorrected or raw data. The upper solid curve is fitted to the corrected data from air and helium runs. The dashed curve shows the effect of a 0.2 atm air admixture on the helium data.

air. The general tendency is for the apparent x-ray ratio to decrease with increasing separation. The decrease in the uncorrected ratio at very close distances is interpreted in terms of coincidence losses of the L x-rays. In order to obtain true intensities, the data must be corrected for coincidence losses and for absorption in the media between the source and the crystal. Transmission of the K x-rays through the 1/4" NaI crystal was estimated to be completely negligible.

The absorbing media between the source and the crystal were the 0.0004" Mylar source covering, the air or helium path which varied from run to run, the 0.00025" aluminum crystal covering, and the very thin oil layer on the crystal (estimated 0.0005" Plexiglas equivalent). The absorption correction factor, f_A, is given by

$$f_A = \frac{e^{-\sum_i \mu_i(K) x_i}}{e^{-\sum_i \mu_i(L) x_i}} \quad . \tag{A5}$$

The linear absorption coefficients, μ, are obtained from the National Bureau of Standards tables (26). These data were extrapolated to determine μ for helium. $\mu(K)$ is the coefficient for the average K x-ray energy, etc.

The L x-ray coincidence losses occurred in the following manner. If an L x-ray arrived at the crystal at the same time as a K x-ray, only one pulse would be produced, and its size would correspond to the high energy side of the K x-ray pulse distribution. In this case, the 100 channel pulse analyzer would record a K event, but no L event. The correction factor, f_C, derived to account for this loss is

$$f_C = \frac{1}{1 - \dfrac{0.744\Omega + 2\tau n_K (N_L/N_K + 0.084)}{N_L/N_K + 0.828}} \quad . \tag{A6}$$

Ω is the solid angle subtended by the crystal in units of 4π steradians, τ is the resolving time of the counter, n_K is the observed total K x-ray counting rate, and N_L/N_K is the ratio of L to K capture. Ω was determined from the formulas of Jaffey (60), with the square crystal approximated by a circular crystal of the same area. The finite size of the source was also taken into account. Unfortunately N_L/N_K depends on the x-ray ratio [see Eq. (7), Part III E]. For a first approximation, the x-ray ratio was determined without making the coincidence correction. The N_L/N_K resulting from this ratio was used to obtain an f_C. This f_C then gave a new x-ray ratio, etc. The process was iterated until the new capture ratio produced no change in the small correction factor. The numerical factors in Eq. (A6) take into account fluorescence and Auger yields, and the relative production of K- and L-shell holes by various processes. Reference 23 was used in evaluating these quantities. Eq. (A6) accounts for true coincidences (between L x-rays that result from K-hole filling by K x-rays) as well as for random coincidences.

The true L/K x-ray intensity ratio is given by

$$(I_{LX}/I_{KX})_{true} = (I_{LX}/I_{KX})_{observed} \cdot f_A f_C \quad . \tag{A7}$$

The upper solid curve in Fig. A 2.2 represents the "true" intensity ratio. Round points are the air data, and triangular points are the helium data. The dashed curve shows where the helium data would be expected, if during the run there were an admixture of 0.2 atmosphere

of air in the helium chamber that was not taken into account. If the flushing of the counter with helium were not complete, then some residual air could be left in the chamber. The possibility of incomplete flushing is probably why the helium point at about 9 cm lies considerably above the solid curve. The indicated errors allow for the statistical uncertainty in the L x-ray counts and for a 10% error in the absorption coefficients (26) used in the corrections.

The significant feature of the corrected(solid)curve is the decrease in apparent L/K x-ray ratio with increasing distance. This effect can be understood in terms of scattering. Table A I lists the ratio of the total scattering coefficients (26) at 10 kev and 60 kev for carbon, nitrogen, oxygen, and copper. 10 kev is near the Ta L x-ray group mean energy (8.7 kev) and 60 kev is near the Ta K x-ray group mean energy (59.3 kev). Since σ_s(L) is larger than σ_s(K), in close geometry, where scattering is important, more L x-rays will be scattered into the crystal than K x-rays. As the distance from the source to crystal increases, less scattered radiation reaches the crystal and hence the apparent L x-ray intensity decreases. Scattering could occur from the source support (Plexiglas $\approx$ C), from the air (= N + O), and from the brass ($\approx$ Cu) counter shield.

Table A I

Ratio of Scattering Coefficients for L and K X-Rays

Element	σ_s (10 kev)/σ_s (60 kev)
C	2.04
N	2.25
O	2.50
Cu	6.25

To obtain the actual x-ray ratio, the curves are extended to a large source-crystal distance to minimize scattering effects. In this manner, the value

$$I_{LX}/I_{KX} = 0.264 \pm 0.013 \qquad \text{(A8)}$$

is obtained for the W^{181} L/K x-ray intensity ratio.

APPENDIX III

INTERNAL CONVERSION COEFFICIENTS

A detailed discussion of the various internal conversion coefficients that are of importance to the arguments of the text will now be given.

A. Compilation of 136 Kev Transition Conversion Coefficient Data

The 136 kev transition in Ta^{181} has been frequently studied both by means of Coulomb excitation of Ta^{181} and by the decay of Hf^{181}. This transition is known* to be of multipolarity mixture M1 + E2. The percentage of E2 contribution can be determined indirectly from conversion coefficient measurements, and directly from δ or δ^2, the multipolarity mixing ratio, obtained by angular correlation or Coulomb excitation experiments. Table A II summarizes most of the relevant experimental results for this transition, along with the corresponding %E2 contribution computed from these measurements. The mixtures calculated from the conversion data have been determined with the use of the theoretical conversion coefficients listed in Table A III. Table A II also shows the average %E2 for each type of experiment and an average of all the results. The K- and L-shell coefficients in Table A III have finite nuclear size and screening corrections included, whereas the conversion coefficients used in the original works of Table A II, in general, were without these corrections, or only had rough empirical corrections.

---

* See the references for Table A II.

Table A II

Percentage E2 Mixture for the 136 Kev Transition in Ta^{181}

Reference	Method *	Results of Experiment		Calculated %E2	
		quantity	value	value	average
a	HD	α_K	1.2 ± 0.2	33.6	23.9
b	CE		1.53 ± 0.18	4.4	
c	HD		1.2	33.6	
d	CE	α_K/α_L	4.8 ± 0.5	19.1	8.4
a	HD		7 ± 1	0.6	
e	CE		6.3	5.5	
c	HD	$\alpha_{L\,I,\,II}/\alpha_{L\,III}$	5.9	17.8	17.8
f, a †	HD γ	$\delta = \sqrt{E2/M1}$	+0.46 ± 0.05	17.4	17.1
g	HD γ		0.45 ± 0.04	16.8	
h	CE	δ^2	0.19	16.0	14.7
i	CE		0.13	11.5	
j	CE		0.20	16.7	
(equally weighted) average				16.1 ± 10**	

* HD = Hf^{181} decay, CE = Coulomb excitation of Ta^{181}, and HD γ = Hf^{181} decay γ-γ angular correlation experiments.

† The original δ (= +0.50) in reference f was computed on the basis of the wrong level assignments. The cited value is from reference a, in which data from reference f were re-evaluated, taking into account the correct level assignments.

** Standard deviation from external consistency.

References for Table A II:

a. (61), Snyder and Frankel, Phys. Rev. (= PR), 106, 755 (1957).

b. (62), McGowan and Stelson, PR, 107, 1674 (1957).

c. (9), Boehm and Marmier, PR, 103, 342 (1956).

d. (63), E. M. Bernstein, PR, 112, 2026 (1958).

e. (64), Bernstein and Lewis, PR, 100, 1345 (1955).

f. (65), F. K. McGowan, PR, 93, 471 (1954).

References for Table A II, continued:

g. (8), Debrunner et al., Helv. Phys. Acta, 29, 463 (1956).
h. (66), Davis et al., PR, 103, 1801 (1956).
i. (67), Heydenburg and Temmer, PR, 104, 981 (1956).
j. (68), Wolicki et al., PR, 105, 238 (1957).

Table A III

Theoretical Conversion Coefficients for a 136 Kev Transition in Ta

Shell	α (M1)	α (E2)	Reference
K	1.58	0.452	(13), (69) *
L_I	0.203	0.046	(13)
L_{II}	0.0177	0.280	(13)
L_{III}	0.00227	0.221	(13)
L_{Total}	0.223	0.547	
M_{Total}	0.103	0.239	(13)
Total (K, L, M)	1.91	1.24	

* Average of values obtained from Rose (13) and Sliv and Band (69).

The final multipolarity mixture result of 16.1% E2 + 83.9% M1 for the 136 kev transition can be combined with the conversion coefficients of Table A III to yield the following values:

$$\alpha_K(136) = 1.40 \qquad \text{(A9a)}$$

$$\alpha_T(136) = 1.80 \ . \qquad \text{(A9b)}$$

The errors in these coefficients are estimated to be of the order of 12%.

B. Conversion Coefficient for the 152 Kev Transition

If the absolute K-shell internal conversion coefficient is known for the 136 kev transition, and if the intensity ratio of the 152 kev to 136 kev transition is known for both the γ-ray and conversion electron spectra, then it is possible to determine the absolute conversion coefficient of the 152 kev transition. The following equation may be derived which relates these quantities:

$$\alpha_K(152) = \alpha_K(136) \cdot \frac{I_{152K}}{I_{136K}} \cdot \frac{I_{136\gamma}}{I_{152\gamma}} \quad . \tag{A10}$$

Debrunner et al. (10) obtained $\alpha_K(152) = 1.0 \pm 0.2$ by essentially this method. However, their $\alpha_K(136)$ (=1.2) was taken from reference c of Table A II and differs from the adopted value of Eq. (A9a). Debrunner's $\alpha_K(152)/\alpha_K(136) = 0.833$ may be combined with the new $\alpha_K(136) = 1.40$ to yield

$$\alpha_K(152) = 1.17 \quad . \tag{A11}$$

By using Eq. (A10), the 152, 136 kev K conversion ratio of Eq. (17c), Part III G, may be combined with the γ-ray intensity ratio of Eq. (19), Part III G, to give an independent value for the 152 kev conversion coefficient of

$$\alpha_K(152) = 1.35 \quad . \tag{A12}$$

A third method of arriving at $\alpha_K(152)$ may be employed, although it is not entirely independent of the previous two determinations. The conversion intensity ratio for the two transitions was estimated from the published curves of Debrunner et al. (10). Conversion line areas were

divided by Hρ to obtain the result

$$I_{152\,K}/I_{136\,K} = 2.12 \quad . \tag{A13}$$

This value must be used with some caution, since no absorption corrections were made. Although Debrunner and co-workers did not indicate that they applied such corrections to their original data, this possibility can not be excluded. When Eq. (A10) is evaluated with Eq. (A13) and Eq. (19) of Part III G, the result is

$$\alpha_K(152) = 1.65 \quad . \tag{A14}$$

These various conversion coefficient determinations are summarized in Table A IV, where their weighted average is also given.

Table A IV

K-Shell Internal Conversion Coefficient for the 152 Kev Transition

Determination	α_K	Assigned Weight
Eq. (A11)	1.17	4
Eq. (A12)	1.35	2
Eq. (A14)	1.65	1
weighted average	1.29	

The conversion coefficient value from Eq. (A11) is given the most weight. This is because Debrunner's (10) published conversion electron spectrum had considerably better signal-to-noise ratio than the spectrum used in obtaining Eq. (A12). The value from Eq. (A14) is given least weight because unknown but necessary corrections may have been omitted as mentioned above. Including a reasonable estimate of the probable error, the final conversion coefficient value becomes

$$\alpha_K(152) = 1.3 \pm 0.2 \quad . \tag{A15}$$

On the basis of this α_K and the theoretical conversion coefficients listed in Table A V, it is possible to draw certain conclusions about the multipolarity of the 152 kev transition. There are three possibilities for the multipolarity: 1) pure M1 [α_K(expt) agrees with α_K(M1) within experimental error]; 2) a mixture of M1 + E2 [the lower experimental limit on α_K (= 1.3 – 0.2) would permit such a mixture]; and 3) a mixture of E1 + M2. Table A VI shows the mixtures calculated for these possibilities, along with the L-shell and total conversion coefficients.

Table A V

Theoretical Conversion Coefficients for a 152 Kev Transition in Ta

Shell	α(M1)	α(E2)	α(E1)	α(M2)	Reference
K	1.17	0.348	0.105	6.37	(13), (69) *
L_I	0.151	0.0359	0.0111	1.35	(13)
L_{II}	0.0129	0.173	0.00249	0.164	(13)
L_{III}	0.00165	0.130	0.00267	0.220	(13)
L_{Total}	0.166	0.339	0.0163	1.73	
M_{Total}	0.073	0.149	0.0060	0.72	(13)
Total (K, L, M)	1.41	0.836	0.127	8.82	

* Average of values obtained from Rose (13) and Sliv and Band (69).

Table A VI

Possible Multipolarity Assignments for the 152 Kev Transition

Possibility	Assumed α_K	Calculated			
		Multipolarity Mixture	α_L	α_T	α_K/α_L
1	1.17	pure M1	0.166	1.41	7.0
2	1.1	91% M1 + 9% E2	0.181	1.36	6.1
3	1.3	81% E1 + 19% M2	0.342	1.77	3.8

From the data available, a clear choice can not be made between possibilities 1) and 2). The best that can be said is that the data indicate pure M1 [since α_K(expt) is really larger than α_K(M1)], but do not rule out the possibility of a small E2 admixture. The choice between 1) and 3) is less ambiguous. The conversion ratio of Cork et al. (6), $\alpha_K/\alpha_L = 8 \pm 2$, strongly suggests 1). Unfortunately, no clear estimate for the K/L ratio could be made from the β-ray spectrometer measurements performed in this laboratory. Debrunner et al. (10) favored possibility 3), although their arguments for this choice depended largely on nuclear model predictions. On the grounds of Cork's (6) results, the 152 kev transition multipolarity will be taken as M1 (+ E2). This must be considered as a weak conclusion, since Cork's intensity ratio was determined by "visual estimate". A redetermination of this K/L conversion coefficient ratio would thus be very desirable.

C. Conversion Coefficients for a 6 Kev Transition in Ta

Theoretical conversion coefficients for a 6.25 kev transition in tantalum have been determined from the tables of Rose (13). The M-subshell coefficients tabulated for several values of Z near 73 were summed to obtain total M-shell coefficients. For each value of k, the energy in $m_o c^2$ units, these total coefficients were plotted on semi-log paper as a function of Z. Values for Z = 73 were interpolated from these graphs. A log-log plot of the interpolated coefficients as a function of k was then used to extrapolate down to 6.25 kev (k = 0.0122). Table A VII shows the results of the interpolation and extrapolation for four different multipolarities.

Table A VII

M-Shell Conversion Coefficients for Z = 73

Energy, k ($m_o c^2$)	α(E1)	α(E2)	α(M1)	α(M2)
0.05	0.878	732	13.2	2210
0.10	0.126	24.3	1.72	78.5
0.15	0.0403	3.34	0.528	13.0
0.20	0.0187	0.888	0.230	3.81
0.0122	47.5	7.7×10^5	850	2.2×10^6
0.0122 (a)	81	1.3×10^6	1.5×10^3	4.0×10^6

Note: (a) Estimated total conversion coefficient, α_T.

An approximate correction* was applied to the M-shell coefficients

* By examining L/K and M/L conversion coefficient ratios for several values of k, it was estimated that α_M(E1, E2) should be

in the next to the last row to obtain the estimated total (M + N + O-shell) coefficients listed in the last row. These coefficients should be used with caution for several reasons. First of all, no screening corrections were made in the calculations, and Rose (38) has estimated that the theoretical M-shell conversion coefficients may be as large as a factor of two because of this. The point nucleus approximation also used may have some effect on the M-shell coefficient values. Finally, it should be noted that the extreme extrapolation to 6 kev was accomplished by drawing a straight line through the points on the log-log plot. For very low energies, this procedure may be questionable and may introduce errors of unknown direction and magnitude. The total 6 kev coefficients in Table A VII, however, should probably be correct within a factor of 5.

---

multiplied by 1.7 and α_M(M1, M2) multiplied by 1.8 to take into account conversion in the N- and O-shells.

APPENDIX IV

LEVEL ASSIGNMENTS - THEORETICAL CONSIDERATIONS

Figs. 4.1 and 4.2 (Part IV A) show possible Ta^{181} level schemes consistent with the present measurements. Rotational level arguments in Part IV B show that the scheme of Fig. 4.1(a), with 11/2- for the 158 kev level assignment, is extremely plausible. The choices of Fig. 4.2 are unlikely because of Cork's (6) data that indicate that the 152 kev transition is M1 (+E2). In addition, the M2 multipolarity of the 476 kev transition requires the 6 kev level to be assigned as 9/2 - . Even without these pieces of evidence, all assignments but the above mentioned possibility [Fig. 4.1(a) with 11/2- 158 kev level] can be excluded. Nuclear model (1), (2), (4) and selection rule (4), (43) arguments will now be presented that show that the other choices of Figs. 4.1 and 4.2 are extremely improbable.

The Nilsson diagram for odd-Z nuclei (4) predicts that the 9/2- [514] level is most likely the first excited odd parity intrinsic state in Ta^{181}. The 7/2- [523] and 11/2-[505] levels might also occur as excited states, but the 9/2- level should appear first. This makes level schemes* 4.1(b), 4.2(b), and the 7/2- 6 kev level choices in 4.1(c) and 4.2(c) improbable.

The 152-158 kev level must either be a rotational state or an intrinsic state. If it is a rotational state based on the 6 kev level, it must have odd parity -- therefore level schemes 4.1(c), 4.2(a), and

---

* For convenience, the level schemes are denoted by the corresponding figure number.

4.2(b) can not be correct. On the other hand, if the 152-158 kev level is an intrinsic state, the Nilsson diagram shows that the only expected even parity intrinsic levels are 1/2+, 3/2+, and 5/2+. (The 7/2+ level is already occupied.) Spin 5/2 has been previously excluded, consequently level schemes 4.1(c), 4.2(a), and 4.2(b) are again ruled out.

Selection rule considerations can be used to exclude level scheme 4.2(c). If the 6 kev level is assumed to be 9/2− [514], then 9/2− is ruled out for the 152 kev level, leaving only the 7/2− [523] possibility. The 146 kev M1 transition from the 152 kev level to the 6 kev level would be classified as unhindered, while both the E1 and M2 transitions to the 7/2+ [404] ground state would be hindered. Since a 146 kev transition is not observed (5), this assumption is not correct. On the other hand, if the 6 kev level is assumed to be 7/2− [523], then the 152 kev level would have to be 9/2− ... either the 9/2− [514] intrinsic state or the 9/2− rotational level based on the 7/2− intrinsic state. In either case, the M1 transition to the 6 kev level is unhindered, while the E1 to the ground state is hindered. As before, the lack of a 146 kev transition means that this assumption is not valid either. Thus nuclear model and selection rule considerations exclude all the possible level schemes of Fig. 4.2.

Level scheme 4.1(b) may also be excluded. With the 6 kev level assumed 7/2−, the 158 kev level must be 9/2− ... either the 9/2− rotational level based on the 6 kev 7/2− [523] intrinsic level, or the 9/2− [514]intrinsic level. In the Hf^{181} decay (see Fig. 4.3), the 346 kev E2 transition between the 5/2+ [402] 482 kev level and the 9/2+ 136 kev level is classified as hindered. The corresponding 324 kev M2 transition between the 482 kev level and a 9/2− level at 158 kev is classified

as unhindered -- for either a 9/2- intrinsic or rotational level. The unhindered M2 transition should compete favorably with the hindered E2 transition, but no 324 kev transition has been observed (5) in the Hf^{181} decay. Consequently level scheme 4.1(b) can not be correct.

In 4.1(a) the 9/2- possibility for the 158 kev level must be ruled out, since the 6 kev level already occupies this state. Branching and ft considerations do not help distinguish between the choices 7/2- and 11/2-. In the Hf^{181} decay (see Fig. 4.3), the 324 kev transition between the 5/2+ 482 kev level and a 7/2- 158 kev level would be classified as hindered E1, and should compete favorably with the 346 kev hindered E2 transition. The lack of an observed 324 kev transition then rules out the 7/2- possibility of 4.1(a). The E3 transition from the 5/2+ 482 kev level to an 11/2- 158 kev level would be classified as unhindered, but it is not inconsistent that the hindered E2 transition should be considerably more intense than the unhindered E3. Thus it is seen that the correct Ta^{181} level scheme must be 4.1(a) with spin 11/2 for the 158 kev level.

REFERENCES

1. S. G. Nilsson, Kgl. Danske Videnskab. Selskab, Mat.-fys. Medd. 29, No. 16 (1955).

2. A. Bohr, Kgl. Danske Videnskab. Selskab, Mat.-fys. Medd. 26, No. 14 (1952); A. Bohr and B. R. Mottelson, Kgl. Danske Videnskab. Selskab, Mat.-fys. Medd. 27, No. 16 (1953).

3. B. R. Mottelson and S. G. Nilsson, Phys. Rev. 99, 1615 (1955).

4. B. R. Mottelson and S. G. Nilsson, Kgl. Danske Videnskab. Selskab, Mat.-fys. Skr. 1, No. 8 (1959).

5. Strominger, Hollander, and Seaborg, Revs. Modern Phys. 30, 585 (1958).

6. Cork, Nester, LeBlanc, and Brice, Phys. Rev. 92, 119 (1953).

7. Bisi, Terrani, and Zappa, Nuovo cimento 1, 651 (1955).

8. Debrunner, Heer, Kündig, and Rüetschi, Helv. Phys. Acta, 29, 463 (1956).

9. F. Boehm and P. Marmier, Phys. Rev. 103, 342 (1956).

10. Debrunner, Heer, Kündig, and Rüetschi, Helv. Phys. Acta 29, 235 (1956).

11. R. L. Garwin, Rev. Sci. Instr. 21, 569 (1950).

12. R. L. Garwin, Rev. Sci. Instr. 24, 618 (1953).

13. M. E. Rose, Internal Conversion Coefficients (North-Holland Publishing Co., Amsterdam, 1958).

14. H. E. Henrikson, Norman Bridge Laboratory of Physics, California Institute of Technology Special Technical Report, 1956 (unpublished).

15. A. T. Nelms, "Energy Loss and Range of Electrons and Positrons", National Bureau of Standards Circular 577 (U. S. Government Printing Office, Washington, D. C., 1956).

16. A. H. Wapstra (private communication).

17. Handbook of Chemistry and Physics, edited by C. D. Hodgman (Chemical Rubber Publishing Co., Cleveland, 1958).

18. J. W. M. DuMond, Ann. Phys. 2, 283 (1957).

19. W. E. Mott and R. B. Sutton, Encyclopedia of Physics, edited by S. Flügge (Springer-Verlag, Berlin, 1958) Vol. 45, p. 86.

20. D. E. Rehfuss and B. Crasemann, Phys. Rev. 114, 1609 (1959).

21. Eastman N. Hatch, Ph. D. thesis, California Institute of Technology, 1956 (unpublished).

22. Hill, Church, and Mihelich, Rev. Sci. Instr. 23, 523 (1952).

23. Wapstra, Nijgh, and Van Lieshout, Nuclear Spectroscopy Tables (North-Holland Publishing Co., Amsterdam, 1959).

24. Asaro, Stephens, Hollander, and Perlman, University of California Radiation Laboratory Report UCRL - 8786, June 1959 (unpublished). F. Asaro, Bull. Am. Phys. Soc. Ser. II, 4, 351 (1959).

25. S. A. Moszkowski, Beta- and Gamma-Ray Spectroscopy, edited by Kai Siegbahn (North-Holland Publishing Co., Amsterdam, 1955), Chapt. 13.

26. Gladys W. Grodstein, "X-Ray Attenuation Coefficients from 10 kev to 100 Mev", National Bureau of Standards Circular 583 (U. S. Government Printing Office, Washington, D. C., 1957).

27. Murray, Boehm, Marmier, and DuMond, Phys. Rev. 97, 1007 (1955).

28. E. H. S. Burhop, The Auger Effect (Cambridge University Press, Cambridge, 1952).

29. W. Laskar, Ann. phys. Ser. 13, 3, 258 (1958).

30. B. B. Kinsey, Can. J. Research 26a, 404 (1948).

31. H. Küstner and E. Arends, Ann. Physik 22, 443 (1935).

32. B. L. Robinson and R. W. Fink, Revs. Modern Phys. 32, 117 (1960).

33. C. E. Roos (private communication, 1960).

34. C. E. Roos, Phys. Rev. 105, 931 (1957).

35. H. Brysk and M. E. Rose, Revs. Modern Phys. 30, 1169 (1958).

36. Debrunner, Heer, Kündig, Rüetschi, and Lindquist, Helv. Phys. Acta 29, 432 (1956).

37. J. M. Jauch, Oak Ridge National Laboratory Report ORNL-1102, 1951 (unpublished).

38. M. E. Rose (private communication), reported in Bunker, Dropesky, Knight, Starner, and Warren, Phys. Rev. 116, 143 (1959).

39. S. A. Moszkowski, Phys. Rev. 82, 35 (1951).

40. R. W. Hoff and J. O. Rasmussen, Phys. Rev. 101, 280 (1956).

41. Gallagher, Sweeney, and Rasmussen, Phys. Rev. 108, 108 (1957). C. J. Gallagher, (thesis), University of California Radiation Laboratory Report UCRL-3928, Sept. 1957 (unpublished).

42. A. J. Bureau and C. L. Hammer, Phys. Rev. 105, 1006 (1957).

43. G. Alaga, Phys. Rev. 100, 432 (1955); Nuclear Phys. 4, 625 (1957).

44. Alaga, Alder, Bohr, and Mottelson, Kgl. Danske Videnskab. Selskab, Mat.-fys. Medd. 29, No. 9 (1955).

45. F. Boehm and A. H. Wapstra, Phys. Rev. 109, 456 (1958).

46. D. M. Chase and L. Wilets, Phys. Rev. 101, 1038 (1956).

47. H. Vartapetian, Compt. rend. 244, 65 (1957).

48. Hatch, Boehm, Marmier, and DuMond, Phys. Rev. 104, 745 (1956).

49. K. Runge, G. Knissel, and U. Hauser (private communication, 1960).

50. C. J. Gallagher, W. F. Edwards, and G. Manning, Nuclear Phys. (to be published).

51. S. A. Korff, Electron and Nuclear Counters (D. Van Nostrand Co., Inc., Princeton, 1955), second edition.

52. B. Rossi and H. Staub, Ionization Chambers and Counters (McGraw-Hill Book Co., Inc., New York, 1949).

53. D. West, Progress in Nuclear Physics, edited by O. R. Frisch (Pergamon Press, London, 1953), Vol. 3, p. 18.

54. S. C. Curran, Beta- and Gamma-Ray Spectroscopy, edited by Kai Siegbahn (North-Holland Publishing Co., Amsterdam, 1955) Chapt. VI; Encyclopedia of Physics, edited by S. Flügge (Springer-Verlag, Berlin, 1958), Vol. 45, p. 174.

55. C. S. Wu, F. Boehm, and E. Nagel, Phys. Rev. 91, 319 (1953). Bernstein, Brewer, and Rubinson, Nucleonics 6, No. 2, 39 (1950).

56. P. Axel, Rev. Sci. Instr. 25, 391 (1954). T. B. Novey, Phys. Rev. 89, 672 (1953).

57. E. Jahnke and F. Emde, Tables of Functions (Dover Publications, New York, 1945).

58. P. R. Bell, Beta- and Gamma-Ray Spectroscopy, edited by Kai Siegbahn (North-Holland Publishing Co., Amsterdam, 1955), Chapt. V.

59. A. Bisi and L. Zappa, Nuovo cimento 12, 211 (1954).

60. A. H. Jaffey, Rev. Sci. Instr. 25, 349 (1954).

61. Snyder and Frankel, Phys. Rev. 106, 755 (1957).

62. McGowan and Stelson, Phys. Rev. 107, 1674 (1957).

63. E. M. Bernstein, Phys. Rev. 112, 2026 (1958).

64. Bernstein and Lewis, Phys. Rev. 100, 1345 (1955).

65. F. K. McGowan, Phys. Rev. 93, 471 (1954).

66. Davis, Divatia, Lind, and Moffat, Phys. Rev. 103, 1801 (1956).

67. Heydenburg and Temmer, Phys. Rev. 104, 981 (1956).

68. Wolicki, Fagg, and Geer, Phys. Rev. 105, 238 (1957).

69. L. A. Sliv and I. M. Band, Leningrad Physico-Technical Institute Report, 1956 [translation: Report 57 ICC K1, issued by Physics Department, University of Illinois, Urbana, Illinois (unpublished)].

70. P. Debrunner (private communication, 1960).